

THE ROLE OF THE LUNG-BRAIN AXIS IN THE OZONE-IMPAIRED AMYLOID
ASSOCIATED ASTROCYTIC AND VASCULAR PHENOTYPE

Chandrama Ahmed

Submitted to the faculty of the University Graduate School
in partial fulfillment of the requirements
for the degree
Doctor of Philosophy
in the Program of Medical Neuroscience,
Indiana University

June 2024

Accepted by the Graduate Faculty of Indiana University, in partial fulfillment of the requirements for the degree of Doctor of Philosophy.

Doctoral Committee

Adrian Oblak, PhD, Chair

Michelle Block, PhD

March 28, 2024.

A. J. Baucum, PhD

Stephanie J. Bissel, PhD

Richard M. Nass, PhD

© 2024

Chandrama Ahmed

DEDICATION

To my father, who taught me it is okay to be different and encouraged me to develop new ideas rather than blindly following the existing ones. To my mother, who taught me that energy is not a construct of just physical strength, and proved time and time again that mountains can be moved with mental energy.

ACKNOWLEDGEMENT

I would first like to thank my mentor and supervisor, Dr. Michelle Block, whose guidance, kindness, and encouragement have shaped not only this dissertation but also my academic growth. I am truly fortunate to have had the opportunity to learn from you, lessons encompassing both research and life, and I hope I can exercise some of these lessons in my life.

I firmly believe I have been very fortunate to have an incredible advisory committee and am grateful for their dedication and expertise. Thank you to Dr. Adrian Oblak for your mentorship, and for always finding the time to talk about my project and progress, and supporting me during times of need. I have always enjoyed my committee meetings and thank you to Dr. A. J. Baucum, Dr. Richard Nass and Dr. Stephanie Bissel for making talking about my project fun.

To Dr. Carla Garza-Lombo, Dr. Hendrik Greve, and Teresa Gomez Ponce thank you for being a tremendous source of support and for providing a space to de-stress and celebrate milestones. I do not think I would be the scientist I am today without any of you in the trenches with me.

A special thanks to all the members of the lab, both past and present, whose collaboration, and encouragement have made this journey both fulfilling and enjoyable. Thanks to George Chittum for always finding ways to facilitate our projects and your leadership. Thanks to Morrent Thang, Jamie Malley, Paloma Sanchez, Windy Woodward, Dr. James Johnson, Angar Tsoggerel, Dr. Lisa Miller, Jo Wanner and Dr. Louis Pay for all your support and always having my back.

I am grateful to SNRI and Medical Neuroscience Graduate Program leadership for giving me this opportunity and facilitating my research. Many times during the course of this PhD journey life outside of PhD took unexpected turns and the program provided immense support every time. Thank you to Dr. William Truitt for making time for progress meetings whenever needed. Special thanks to Rene Baugh for always keeping me on track, supporting us and appearing as a life saver every time any administrative paperwork needed to be done.

I would like to extend my appreciation for all LARC stuffs and veterinarians for taking care of our mice and always making sure our work continues smoothly. Thank you to all SNRI stuffs for your support and particularly to Stacy Walton for looking out and all the encouragements and banter.

Thank you to all our funding sources, National Institute of Environmental Health Sciences, National Institute of Aging and Veterans Affairs for making this work possible.

I would like to express my deepest gratitude to my family, my parents, Dr. Salim Ahmed, and Dr. Nasreen Sultana, my sister, Dr. Amrita Ahmed, and my husband, Rifat Mueid for their endless sacrifices, patience, encouragements, and support throughout my PhD journey. Your unwavering belief in me made this journey possible for me. I am grateful for my family for keeping me grounded and giving me an incredible life beyond being a PhD candidate.

Chandrama Ahmed

THE ROLE OF LUNG-BRAIN AXIS IN OZONE IMPAIRED AMYLOID
ASSOCIATED ASTROCYTIC AND VASCULAR PHENOTYPE

Air pollution has been associated with an increased risk of Alzheimer's Disease (AD). Studies show ozone (O_3), a major component of urban air pollution, can exacerbate amyloid pathology. However, O_3 reacts in its entirety with lung epithelial lining after inhalation, hence does not translocate to brain. Studies have implicated the lung-brain axis in O_3 induced central nervous system (CNS) pathology. However, the mechanistic underpinnings of its role in amyloid pathology is obscure. Here, we explored the impact of O_3 on the astrocytic and vascular response to amyloid plaque in 5xFAD mice and its link to the O_3 lung response. O_3 exposure increased GFAP positive astrocyte density correlating with increased plaque burden in the cortex. Focusing on the plaque microenvironment, we found O_3 qualitatively altered plaque associated astrocytes, evidenced by both proteomic and transcriptomic changes. Along with loss of protein expression, proteomic changes reflected increased cell-cell interaction in plaque microenvironment. Specifically, we found increased astrocyte-microglia contact selectively in periplaque space from O_3 exposure. Transcriptional analysis of periplaque astrocytes revealed an accelerated shift towards disease associated astrocyte (DAA) phenotype. Elevated circulating HMGB1 was previously found from O_3 exposure. In this study we demonstrate deleting HMGB1 selectively in peripheral myeloid cells and not in CNS microglia ameliorates the lung immune response to O_3 as well as downregulates DAA marker in the CNS, providing a potential link between peripheral HMGB1 and O_3 induced astrocytic dysregulation. On examining vascular response to O_3 we found

increased vascular amyloid accumulation associated with an altered vascular proteomic profile. Our analysis indicates O₃ potentially disrupts vascular function such as amyloid clearance. Taken together, our study demonstrates that astrocyte and neurovasculature are contributors to O₃ lung-brain axis with important implications towards amyloid pathology progression and identifies peripheral myeloid HMGB1 as its potential modulator. Further studies are required to fully understand the consequences of this impact and its role in amyloid pathology.

Adrian L. Oblak, PhD, Chair

Michelle L. Block, PhD

A. J. Baucum, PhD

Stephanie J. Bissel, PhD

Richard M. Nass, PhD

TABLE OF CONTENTS

List of Tables	xi
List of Figures	xii
List of Abbreviations	xiv
Chapter One: Introduction	1
Introduction.....	1
Literature Review.....	3
Alzheimer’s Disease	3
Astrocytic Response in AD.....	4
Role of the Vasculature in AD Pathology.....	6
Peripheral Immune Responses in AD.....	9
Air Pollution.....	10
O ₃ Pollution.....	12
Respiratory and Neurological Effects of O ₃ Pollution.....	14
Lung–Brain Axis.....	16
Knowledge Gap and Research Outline	17
Chapter Two: Peripheral HMGB1 is Linked to O ₃ Pathology of Disease-Associated	
Astrocytes and Amyloid	20
Background	20
Methods.....	22
Results.....	32
Discussion.....	37
Chapter Three: Role of VEGF in O ₃ Induced Altered Vascular Phenotype.....	76

Introduction	76
Methods.....	78
Results.....	85
Discussion.....	88
Chapter Four: Conclusion.....	100
References.....	109
Curriculum Vitae	

LIST OF TABLES

Table 2.1: Antibodies and chemical stains used in specific applications.	58
Table 2.2: Primer sequences for qPCR.	59
Table 2.3: TaqMan probes.	59
Table 2.4: Other reagents used in Methods.	60
Table 2.5: Reagents used in GeoMx DSP.....	61
Table 2.6: Pathogen Exclusion List in Indiana University Mouse Colony.....	63
Table 2.7: List of altered proteins in GeoMx DSP assay.....	64
Table 2.8: List of Altered targets from GeoMx Whole Transcriptomic Assay.	66
Table 2.9: Selected Upregulated Pathways from GeoMx Whole Transcriptomic Assay.....	68
Table 2.10: Selected Downregulated Pathways from GeoMx Whole Transcriptomic Assay.....	74
Table 3.1: List of altered proteins in GeoMx DSP assay.....	98

LIST OF FIGURES

Figure 1.1: O ₃ alters amyloid associated astrocytic and neurovascular phenotype reflecting on the impact of lung immune dysregulation on CNS pathology.	19
Figure 2.1: Ozone exposure increases astrocyte density in the cortex of 5xFAD mice. ...	43
Figure 2.2: Ozone exposure increases astrocyte density in the cortex in 5xFAD mice, which is associated with increased plaque number and independent of plaque localization.....	45
Figure 2.3: Ozone altered the astrocytic protein expression pattern, dependent on spatial localization with plaques.	47
Figure 2.4: Ozone increased astrocyte–microglia cell contacts in the plaque microenvironment.	49
Figure 2.5: Ozone increased astrocyte-microglia cell-contact in plaque microenvironment.	51
Figure 2.6: Ozone alters the astrocytic transcriptional profile in the plaque microenvironment.	52
Figure 2.7: Peripheral HMGB1 modulates ozone-induced astrocytic dysregulation.	54
Figure 2.8: Plaque-associated astrocytes and peripheral myeloid cells interact in the O ₃ -dysregulated lung–brain axis: Implications for Alzheimer’s disease.	56
Figure 3.1: O ₃ increases vessel associated A β and decreases vascular density in plaque microenvironment.	92
Figure 3.2: O ₃ alters vasculature associated protein expression in plaque microenvironment.	94
Figure 3.3: Role of VEGFA in O ₃ Induced Exacerbated Amyloid Pathology.	96

Figure 3.4: O₃ Potentially Alters Vascular Wall-Astrocytic Association.....97

LIST OF ABBREVIATIONS

5xFAD	5x familial Alzheimer's disease
AD	Alzheimer's disease
AHR	Airway hyperactivity
Aldh1l1	Aldehyde dehydrogenase 1 family member L1
ANOVA	Analysis of variance
APO	Apolipoprotein
APOE	Apolipoprotein E
APOJ	Apolipoprotein J
APP	Amyloid precursor protein
AQG	Air Quality Guidelines
AQP4	Aquaporin4
A β	Amyloid beta
BAL	Bronchoalveolar lavage
BBB	Blood-brain barrier
CAA	Cerebral amyloid angiopathy
CBF	Cerebral blood flow
cDNA	complementary DNA
CNS	Central nervous system
COPD	Chronic obstructive pulmonary disease
CSF1R	Colony stimulating factor 1 receptor
DAA	Disease-associated astrocyte
DAMP	Damage associated molecular pattern

DCLN	Deep cervical lymph node
DSP	Digital spatial profiling
DTT	Dithiothreitol
ECE	Endothelin converting enzyme
ELF	Epithelial lining fluid
EPA	Environmental Protection Agency
GAPDH	Glyceraldehyde 3-phosphate dehydrogenase
GFAP	Glial fibrillary acidic protein
GLAST-1	Glutamate aspartate transporter 1
GLT-1	Glutamate transporter 1
HBSS	Hanks Balanced Saline Solution
HCL	Hydrochloric acid
HEPA	High efficiency particulate air
HMGB1	High mobility group box 1
IACUC	Institutional animal care and use committee
IBA-1	Ionized calcium-binding adaptor molecule 1
IDE	Insulin-degrading enzyme
IHC	Immunohistochemistry
IL-1	Interleukin-1
IL-9	Interleukin 9
IUSM	Indiana University School of Medicine
LMM	Linear mixed model
MBP	Myelin basic protein

MCI	Mild cognitive impairment
MMSE	Mini-mental state examination
NFκB	Nuclear factor kappa-light-chain-enhancer of activated B cells
NGS	Next generation sequencing
NIH	National institute of health
NLRP3	Nucleotide-binding domain, leucine-rich-containing family, pyrin domain-containing-3
NO	Nitric oxide
NO ₂	Nitrogen di-oxide
NVU	Neurovascular unit
O ₃	Ozone
OCT	Optimal cutting temperature compound
PBS	Phosphate buffered saline
PET	Positron emission topography
PFA	Paraformaldehyde
PM	Particulate matter
PPM	Particle per million
PSEN1	Presenilin-1
RAGE	Receptor for advanced glycation endproducts
RNA	Ribonucleic acid
ROI	Region of interest
RT-qPCR	Reverse transcription-quantitative polymerase chain reaction
SAA	Serum amyloid A

SEM	Standard error of the mean
TJ	Tight junction
TLR4	Toll like receptor 4
T-PER	Tissue Protein Extraction Reagent
TREM2	Triggering receptor expressed on myeloid cells 2
US	United States
UV	Ultraviolet
VEGF	Vascular endothelial growth factor
VEGFA	Vascular endothelial growth factor A
VEGFR2	Vascular endothelial growth factor receptor 2
VOC	Volatile organic compound
WHO	World Health Organization
WTA	Whole transcriptome atlas

CHAPTER ONE

INTRODUCTION

Introduction

Air pollution is a critical environmental concern with severe implications for human health [1]. The association between air pollution and respiratory as well as cardiovascular diseases is well documented [1–7], and recent research has suggested a link between air pollution and neurodegenerative disorders, including Alzheimer's disease (AD) [8–12]. Research on AD has typically focused on genetic risk factors; however, emerging studies have uncovered lifestyle [13,14] as well as environmental risk factors, including multiple components of air pollution [8–10,15–18]. One such component, Ozone (O₃), which is prevalent in urban air pollution, has been associated with higher risk of AD [19,20]. While AD is the most common form of dementia [21], a clear definition of its etiology remains lacking and treatment options remain limited, underscoring the importance of investigating the role of non-genetic factors in AD progression. Although epidemiological reports have implicated air pollution as an AD risk factor, its role in the development and progression of AD pathology is poorly understood.

Along with epidemiologic studies, animal studies have uncovered several potential mechanisms involved in air pollution mediated brain pathologies [22–27] and Lung–brain axis has been suggested as one of the mechanistic pathways regulating brain pathology from air pollution [22,26,28]. Researches focusing on air pollution induced AD pathology have found increased amyloid, oxidative stress response, neuronal damage, neuroinflammatory response as well as blood–brain barrier (BBB) damage

[22,23,25,27,29]. Amyloid plaque microenvironment, an important research focus for understanding plaque pathology and responses of central nervous system (CNS) cellular population to it [22,30–32], has been shown to be altered with O₃ exposure as well [22]. However, how the individual cellular components, including astrocyte and neurovasculature, in this plaque microenvironment are affected by air pollution is not known.

To address this research gap our focus in this study was to investigate how subchronic O₃ exposure alters astrocytic and vascular characteristics in the plaque microenvironment using 5xFAD mice, a well-defined AD mouse model for amyloid pathology [33], thereby aiming to understand how O₃ exposure impedes their normal function in plaque microenvironment potentially contributing to accelerated pathology progression. O₃ being highly reactive [34], reacts in its entirety inside the lung barrier and does not reach CNS. Hence, we also explored the role of the lung-brain axis in regulating these changes, as well as the involvement of circulating factors in its dysregulation. Our findings suggest that both astrocytic and vascular phenotypes are affected by O₃ exposure depending on proximity to plaque deposition site, altering their communication with other cellular components in the microenvironment. We also demonstrate peripheral myeloid cell specific as well as circulating high mobility group box 1 (HMGB1) has the potential to modulate these O₃ induced effects suggesting a role of lung-brain axis in AD pathology.

These findings build on the existing knowledge of AD pathology and provide important insight into how air pollution exacerbates its progression, strengthening the idea that complex, multifaceted responses are likely involved in this process, highlighting

the importance of further investigation. It also elucidates the role of peripheral components in AD providing potential biomarkers and therapeutic target.

Literature Review

Alzheimer's Disease

AD is a progressive neurodegenerative disorder that primarily affects the central nervous system (CNS), leading to a decline in cognitive function and memory loss [21]. Gustavsson et al. estimated the global prevalence of AD dementia, prodromal AD, and preclinical AD to be 32, 69, and 315 million, respectively, constituting 22% of people older than 50 years overall [35]. In the United States (US), the number of AD patients over 65 years of age is predicted to double by 2060, increasing from 6.7 million in 2023 to approximately 13.8 million [36,37]. Enormous advancements have been made in defining AD pathology and identifying many risk factors since AD pathology was first described over one hundred years ago by Alois Alzheimer [38]. However, there is still a vast gap in our understanding of the etiology of this disease, impeding therapeutic development and patient care.

AD pathology is classically defined by extracellular amyloid plaque deposition resulting from Amyloid-beta ($A\beta$) protein aggregation and intracellular neurofibrillary tangles resulting from misfolded tau protein accumulation [21]. Abnormal $A\beta$ and tau protein accumulation is a multifaceted process involving abnormal protein processing, deficient degradation pathways, and defective clearance mechanisms [39], with effects including synaptic dysfunction, synapse loss, and disruption of neuronal homeostasis and function, contributing to neuronal toxicity and neuron loss [21]. Clinical manifestation of

symptoms follows a progressive course starting with memory concerns leading to mild cognitive impairment (MCI), transitioning into dementia of varying progressing severity [40–42].

More recently the neuron centric description of AD pathology has diverged into other cellular components of the CNS [43]. A considerable number of genes associated with high risk of AD are mostly expressed by these non-neuronal cells shifting significant the research focus towards microglia and astrocyte [44]. Recent research are also targeting their responses for biomarker identification [45] and therapeutic development [46,47]. The findings however show complex responses from each of these cells suggesting contributions towards both neuronal protection and toxicity [43,48–54] potentially depending on the disease progression timeline [51,55]. Along with the role of these non-neuronal populations, condition and response of CNS vasculature are shown to be extremely important in disease progression. [56,57]. Among these, microglia, the resident immune cell in CNS, have been studied and characterized most extensively in the context of AD [49,54,55,58]. While researchers are increasingly studying astrocytic [43,44,59] and vascular responses [56,57,60,61], their roles in disease progression remain poorly understood. More importantly their interconnected communication and its disruption requires further investigations.

Astrocytic Response in AD

The main function of astrocytes is to maintain the homeostatic health of CNS, including synapse formation and elimination [62,63], maintaining synaptic homeostasis and health via modulation of extracellular ions and neurotransmitters [62–64], and providing metabolic and trophic support to neurons maintaining brain energy homeostasis

[39,43,44], maintaining communication with vessels as well as maintaining neurovascular unit [56,65,66], take active part in neuroinflammatory response [67]. Astrocytes are a vital part of the neurovascular unit (NVU), and their endfeet form the outer layer of the BBB [68], controlling its permeability and facilitating the glymphatic pathway [69,70], defined as, brains waste clearance mechanism via paravascular fluid circulation [71]. The importance of astrocytes in brain health maintenance suggests that these cells are likely impacted by AD pathology and play an important role in the disease process. Recent research has elucidated some astrocytic responses to AD pathology [43,72,73]. However, owing to the complex nature of AD, the dynamic progression of its pathology and non-uniformity of disease models, fully characterizing astrocytic response and its role in AD has been challenging.

Alois Alzheimer noted astrogliosis while describing AD [43]. Both atrophic with reduced branching suggesting astrodegeneration and hypertrophic astrocytes, have been found in AD [44]. Hypertrophic astrocytes with enlarged cell body and branches is a feature of reactive astrocytes commonly seen in most neuropathological condition including AD [43], particularly near A β plaque deposition sites [44]. Along with the morphological changes, reactive astrocytes feature differential expression of several proteins, suggesting a mix of protective [74–76] and deleterious effects on neurons [43,48,77,78]. Reactive astrocytes potentially contribute to increased A β production and secretion, as evidences by increased APP and BACE1 expression [43,62,79]. Decreased glutamate transporter 1 (GLT-1) and glutamate aspartate transporter 1 (GLAST-1) expression in reactive astrocytes [80–82] suggest reduced glutamate uptake, indicating excitotoxicity [43,83]. However, A β degradation is also facilitated by reactive astrocytes,

as suggested by the increased expression of the A β proteolytic enzymes neprilysin, the insulin-degrading enzyme (IDE), and endothelin converting enzyme (ECE) [43,74–76]. Astrocytes facilitate clearance mediated by apolipoproteins (APOs), such as APOE and APOJ [43,84,85]. As AD pathology progression is a decades-long process [86] and the astrocytic response precedes plaque aggregation [43], astrocytic responses are likely dynamic and depend on the disease stage.

Single-nucleus RNA sequencing has enabled the characterization of the astrocytic population associated with AD [73,87,88]. Habib et al. 2020 showed differences in these populations in normal aged and AD mice and identified a specific disease-associated astrocyte (DAA) population with a unique transcriptional signature that was not present in aged mice [73]. More interestingly, they explored how these changes progress with age, indicating the early onset of astrocyte changes at the initial stages of the disease. However, what initiates and drives these shifts remains largely unknown. Consistent with earlier findings, the expression levels of genes involved in amyloid metabolism and clearance were elevated in the DAA population [73]. Other researchers have found astrocytic subpopulations with transcriptional shifts and some overlapping characteristics [48,87–89]. It has recently been demonstrated that cellular responses are dependent on their proximity to plaque deposition site [22,50,73]; thus, it is critical to evaluate A β plaque microenvironment changes in AD pathology in addition to cellular changes.

Role of the Vasculature in AD Pathology

The brain's dense network of blood vessels provides oxygen, metabolites, and nutrients to the CNS; thus, healthy neurovasculature is critical for maintaining neuronal health [61,65]. Neurovascular coupling controls cerebral blood flow (CBF) to

accommodate exceptional oxygen consumption in the brain during the active cycle [65]. Thus, disruption of mechanisms involved in CBF regulation likely affects neuronal health and vice versa. The neurovascular system also restricts the entry of blood-derived molecules into the brain via the BBB [61]. Different components of the NVU, such as, luminal endothelial cell layer, extracellular matrix structure basement membrane, pericytes, smooth muscle cells, and astrocytic endfeet perform different functions in BBB formation and maintenance [65,90]. These components are differentially affected by CNS pathological conditions, including AD, influencing their function and impacting brain health [65].

Neurovascular dysfunction contributes substantially to A β accumulation [56]. The basement membrane and astrocytic endfeet regulate perivascular drainage with their dysfunction compromising A β clearance [69,90]. In AD, the low-density lipoprotein receptor-related protein 1 (LRP1) [61,90] and p-glycoprotein [91] expression, important for A β efflux have shown to be reduced in endothelial cells. Whereas, receptor for advanced glycation endproducts (RAGE) expression is increased promoting increased A β re-entry into the brain [61] and subsequent A β accumulation [92]. In line with vascular amyloid clearance dysfunction, eighty percent of AD patients demonstrate cerebral amyloid angiopathy (CAA) [90], characterized by cerebrovascular A β deposition [93].

Reduced CBF and increased BBB permeability occur at the early stages of AD before clinical manifestations arise [61,65]. Basement membrane thickening contributes to disrupted neurovascular coupling and CBF in AD patients [90]. Reduced endothelial cell coverage by pericytes and pericyte degeneration have also been reported in AD [61,90,94]. Pericytes are major regulators of neurovascular coupling as well as vessel

constriction and relaxation, with its dysfunction being responsible for CBF disruption [90,95]. They also has been shown to contribute in BBB breakdown in an APOE4 dependent pathway [96]. Endothelial cells in AD exhibit shortened tight junctions (TJs) and reduced TJ proteins [90], compromising BBB integrity [90].

One of the mechanistic pathways implicated in driving increased BBB dysfunction involves dysregulated vascular endothelial growth factor (VEGF) levels [97–99]. VEGF is an angiogenic factor [100] important for the formation of blood vessels and maintenance of vascular health and density [101]. However, brain injury and pathological conditions have been shown to increase VEGF levels, contributing to increased BBB permeability [97–99]. Interestingly, astrocytes are a known source of pathological VEGF levels [97,98]. In AD, increased VEGF levels likely arise due to hypoxia and reduced CBF [101]. However, both pathological [102–104] and beneficial [105–107] roles of VEGF has been found in AD. While, VEGF-A plays a dominant role in angiogenesis [100] and is the most studied member of VEGF family; not all studies specify which VEGF protein was investigated, potentially contributing to inconsistent findings. The stage of pathology [108] and site of examination [103,104] could also be causes of inconsistency, suggesting a complex and dynamic role of VEGF. More recently, Ali et al. demonstrated that peripheral inhibition of VEGF-A increased CBF, decreased BBB permeability, and increased TJ protein levels [104]; hence, further investigation is needed to determine the source of VEGF-A, the stimulators of its release, and its role at different stages of AD pathology.

Peripheral Immune Responses in AD

The contribution of peripheral myeloid cells in AD has been implicated, but is often overlooked. Most studies concerning peripheral myeloid cells have investigated A β plaque-associated myeloid cells [109,110]. Interestingly, AD pathology has been shown to influence the peripheral myeloid cell phenotype [111], dynamically altering myeloid-derived suppressor cells [112]. Ongoing AD pathology have been shown to regulate the immune response in the lungs [22], and neutrophils in cerebral blood vessels play a role in AD pathology [113], affecting BBB integrity and facilitating capillary stalls [104,114]. Neutrophils have been observed near plaque sites in individuals with AD and AD mouse models [113,115]. However, the contribution of peripheral immune cells to AD remains largely unexplored, particularly the mechanisms underlying their pathological modification.

HMGB1, in physiological conditions, is a nucleus bound transcriptional cofactor, with DNA bending properties [116]. In pathological conditions such as during oxidative stress, inflammatory insult, cellular injury and necrotic cell death, however, HMGB1 goes through passive or active release [116–118], depending on the nature of its post-translational modification [116,118], into cytosol and extracellular space and act as damage associated molecular pattern (DAMP) mediating cytokine like pro-inflammatory properties [116,117,119]. A number of receptors have been shown to be involved in its signaling pathway, however toll like receptor 4 (TLR4) and RAGE are the most commonly studied ones [120]. Along with pro-inflammatory cytokine like activities in different conditions, HMGB1 has also been shown to play anti-inflammatory, tolerogenic role, primarily depending on its oxidative states [117,121]. Monocytes and tissue

macrophages secrete HMGB1 in response to pro-inflammatory stimuli [116,122,123], on the other hand, HMGB1 is able to stimulate macrophages towards pro-inflammatory activation during tissue injury. Particularly in the event of lung injury HMGB1 has been shown to promote immune cell activation and recruitment [116,124–126]. Extracellular HMGB1 activity has been associated with neurological disorders including AD [127–129], with its inhibition shown to play a beneficial role [130,131], including prevention of neurite degeneration [131]. Studies have found elevated circulating HMGB1 in AD patients [127,132], which correlated with A β levels [127]. O₃ exposure in 5xFAD mice resulted in circulating HMGB1 increase [22], whereas in a separate experiment increased circulating HMGB1 in C57s resulted in reduced CNS triggering receptor expressed on myeloid cells 2 (TREM2) levels [22] which is required for disease associated microglial response [49] and plaque association [50]. More importantly, while O₃ exposure reduced CNS TREM2 levels, selective deletion of HMGB1 in peripheral myeloid cells, but not in CNS microglia diminished that reduction [22], implicating an important role of peripheral myeloid specific HMGB1 in amyloid pathology. It is important to fully characterize the role and effect of peripheral HMGB1, its impact on myeloid cell recruitment in AD and how that affects astrocytes and other CNS components, to identify pharmacological inhibition of peripheral HMGB1 as a therapeutic intervention.

Air Pollution

Air pollution is becoming one of the most common risk factors for global public health [133]. Indeed, a Global Burden Disease Study revealed air pollution as one of the five top risk factors, accounting for 11.3% of all female deaths and 12.2% of all male deaths [1]. Although long-term air pollution-associated respiratory illnesses have been

the primary target of investigation [133], increasing evidence has demonstrated an association between air pollution and increased risk for neurological disorders [10]. The 2021 World Health Organization (WHO) Air Quality Guidelines highlight the contribution of increasing air pollution to the global health burden associated with these noncommunicable diseases [134].

Air pollution comprises a complex mix of components [133]. The 2021 WHO Air Quality Guidelines provide air quality guidelines (AQGs) for PM₁₀, PM_{2.5}, O₃, nitrogen dioxide, sulfur dioxide, and carbon monoxide, highlighting these air pollution components as a priority [134]. These components were prioritized due to their effects on health outcomes; most contributing to total mortality and cardiovascular effects, and all cause respiratory effects [134]. However, to date, the estimated global disease burden only includes PM_{2.5} and O₃; thus, the total effect of air pollution on global health is underestimated [134]. The disproportionate availability of monitoring systems for these individual pollutants makes it challenging to model their contributions to the global health burden [134].

One of the major outcomes of long term air pollution exposure is increased risk of dementia supported by an increasing body of epidemiologic studies [11,16,19,135–139]. More importantly, some of the studies demonstrate increased dementia risk with long term exposure to even relatively low levels of air pollution [12,140,141], including one study in Ontario, with one of the lowest air pollution levels [140]. A similar study found higher incidences of dementia among population living near heavy traffic roadside [15]. Importantly, Mork et al 2023 demonstrates lagged hospitalization with dementia from air pollution exposure from decades earlier [12], which is consistent with dementia etiology

being a decades long process [86]. Along with dementia incidences and hospitalizations, post mortem analysis of adults and children living in cities with high air pollution have found increased A β and hyperphosphorylated tau [136,137]. Studies using animal models have recapitulated air pollution induced memory deficit and cognitive decline symptoms [142–146] as well as fibrillar A β deposits [23] and increased A β plaques [22,25,147]. Increased oxidative damage along with decreased glutamate receptors, neuritic damage and decreased neurite density have been observed in some of these studies associated with increased amyloid pathology [22–25]. While plaque deposition take a longer time frame to form, some studies show increase in A β ₄₂ levels, the longer form of the peptide that is more prone to aggregation [148], from just a single exposure to some air pollutants [142,149,150]. Some form of neuroinflammatory signatures have been most commonly found in air pollution exposed rodent brains including microgliosis, astrogliosis, increased cytokines from interleukin family, increased NF κ B, as well increased NLRP3 [22,26,27,29,143,151–154]. However air pollution is a complex mixture of several components, whose composition, hence human exposure to them, differ in different regions depending on their sources and climate of the region [155], making it challenging to study the mixed effect of these pollutants on human health [142,156]. Most animal studies are conducted with one form of pollutant and their differing composition, dose, route of administration or mode of exposure as well as use of diverse animal models confound the translatability of these findings.

O₃ Pollution

Ground-level O₃ is a major component of air pollution [134]. However, O₃ has received less attention than PMs, which is the focus of most air pollution studies.

Nonetheless, recent research has demonstrated the deleterious effects of O₃ exposure on human health, with Malashock et. al. reporting a 46% increase in O₃-attributable mortality from 2000 to 2019 [157]. The extensive effects of O₃ exposure on pulmonary function and its robust positive association with cardiorespiratory illnesses have been well documented [2,158–160]. More recent research has identified adverse effects on cognitive health, with an increasing number of studies finding increased dementia and AD risk with increased O₃ exposure [16,19,20]. Overall, the global O₃ incidence has increased despite considerable mitigation efforts in various parts of the world [134,157]. Malashock et al. reported an average 10% worldwide increase between 2000 and 2019 in population-weighted mean O₃ levels despite varying degrees of decreasing trends in high-income North American, European, and East Asian countries [157]. The considerable regional variation in O₃ levels has resulted in disproportionate O₃-attributable health effects and mortality [157].

Natural influx from the stratosphere provides a low background O₃ level in the troposphere (ground-level O₃) [161]; however, the two main sources of ground-level O₃ are oxides of nitrogen and volatile organic compounds (VOCs) [158,161]. Generally, the equilibrium state reaction between oxides of nitrogen keeps O₃ accumulation at check with nitrogen dioxide (NO₂), via photolysis, indirectly giving rise to O₃ and nitric oxide (NO) and in return nitric oxide scavenging O₃ to produce nitrogen dioxide [161]. These reactions result in O₃ accumulation when an imbalance in ratio of NO₂ and NO occurs [161]. One of the dominant pathways of disrupting this imbalance is via VOCs, which result from fossil fuel combustion and are present in vehicular exhaust fumes [158,161]. Atmospheric VOCs give rise to a series of reactions resulting in NO scavenging and,

consequently, O₃ accumulation [158,161]. The dissociation of NO₂, a photochemical reaction of O₃, also largely depends on sunlight and increased temperature. Hence, climate change and continued global increases in temperature makes it even a greater threat [158].

Respiratory and Neurological Effects of O₃ Pollution

O₃-induced lung damage and the resulting loss of respiratory function have been extensively studied in rodent models [162] and humans [2,163]. The upper respiratory tract is the only route of O₃ entry [34,164]. O₃ is very reactive and is absorbed entirely by the epithelial lining fluid (ELF) in a manner termed as “reactive absorption” [161], where it reacts with the constituents of ELF, generating lipid ozonation and peroxidation products and aldehydes [161,165], which has the potential to trigger downstream immune responses and lung damage [3,166]. Additionally, the thickness of the ELF is not uniform across the lower respiratory tract, exposing the epithelial cell layer to direct O₃ damage similarly triggering an immune response [166]. Evidence of cytokine upregulation, including that of IL-1 family members, has been observed following O₃ exposure, accompanied by increased myeloid cell (dominated by neutrophils and macrophages) and lymphocyte infiltration [166]. The combined effect of these responses leads to airway hyperactivity (AHR), as evidenced by human [163] and rodent studies [162,166], which is also observed in asthma [166,167]. Prolonged lung damage from continued exposure to O₃ results in emphysema, which is also observed in chronic obstructive pulmonary disease (COPD) patients [166]. In fact, O₃ exposure has been linked to impaired lung development, increased risk of developing asthma [168,169], and exacerbation of asthma [170–172] and COPD [173–175].

Along with respiratory illness, emerging epidemiologic studies have implicated O₃ pollution in increased cognitive deficit and AD risk [16,141]. Many of the initial studies linking air pollution and O₃ to neuropathology were conducted in Mexico City [176–179]. These studies examined the neuropathological effects of people living in cities with high levels of air pollution, including O₃, and revealed hyperphosphorylated tau, diffuse plaque, markers of oxidative stress, inflammatory responses, and BBB dysregulation in the brains of autopsied children and young adults [137,179]. More recent studies have been conducted with the advancement of ground-level O₃ estimation and monitoring approaches, revealing a striking association between O₃ exposure and cognitive impairment with findings like 10.4% increased risk of cognitive impairment according to Mini-Mental State Examination (MMSE) scores was reported to be associated with a 10 µg/m³ increase in O₃ in China [16], and a case study in Taiwan revealed a 211% increase in AD risk associated with a 10.91 ppb increase in O₃ [19]. Cleary et al. also reported an increased rate of cognitive decline with increased O₃ exposure in the US, which was worsened by the presence of one or more APOE4 alleles [141]. Deleterious effects of air pollution, including O₃, have also been observed in children including impaired brain development and dysfunction [180,181].

Evidence of O₃-induced neuropathology has also been investigated in rodent models. Increased oxidative stress and mitochondrial dysfunction [182] leading to the overproduction of Aβ were found in the rat hippocampus after O₃ exposure [183], as were memory deficits [145,146,184,185]. Avila-Costa et al. demonstrated reduced dendritic spines in the hippocampus of O₃-exposed rats exhibiting memory deficits [145]. Similar neuropathologies have been observed in mouse models of AD, in which O₃

aggravated amyloid pathology and neuronal damage [22,147]. However, a few studies have presented evidence of CNS BBB damage and increased permeability with O₃ exposure [150,186,187]. Microglial migration towards and association with plaques has been shown to mediate protective barrier function, facilitating plaque clearance and attenuating toxicity [50,110]. Although few previous studies have shown a microglial proinflammatory response [26,150], more recent work shows decreased microglial association with plaque, as well as altered periplaque protein expression profile with subchronic O₃ exposure [22].

These advancements in knowledge illustrate glimpses of potential mechanistic pathways underlying the impact of O₃ on amyloid pathology. However, it also elucidates the gaps in our understanding of the underlying mechanism. Astrocytic and neurovascular responses are tremendously important aspects of AD pathology. Yet, little is known about how O₃ influences their responses, and nothing is known about how O₃ affects their phenotypes in plaque microenvironment.

Lung–Brain Axis

Even though many components of air pollution are able to translocate into the brain and thereby exert a direct effect [136,180,188–191], that cannot be the case for O₃, it being a very reactive gas [34]. Studies have shown that O₃ is completely absorbed by the ELF or within the epithelial cell bilayer; no traces are observed beyond this region, including in the CNS [34,164]. The lung–brain axis hypothesis posits that the byproducts of O₃-induced lung damage, such as inflammatory cytokines and DAMPs, spill into the circulation and travel to the brain, possibly facilitating negative effects including BBB dysfunction, microglial response, oxidative stress, and neuronal damage. This axis may

represent the underlying mechanism behind the impact of O₃ on the CNS, and findings from animal studies support the lung–brain axis hypothesis [22,26,28]. Interestingly, the serum of O₃-exposed rats has been reported to be bioactive and can induce a microglial response *ex vivo* in the absence of a traditional circulating cytokine signature [26]. Erickson et al, on the other hand, observed increased serum amyloid A (SAA) and its influx into the brain parenchyma, implicating circulating factors as mechanistic contributors to the CNS effect of O₃ [28]. Greve et al. demonstrated subchronic O₃ exposure has the potential to aggravate amyloid pathology in an AD mouse model along with upregulation of circulating HMGB1, VEGF and IL-9. Elevated circulating HMGB1 was found in AD patients and although there are inconsistent findings showing both increase and decrease of circulating VEGF levels correlating with AD disease progression, taken together they implicate a role of these circulating factors in AD. While their presence in the serum has been reported and sometime correlated with disease progression, how they mediate O₃-associated CNS effects remains largely unexplored, as does their role in the pulmonary response.

Knowledge Gap and Research Outline

O₃ causes lung damage in humans and animal models [2,166]. It is associated with an increased risk of dementia in humans [16] and aggravated amyloid pathology in rodent models [22]. Greve et al. investigated the mechanistic underpinnings of O₃-induced increases in the A β plaque burden, revealing an impaired microglial association with plaque and overall altered protein expression in the plaque microenvironment [22]. However, how other cellular components in the plaque microenvironment, including

astrocytes and neurovascular units, are influenced by O₃ is not known. The role of peripheral signaling in mediating the impact of O₃ on these cellular components in amyloid pathology has not been investigated.

Hence, we investigated how O₃ affects the astrocyte phenotype by analyzing astrocytic proteomic and transcriptomic characteristics after subchronic O₃ exposure in an AD mouse model. Additionally, we examined the role of peripheral HMGB1 in regulating this phenotype. In Chapter Two, our findings show that an altered astrocytic phenotype leads to increased physical interactions between astrocytes and microglia in the plaque microenvironment and that peripheral deletion of HMGB1 has the potential to regulate this phenotype. We also explored how neurovasculature is modulated by O₃ exposure and as illustrated in Chapter three, demonstrate subchronic O₃ exposure alters neurovascular phenotype in plaque microenvironment. Overall, we provide evidence that O₃-induced dysregulation of the lung–brain axis modifies astrocytic and neurovascular responses (Figure 1.1), thereby potentially contributing to exacerbated amyloid pathology.

Figure 1.1: O₃ alters amyloid-associated astrocytic and neurovascular phenotype reflecting on the impact of lung immune dysregulation on CNS pathology.

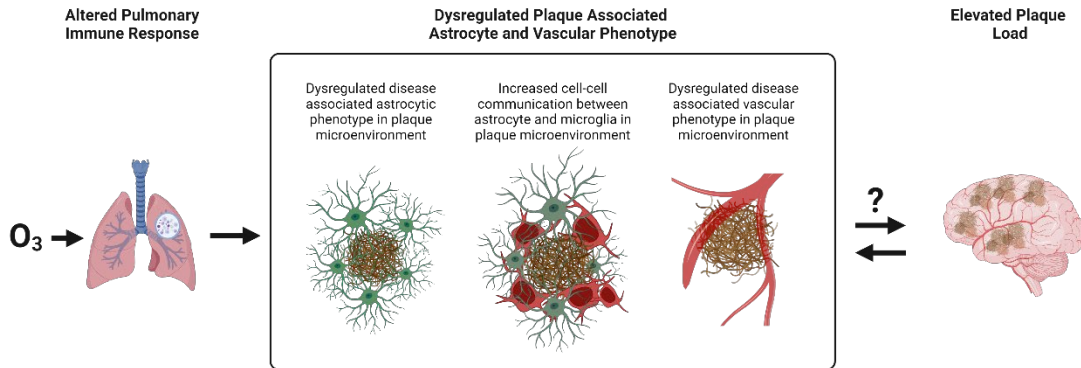


Figure 1.1: O₃, a reactive component of air pollution, is unable to translocate to the brain, has been associated with dementia and found to exacerbate amyloid pathology in the brain. After inhalation it reacts entirely in the lungs, inducing tissue damage and initiating immune cell trafficking. Lung–brain axis dysregulation has been implicated in O₃ mediated CNS pathology and here we demonstrate astrocytes and vasculature are important components of the O₃ lung–brain axis. Analysis of O₃ induced altered astrocytic and neurovascular phenotype highlighted changes in cell-cell interaction in the plaque microenvironment. These findings provide important insight into how air pollution impact CNS physiology and reflect the importance of understanding influences of peripheral immune dysregulation in AD pathology.

CHAPTER TWO

PERIPHERAL HMGB1 IS LINKED TO O₃ PATHOLOGY OF DISEASE-ASSOCIATED ASTROCYTES AND AMYLOID

Background

Alzheimer's disease (AD) is the most common neurodegenerative disease and the leading cause of dementia; however, its etiology is largely unknown and there are few disease modifying treatments [21,86]. Increasing evidence points to a role for environmental factors in AD risk [154,192–196], where several studies implicate several components of urban air pollution in increased AD risk and cognitive deficits [16,197–204]. Urban air pollution is a complex mixture comprising several chemical, particulate, and gaseous components, such as ozone (O₃), which is a prevalent and chronic exposure with health effects spanning several organ systems [134,158], including the central nervous system (CNS). In the United States (US), in 2022 alone, over 85 million people were exposed to air pollution levels exceeding EPA safety standard [205], emphasizing the importance of understanding how these inhaled exposures could be affecting the brain, particularly AD pathology.

O₃, one of the components of urban air pollution and a common ground-level air pollutant component [134,205], increases mortality [1,134,206,207] with a global burden of disease study attributing 12.1% of all male deaths in 2019 to ambient ozone pollution along with ambient air pollution [1]. Increased temperatures catalyze ground-level O₃ accumulation [161]; thus, climate change is a concern regarding increasing O₃-associated health effects [205]. Recent epidemiology studies have implicated O₃ as a strong risk factor for cognitive decline [16,141,208] and AD risk [19,20], with one study finding

10.4% increase in cognitive impairment risk with increased O₃ [16]. Prior rodent studies support that inhalation of O₃ affects the brain, demonstrating increased oxidative stress, mitochondrial dysfunction, neuronal damage as well as memory deficits [22,145–147,150,182,187,209,210]. Increased amyloid β (A β) PET signals in response to ambient air pollution have been observed in humans [200]; however, the underlying cellular mechanisms remain unclear. O₃ is a highly reactive gas and cannot transfer to the brain after inhalation [34,164,165]; thus, circulating factors or trafficking peripheral immune cells have been implicated to contribute to O₃-induced CNS effects in a pathway named “the lung–brain axis” [22,26,28] among other pathways [211,212]. While the majority of the inhaled O₃ reacts with the alveolar lining fluid and O₃ exposure extensively linked to myeloid cell infiltration in prior studies [22], the cell-specific and peripheral mechanisms underlying the impact of O₃ on amyloid pathology are unclear.

A β plaque deposition is a hallmark of AD [39,43,213,214]. Astrocytes [72] and microglia [49] surround plaques to form a protective barrier, restricting plaque toxicity to the surrounding neuropil and facilitating plaque clearance [49,50,72,73,110,215,216]. Disease-associated astrocytes (DAAs), a recently identified reactive astrocyte subset with a unique transcriptional signature and high glial fibrillary acidic protein (GFAP) expression, surround plaques in human and 5xFAD mouse tissue [73]. We previously demonstrated that O₃ exposure impacts plaque-associated microglia in 5xFAD mice [22]; however, little is known regarding how air pollution, including O₃, affects astrocytes and their plaque microenvironment localization.

Increasing evidence suggests that peripheral and systemic immune mechanisms contribute to AD pathobiology [22,217]; e.g., peripheral myeloid cells are implicated in

AD and amyloid pathology [22,112]. How these cells are pathologically modified and contribute to neurological disease is unknown, but urban air pollution exposure could play a role [22]. High mobility group box 1 (HMGB1) is a ubiquitous nuclear DNA-binding chaperone actively secreted by immune and damaged cells, acting as an autocrine and paracrine signal/cytokine [116]. Importantly, circulating HMGB1 is elevated in O₃-exposed 5xFAD mice, but CNS HMGB1 expression level changes are absent [22]. Circulating HMGB1 is elevated in some AD patient populations [127,131], implicating peripheral circulating HMGB1 but the role of HMGB1 as a transcription factor regulating specific cellular functions in AD is less known. The roles of these peripheral mechanisms in DAA phenotype development and amyloid pathology are unclear.

In the current study, we began to address these unresolved questions in the field by exploring: 1) How O₃-induced changes in the periphery may regulate the astrocyte phenotype (transcriptomic, proteomic, cell number, and cell contact) and how this is modified by localization with plaques; 2) the potential role of peripheral myeloid cells in this process; and 3) whether the loss of peripheral myeloid cell HMGB1 is linked to changes in the DAA phenotype.

Methods

Reagents

All reagents are listed in Tables 2.1–2.5.

Animals

Male transgenic 5xFAD mice hemizygous for five familial AD mutations (APP K670N/M671L, Swedish; I716V, Florida; V717,I London; PSEN1 M146L; and PSEN1,

L286V) [33], littermate controls on a C57Bl/6J background (B6. Cg-Tg(APP^SwF^Lon,PSEN1*^{M146L}*L286V)6799Vas/Mmjax; RRID:MMRRC_034848-JAX), C57BL/6J (RRID:IMSR_JAX:000664), and *LysM-Cre* (B6.129P2-Lyz2tm1(cre)Ifo/J; RRID:IMSR_JAX:004781) mice were obtained from the Jackson Laboratory. Female 5xFAD mice exhibit markedly exacerbated amyloid pathology that increases rapidly over time [218,219], risking a ceiling effect when combined with O₃ exposure; thus, to prevent potentially confounding analyses, only male mice were employed in the current study. Homozygous HMGB1 floxed (*HMGB1*^{fl/fl}) mice [220] were obtained from Riken (B6.129P2-Hmgb1<tm1Ttg>; BRC No. RBRC06240). *Hmgb1*^{fl/fl} mice were crossed with *LysM-Cre*^{+/+} mice to generate *Hmgb1*^{fl/fl}.*LysM-Cre*⁺ mice with deletion of HMGB1 in only peripheral myeloid cells [22]. *Hmgb1*^{fl/fl}.*LysM-Cre*^{+/-} mice were bred to produce the experimental *Hmgb1*^{fl/fl}.*LysM-Cre*⁺ mice and control *Hmgb1*^{fl/fl}.*LysM-Cre*⁻ littermates. All *Hmgb1*^{fl/fl}.*LysM-Cre* mice were genotyped to confirm the presence or absence of Cre recombinase and homozygous floxed *HMGB1* alleles.

The mice were acclimated to the housing facility for at least 1 week before all studies. All mice were maintained on a 12-hour light/dark cycle (7:00 AM–7:00 PM) in a specific pathogen-free environment, excluding *Helicobacter*. The complete list of pathogen exclusions is provided in Table 2.6. Experimental mice were individually housed in HEPA-filtered ventilated polycarbonate cages with food and acidic water (pH 2.2–2.7) provided *ad libitum*. All experiments were completed in strict accordance with the IUSM IACUC protocols (29002 and 27001) and NIH guidelines for housing, breeding, and experimental use. All mice were treated humanely to alleviate suffering.

O₃ Exposure

Mice were exposed to O₃ in full-body Hinner's inhalation chambers [221] as previously described [22]. Briefly, O₃ was produced with an HFL-10 O₃ generator (Ozonology, Northfield, IL, USA). The O₃ concentration was continuously monitored using a UV photometric O₃ analyzer (465L, Teledyne API, San Diego, CA), and the temperature was maintained at 21 ± 2°C. Rodents have lower sensitivity to O₃ toxicity than primates [222,223] due to their complex nasal turbinates, lung morphological differences, and unique airway surfactant [223,224]. Thus, increasing exposure by a factor of 3 is traditionally accepted for extrapolating to environmentally relevant human exposures [222]. O₃ concentrations of 0.2–0.3 ppm are frequent in areas of high air pollution, similar to 1 ppm O₃ exposure in rodents [26,225]. Regarding single exposures, 2 ppm was used to compensate for rodent insensitivity, as previously reported [28]. Rochester-style Hinner's chambers were used for whole-body O₃ inhalation exposure. The mice were placed in wire mesh individual housing cages that were transferred to the chambers for exposure. Before the experiment, mice were habituated to the exposure chambers for 5 consecutive days (4 hours/day).

Exposure-Specific Experimental Design

For each study, animals were assigned to experimental groups using a randomized block design. Random numbers were generated using <http://www.jerrydallal.com/random/randomize.htm>.

Subchronic O₃ Exposure

For the subchronic O₃ exposure experiments exploring how astrocytes are modified during O₃-augmented amyloid plaque pathology, one hundred twenty 10- to 11-

week-old male 5xFAD mice and littermate controls were exposed in two separate experiments (60 for CNS and 60 for pulmonary measures) to filtered air (FA), 0.3 ppm, or 1.0 ppm O₃ for 4 hours/day, 3 consecutive days/week, for 13 weeks (n = 10 per group). The mice were then euthanized, and samples were collected 18–24 hours after the last exposure, as reported previously [22]. Because the purpose of the study was to determine how O₃ modified the astrocyte phenotype during ongoing O₃-augmented amyloid pathology, the littermate control strain (no plaques) and the mice exposed to 0.3 ppm O₃ (no O₃-induced change in plaque pathology [22]) were excluded from processing and analysis.

Single O₃ Exposure

Two studies were conducted to investigate the effects of O₃ in *Hmgb1*^{fl/fl}.*LysM*-Cre⁺ mice. For the single 1.0 ppm exposure, seventeen 6- to 8-week-old male *Hmgb1*^{fl/fl}.*LysM*-Cre⁺ mice and *Hmgb1*^{fl/fl}.*LysM*-Cre⁻ mice were exposed to 1.0 ppm O₃ or FA once for 4 hours (n = 4–5 mice). Samples were collected 18–24 hours after exposure. To obtain clear neuroimmune measurements in this unique strain and genetic background, the exposure was increased to a single 2.0 ppm O₃ exposure, which results in increased neuroimmune responses in the control *Hmgb1*^{fl/fl}.*LysM*-Cre⁻ mice [22]. As such, thirty-eight 6- to 8-week-old male *Hmgb1*^{fl/fl}.*LysM*-Cre⁺ mice and *Hmgb1*^{fl/fl}.*LysM*-Cre⁻ mice were exposed to 2.0 ppm O₃ or FA once for 4 hours (n = 4–5 mice). Tissue samples were collected approximately 24 hours after exposure.

rHMGB1 IV Administration

Sixteen male C57Bl/6J mice (6–7 weeks old; n = 8) were injected intravenously by tail vein with 32.5 µg rHMGB1 (Thermo Scientific, 34-8401-85) in 200 µL vehicle

(20 mM Tris HCl, pH 8.0, 0.2 M NaCl, 1 mM DTT). Three hours after injection, the mice were euthanized, and samples were collected. Samples were excluded from analysis when identified as statistical outliers, resulting in a final sample size of $n = 6-8$.

Sample Collection

Brain Tissue

Mice were euthanized with isoflurane. One brain hemisphere was microdissected (cortex, hippocampus, and midbrain), flash-frozen in liquid nitrogen, and stored at -80°C . The other half of the brain was fixed in 4% paraformaldehyde (PFA, Electron Microscopy Sciences, 1921) by immersion for 2 days, followed by cryopreservation in 30% sucrose in phosphate-buffered saline (PBS) for another 2 days. Then, the entire hemisphere was embedded with optimal cutting temperature compound (OCT, 4583, Sakura Finetec, Terrance, CA) in cryomolds (Tissue-Tek, 4557, Sakura Finetec, Terrance, CA).

Pulmonary Samples

Bronchoalveolar lavage (BAL) fluid was collected from euthanized mice by lavaging the lung twice with 1 mL Hanks Balanced Saline Solution (HBSS, 21-622CV, Corning, Manassas, VA) without Ca^{2+} and Mg^{2+} . BAL fluid samples were centrifuged at $1500 \times g$ for 10 minutes at 4°C , and the cell pellets were resuspended in 250 μL of PBS. Total cell counts were determined using a TC-10 automated cell counter (Bio-Rad, Hercules, CA), applied to slides using a Shandon Cytospin centrifuge (Thermo Scientific, Waltham, MA), and stained with Wright-Giemsa (89013, Thermo Scientific, Waltham, MA). Cell differentials were determined at $40\times$ by a blinded observer counting at least 300 cells per sample.

Fluorescent Immunohistochemistry (IHC)

Sagittal sections (40 μ M) were collected using a freezing stage microtome (Microm HM 450, Thermo Scientific, Waltham, MA). For all following IHC endpoints, three evenly spaced sections approximately 0.24 mm apart spanning the motor cortex starting at the sagittal plane \sim 0.6 mm lateral to the midline [226] were stained per brain. All sections were washed for 10 minutes in 0.1% PBST prior to antigen retrieval. Antigen retrieval was performed in 1 M sodium citrate solution at 85°C for 15 minutes with subsequent cooling to room temperature for 20 minutes. Blocking was performed with normal donkey serum for 1 hour, followed by overnight incubation in primary antibody diluted (1: 500) in blocking serum. Rabbit anti-GFAP (Agilent DAKO, Z0334; RRID AB_10013382) and goat anti-IBA1 (Novus Biologicals, NB100-1028) were used to stain astrocytes and microglia, respectively. Sections were washed three times in 0.1% PBST and incubated with secondary Alexa Fluor antibodies diluted (1: 1000) in blocking serum at room temperature for 1 hour, followed by three washes with 0.1% PBST. Donkey anti-rabbit 647 (Invitrogen A-31573; RRID AB_2536183) and donkey anti-goat 488 (Invitrogen A11055; RRID AB_2534102) were used as secondary antibodies for GFAP and IBA-1 staining, respectively. Sections were mounted on slides with Prolong Gold (P36930, Life Technologies, Eugene, OR), coverslipped, and dried overnight in the dark. Slides were stored at -20°C before imaging. To stain for A β plaques, sections were washed in 0.1% PBST for 5 minutes and Methoxy x34 (SL 1954, Millipore Sigma, St Louis, MO) solution (0.04 g X34 in 400 mL 100% ETOH and 600 mL DI H $_2$ O) for 10 minutes. The slides were then sequentially washed five times with DDH $_2$ O and 0.1% PBST for 5 minutes before the addition of Prolong Gold and coverslipping.

Imaging

Whole-Cortex GFAP Expression

The entire hemisphere was scanned at 10× using a Leica Aperio Versa slide scanner (Leica Microsystems Inc., Deerfield, IL) to determine whole-cortex astrocyte expression. Images were processed and analyzed using ImageJ (FIJI, version 2.9.0, NIH). The region of interest (ROI) was drawn around the entire cortex and manually thresholded. The Analyze Particles plugin was used to quantify the GFAP-positive area and cell number. A sample size of 8–10 mice per group was analyzed per endpoint. Statistical outliers were excluded.

Plaque-associated Astrocyte Quantification

For plaque-associated astrocyte quantification, 1 μm Z-stacks were acquired at 40× with oil immersion with a Nikon A1R confocal microscope (Nikon, Tokyo, Japan) in the primary motor region of the cortex due to ease of identification of the finite region using confocal microscopy. Images were analyzed in NIS Elements AR (Nikon, Tokyo, Japan) using the General Analysis 3 module. Image stacks were thresholded using consistent criteria across the entire analysis. To consistently define the plaque microenvironment, a 50 μm diameter circle was drawn around a plaque-positive area of this specific size, defining the periplaque ROI. A blinded observer counted GFAP-positive cell bodies manually in the maximum intensity projection image. Astrocytes were considered periplaque astrocytes if either the cell body or any branches were contained in the ROI. A sample size of 8–10 mice per group was analyzed per endpoint. Statistical outliers were excluded.

Colocalized Astrocyte–Microglia Volume Quantification: Cell–Cell Contact

To assess astrocyte–microglia colocalization, 1 μm spaced Z-stacks were acquired from the primary motor region of the cortex at 40 \times with oil immersion with a Nikon A1R confocal microscope. Images were analyzed in NIS Elements AR using the General Analysis 3 Module. Image stacks were thresholded using criteria maintained across the entire analysis. Within a 50 μm diameter ROI, areas double-positive for GFAP and IBA-1 were quantified per stack. The total colocalized volume was obtained by adding the colocalized area of all the stacks in the image and normalized by the total GFAP volume. A sample size of 8–10 mice per group was analyzed per endpoint. Statistical outliers were excluded.

NanoString GeoMx Digital Spatial Profiling: Protein Expression

Fixed 10 μm coronal sections were acquired with a cryostat (CM1900, Leica) and stored at $-20\text{ }^{\circ}\text{C}$ before processing. Slides were processed per the NanoString Slide Prep manual for protein analysis. Briefly, slices were incubated with the NanoString GeoMx Alzheimer's Morphology kit, which contains the A β antibody for plaque visualization and Alexa Fluor 647-conjugated mouse anti-GFAP antibody (BioLegend, 837512; RRID AB_2734611) for astrocyte identification, along with NanoString panels (Neural Cell Profiling Core, Alzheimer's Disease Panel, Alzheimer's Disease Extended Panel, Glial Subtyping Panel) containing approximately 60 antibodies with unique photo-cleavable oligonucleotide tags. Slices were scanned in the NanoString Digital Spatial Profiler, and polygonal ROIs were drawn around plaque-associated and non-plaque-associated astrocytes in the cortex. The GFAP-positive area within each ROI was delineated for photocleavable oligonucleotides collection. The collected oligonucleotides were

hybridized with NanoString codeset, per the NanoString user manual, to map the counts to corresponding antibodies and region from where the oligonucleotides was collected. Digital counts were generated on an nCounter Max/Flex system (NanoString Technologies, Seattle, WA). The differential protein expression analysis was performed using the NanoString GeoMx Digital Spatial Profiling (DSP) Analysis Suite. The digital counts were tested for quality control and normalized to the housekeeping protein (GAPDH and histone H3) counts. Three sections were scanned per brain from a sample size of 4 animals per exposure group (FA or 1.0 ppm O₃) for the analysis, resulting in 68–70 ROIs analyzed per experimental group. ROIs that did not pass the quality control checks were excluded.

NanoString GeoMx Digital Spatial Profiling: Whole Transcriptome Assay

Fixed frozen 10 µm coronal brain sections were processed with the NanoString Mouse Whole Transcriptome Atlas (WTA) panel per the NanoString user manual for spatial transcriptomic analysis. Plaques and astrocytes were visualized using Alexa Fluor 594-conjugated mouse anti- Aβ antibody (BioLegend 803019; RRID AB_2734552) and Alexa Fluor 647-conjugated mouse anti-GFAP antibody (BioLegend; 837512 RRID AB_2734611), respectively. Sections were scanned in the NanoString Digital Spatial profiler, and polygonal ROIs were drawn around plaque-associated astrocytes in the cortex. Photocleavable oligonucleotides were collected only from the GFAP-positive segments. Collected oligonucleotides were sequenced using the Illumina Next Generation Sequencing (NGS) Platform (NanoString Technologies, Seattle, WA). Differential gene expression and enriched pathway analyses were conducted using the NanoString GeoMx DSP Analysis Suite. Normalization was performed using the ubiquitous astrocyte marker

Aldh111 [227,228] since its expression was unchanged in both groups. For the analysis, 2–5 sections were scanned per brain from a sample size of 3 animals per group, with 90–92 ROIs analyzed per experimental group. ROIs were excluded from the analysis if they did not pass the quality control test.

RNA Isolation and RT-qPCR

Microdissected whole cortex (including corpus collosum) and midbrain tissue were homogenized in Tissue Protein Extraction Reagent (T-PER) with protease and phosphatase inhibitors. An equal volume of TRIzol™ was added to each homogenate, and RNA was extracted per the manufacturers' protocol. RNA was treated with DNase for purification using an Ambion DNA-free kit (Invitrogen AM1906) and reverse-transcribed using a Maxima First Strand cDNA synthesis kit (Invitrogen, K1641). RT-qPCR was performed with 1 µL cDNA and TaqMan probes and primers (Tables 2.2 and 2.3) on a QuantStudio™ 6 Flex RT-PCR system (Applied Biosystems, Waltham, MA). *Gapdh* was used as the housekeeping control for $2^{-\Delta\Delta CT}$ quantification. For a complete list of primers and probes used, see Tables 2.2 and 2.3.

Statistical Analysis

Experimenters were blinded to the experimental groups. The sample size was determined according to prior reports, and power analyses were calculated for 80% power. Data were analyzed in GraphPad Prism 8.0 (GraphPad Prism, San Diego, CA, USA). Outliers were determined using the ROUT method with $Q = 1\%$ and removed from all analyses. Normal distribution was tested using the Shapiro–Wilk test. Welch's t test was performed for data that passed the normality test. A 2-way ANOVA with Bonferroni's post hoc analysis was performed when applicable. A t test was used for

GeoMx DSP protein profiling and a linear mixed model with Benjamini–Hochberg post hoc correction for the whole transcriptome assay. Data are expressed as the mean \pm standard error of the mean (SEM). A P value $<.05$ was considered to indicate significance.

Results

Ozone Exposure Increases GFAP Astrocyte Density in the Cortex

The role of astrocytes in maintaining neuronal health and function has been extensively studied and described [43,73]. Astrocytes are a heterogeneous and highly complex population of cells with unique phenotypic responses depending on pathological conditions. Some common characteristics of reactive astrocytes have been identified, such as the overexpression of GFAP with enlarged morphology [43,72,73], which is a characteristic of AD [43,72]. However, the instigating events responsible for astrogliosis in AD and how astroglia respond to air pollution are poorly understood. Here, cortical GFAP-positive astrocytes were found to increase in number in response to O₃ exposure, as evidenced by increased O₃-elevated GFAP-positive cell counts and increased total cortical GFAP expression in 5xFAD mice (Figure 2.1A and 2.1B). To explore whether the O₃-induced increase in cortical astrocyte density is affected by plaque proximity, we quantified the plaque-associated and plaque-distant astrocyte numbers in confocal images of the primary motor cortex. Consistent with prior reports [22], subchronic O₃ exposure increased the plaque number (Figure 2.1C and 2.1D). O₃ also increased the periplaque astrocyte number; however, only a trend toward an O₃-induced increase was observed in the number of nonplaque astrocytes (Figure 2.2A and 2.2B). No significant difference in

the number of periplaque astrocytes per plaque was identified (Figure 2.1E, 2.2C and 2.2D), suggesting that the close proximity of astrocytes to the increased number of plaques may be associated with the increased number of astrocytes. This association is further supported by the significant correlation between periplaque astrocytes and plaque number irrespective of O₃ exposure (Figure 2.1F). However, the number of nonplaque-associated astrocytes increased with O₃ exposure with no significant association with plaque number (Figure 2.1G), suggesting that O₃ affects astrogliosis differently depending on plaque localization.

Ozone Alters Astrocyte-Associated Protein Expression in the Periplaque Space

To understand how O₃ exposure and plaque localization could interact to affect the astrocyte phenotype and obtain insight into potential functional changes, we next sought to spatially profile cortical astrocyte protein expression according to their proximity to or distance from amyloid plaques. As such, we compared the protein expression pattern in periplaque astrocytes to that in astrocytes distant from the plaque deposition site (nonplaque) in both O₃- and FA-exposed mice. More specifically, we sought to elucidate how the astrocyte protein response to plaque deposition changes with O₃ exposure. DSP analysis revealed a baseline change in 25 astrocyte-associated proteins (Table 2.7) in periplaque astrocytes, consistent with prior findings [72,73]. Notably, the expression of 16 proteins changed regardless of O₃ exposure (Figure 2.3B). However, when comparing plaque-associated and plaque-distant astrocytes, 9 proteins (Figure 2.3B and 2.3C) were changed in only FA-exposed mice, including neprilysin and Ki-67, indicating a unique baseline change in plaque-associated astrocyte proteins that occurs without O₃ exposure. Thus, O₃ exposure appears to impede this shift in protein

expression. However, myelin basic protein (MBP), CSF1R, and Clec7a protein expression levels were increased in response to O₃ in plaque-associated astrocytes (Table 2.7). The upregulation of microglia-associated proteins in response to O₃ in GFAP-positive tissue indicated increased cell-to-cell physical overlap, suggesting that O₃ may modify astrocyte–microglia communication in the plaque microenvironment.

Ozone Increases Astrocyte and Microglia Colocalization in the Plaque

Microenvironment

The overlapping GFAP-positive and IBA-1-positive volume in the motor cortex periplaque space was calculated to directly test whether ozone exposure affects astrocyte–microglia cell–cell contact around plaques (Figure 2.4A and Figure 2.5A). The data demonstrated that O₃ exposure increased astrocyte and microglia colocalization in the plaque microenvironment (Figure 2.4B) but not in nonplaque regions (Figure 2.4C and 2.4D), suggesting that O₃ modifies glial cell–cell communication only near amyloid plaques. We have previously seen a O₃-induced decrease in plaque associated microglia [22], making this increased colocalization even more intriguing. To verify that this increased colocalization is not simply a result of increased GFAP in the periplaque space, we normalized the data to total GFAP (Figure 2.4B). The significant difference was retained regardless of the source of GFAP volume.

Ozone Triggers an Astrocytic Transcriptional Shift

Large-scale astrogliosis is observed in AD, and impaired clearance of A β by astrocytes is thought to be deleterious [72]. A recently identified DAA population displays a somewhat distinct transcriptional phenotype when localized around plaques; however, this transcriptomic fingerprint is also closely linked with astrocyte

subpopulations in the aged brain [73]. Very little is known about how air pollution exposure changes astrocytes, particularly the transcriptional phenotype of plaque-associated astrocytes. Thus, we used DSP and the NanoString WTA to assess the transcriptional changes in periplaque versus plaque-distant astrocytes in FA- and O₃-exposed 5xFAD mice. O₃ exposure triggered a unique transcriptional shift in periplaque astrocytes (Figure 2.6A and 2.6B). On closer examination of the differentially expressed genes in these astrocytes (Table 2.8), an accelerated DAA phenotype was present, highlighted by increased expression of *serpina3n*, a serine protease inhibitor associated with increased amyloid accumulation [73,229], *ctsb* and *ctsd*, lysosomal cysteine proteases associated with amyloid precursor protein processing [73,230], and *clqa*, a complement factor associated with astrocyte-mediated synapse elimination [231]. However of the protein targets upregulated in the O₃ group, only *csflr*, *cd9* and *ctsd* were also significantly transcriptionally upregulated with DSP analysis. Pathway analysis revealed that O₃ upregulated several functional categories of genes in periplaque astrocytes, including cell–cell communication and gap junction trafficking pathways (Figure 2.6C and Table 2.9 and 2.10). O₃ also resulted in the downregulation of genes in other critical categories in periplaque astrocytes, such as matrix metalloproteinase activation (Figure 2.6D), suggesting that extracellular matrix modifications potentially underlie the spatially defined differences. Overall, these results suggest that O₃ exposure triggers a potentially pathologically dysregulated astrocyte phenotype that occurs concomitantly with higher A β accumulation.

Peripheral HMGB1 Mediates O₃-induced Dysregulation of Astrocytes

We previously demonstrated that peripheral HMGB1 regulates the microglial response to O₃ in 5xFAD mice [22]; however, the impact on astrocytes is unknown. Here, HMGB1 mRNA levels were found to be downregulated in O₃-exposed BAL fluid (Figure 2.7A), predominantly comprising infiltrating myeloid cells consistent with prior studies in other tissues [22,232]. Thus, we hypothesized that peripheral myeloid cell HMGB1 is involved in the association between astrocytes and amyloid pathology. To test this hypothesis, we used the previously described *Hmgb1fl/fl.LysM-Cre⁺* mouse strain [22], with HMGB1 specifically deleted in only peripheral myeloid cells, including BAL fluid cells. A single 4-hour O₃ exposure (1 ppm) reduced neutrophil and lymphocyte infiltration into the BAL fluid in *Hmgb1fl/fl.LysM-Cre⁺* mice (Figure 2.7B), indicating that myeloid cell HMGB1 plays an important role in peripheral immune cell trafficking and the pulmonary immune response to O₃. Given the reduced HMGB1 mRNA in these cells in 5xFAD mice after 13 week exposure, we hypothesize that ongoing AD pathology and extended exposure length could have a differential impact on HMGB1 mRNA expression in these cells. Interestingly, *serpina3n* levels in the midbrain of *Hmgb1fl/fl.LysM-Cre⁺* mice were reduced in response to O₃ exposure (Figure 2.7C), further suggesting that peripheral myeloid cells and HMGB1 influence the expression of astrocyte genes in the lung–brain axis.

Circulating HMGB1 has previously been shown to be upregulated in 5xFAD mice in response to O₃ [22]. Thus, we treated C57 mice with 32.5 µg recombinant HMGB1 protein intravenously, as previously reported [22,233], to determine whether circulating HMGB1 can regulate the DAA phenotype. Circulating HMGB1 increased *gfap* mRNA

expression in the midbrain, and there was a trend toward an increase in *c3*, and *aqp4* mRNA expression (Figure 2.7D). Most of these DAA markers were demonstrated above to be modified by O₃ in the cortex in 5xFAD mice (Table 2.8). Overall, these data suggest that peripheral myeloid cell HMGB1 is modified by O₃ exposure and may play an important role in immune cell trafficking and modulating the astrocytic response to O₃ exposure.

Discussion

O₃ is a major component of urban air pollution and abundant at levels deleterious to human health across the US and worldwide [161]. High O₃ levels have recently been strongly associated with increased AD risk [19]. In addition, O₃ is associated with chronic obstructive pulmonary disease (COPD) and is a well-known asthma irritant [172,234], and recent studies have linked both asthma [235] and COPD [236] to increased dementia risk, further emphasizing the importance of understanding the underlying disease mechanisms. In the current study, using 5xFAD mice, we explored the mechanistic underpinnings of how an inhaled gas incapable of translocating to the brain (O₃) could impact the brain and cellular pathology in the CNS parenchyma in association with peripheral immune responses. We define peri-plaque DAAs and demonstrate the involvement of peripheral myeloid cells in their regulation to delineate an overlooked component of the lung–brain axis that potentially influences how urban air pollution promotes AD pathobiology (Figure 2.8).

In the current study, we demonstrated that GFAP astrocyte density in the cortex of 5xFAD mice increases in response to O₃ exposure (Figure 2.1A and B). The number of

plaque-associated astrocytes increased with O₃ exposure; however, the number of astrocytes surrounding each plaque did not increase. Thus, the increase in cortical astrocytes was likely due to the increase in the number of plaques in response to O₃ exposure (Figure 2.1E). Importantly, the astrocytes surrounding plaques, which are important for plaque clearance and reducing toxicity [215,216], were found to be qualitatively different after O₃ exposure (Figure 2.3, 2.4, 2.5). Periplaque astrocytes from 5xFAD mice exposed to O₃ exhibited a localization-dependent altered astrocytic proteomic profile (Figure 2.3). On closer examination, many of the proteomic changes occurring only with O₃ exposure in plaque-distant versus periplaque astrocytes involved the loss of several key proteins (Figure 2.3). Some unexpected proteins, such as MBP, were upregulated in plaque-associated astrocytes in response to O₃ exposure (Table 2.7). This finding suggests that astrocytes may take up MBP during neurite breakdown, consistent with our prior work showing that O₃ enhances dystrophic neurites in the periplaque space [22].

Importantly, the upregulation of microglia-specific proteins in astrocytes (Table 2.7) likely reflects an increase in cell–cell interactions and communication between astrocytes and microglia in the plaque microenvironment. We directly tested increased astrocyte–microglia interactions by immunohistochemistry (Figure 2.6) and demonstrated that O₃ increases astrocyte–microglia contact only in the periplaque space. Additionally, these periplaque cells differ transcriptionally from plaque-distant astrocytes, demonstrating altered cell–cell communication and gap junction trafficking pathway genes in the plaque microenvironment (Figure 2.6). It has been previously reported that microglia and astrocyte cell–cell contact may be important for amyloid clearance [237].

We hypothesize that increased astrocyte–microglia communication may signify a coordinated effort between these cell types in compensating for the O₃ exposure–induced dysregulation of protective functions in the periplaque space.

While O₃ mainly induced a loss of protein expression in periplaque astrocytes, a larger transcriptional inquiry revealed the upregulation of genes such as *serpina3n*, *c1qa*, *c1qb*, and *ctsb*, indicating that O₃ exposure shifted the astrocyte transcriptional signature toward a more enriched DAA phenotype. Among the DAA genes upregulated by O₃ only in the periplaque space, *serpina3n* is associated with increased A β deposition and could contribute to increased plaque burden [73,229]. Notably, DAA astrocytes precede plaque deposition in 5xFAD mice and accumulate over time [73]. Here, exposure to O₃ appears to accelerate the DAA phenotype in 5xFAD mice. However, while this O₃-accelerated DAA phenotype correlated with an O₃-induced increase in plaque burden in the current study, the beneficial or deleterious consequences of the O₃-modified astrocyte genes in the periplaque space remain unclear and require substantial further investigation.

The transcriptional data emphasize that O₃ exposure qualitatively changes periplaque astrocytes, revealing multiple important potential targets for future mechanistic inquiry. For example, O₃ exposure has a well-established impact on stroke and vascular pathology [150,186,187], and the astrocyte gene expression pathway analysis in the current study denotes changes in pathways involving vascular wall communication, vegfa–vegr2 communication (which occurs in vascular endothelial cells), and aquaporin communication, all of which point to O₃-induced phenotypic changes in plaque-associated astrocytes that may be linked to neurovascular dysfunction or pathology. Interestingly, gene expression changes in neurotransmitter pathways were

also altered, which is unsurprising because astrocytes are known to maintain neurotransmitter homeostasis, the disruption of which is neurotoxic. This finding supports our previous data showing that O₃ exposure augments neuritic dystrophy [22].

We next sought to better understand the mechanisms underlying these changes in the periplaque astrocyte phenotype. Peripheral immune cells traffic to the lung upon O₃ inhalation [3], and these cells and their associated circulating factors are key components of the lung–brain axis [26]. Here, we discovered that with subchronic O₃ exposure in 5xFAD mice, when the plaque load was increased and the proteomic and transcriptomic DAA phenotype was disrupted, HMGB1 gene expression was lowered in the immune (predominantly myeloid) cells that trafficked to the lung (Figure 2.7). While this decrease in gene expression does not demonstrate a direct impact on A β plaque load it implies a potential relation to be directly tested in future studies. Furthermore, Peripheral myeloid cell-specific HMGB1 deletion reduced immune cell infiltration into the lung and midbrain *serpina3n* expression (Figure 2.7), implicating the lung–brain axis in modulating the astrocytic transition to the DAA phenotype. Our data demonstrating that circulating HMGB1 upregulates DAA marker expression further indicate that peripheral HMGB1 influences the periplaque astrocyte phenotype.

Overall, our findings demonstrate that O₃ triggers a qualitative change in periplaque astrocytes, dysregulates cell–cell communication and cellular function in the plaque microenvironment, and accelerates the astrocyte transcriptomic shift toward the DAA phenotype, which is associated with an increased plaque number. These findings identify astrocytes, particularly periplaque astrocytes, as a key mechanistic component of the lung–brain axis associated with the effect of air pollution on AD pathology. Finally,

we demonstrate the important role of peripheral HMGB1 in this process, highlighting a critical need to investigate this highly complex mechanistic pathway further.

One limitation of this study is the use of the 5xFAD mouse model. While this model is popular for investigating amyloid pathology, the Alzheimer's disease phenotype is aggressive, particularly in female mice. This prevented us from assessing female mice in this study, and sex-based differences may exist. Additionally, the focus of this study was astrocytic dysregulation in the context of amyloid pathology. To fully elucidate the role of the lung–brain axis in astrocytic dysregulation in AD, its effects on tau pathology must be investigated in the future.

While O₃ is unable to directly interact with the brain parenchyma after inhalation, it is important to note that in addition to the pulmonary epithelium, O₃ also reacts with nasal epithelium potentially causing some lesions and generating cytokines among other factors which could also be an indirect pathway signaling ozone-induced CNS effects, which is a point of future study, to fully elucidate how O₃ affects brain.

This manuscript introduces a complex mechanism implicating astrocytes in the lung–brain axis that will require extensive multidisciplinary studies to fully elucidate. The following prospects for future inquiry were identified according to our results: 1) The identification and localization of the culpable immune cell cascade, tracing the first immune cell response in the periphery to the transfer of the cascade to the brain parenchyma and subsequent follow-up of chronic consequences. 2) An exploration of the CNS cellular contribution and the role of cell–cell contact, including the CNS vasculature unit and border-associated macrophages, in how O₃ communicates with the brain and impacts astrocyte and amyloid pathology. 3) Rescue studies investigating whether

peripheral circulating factors can ameliorate the O₃-augmented astrocyte and amyloid pathology. 4) Investigations into the O₃ lung-brain axis exposome and its role in this process, comparing identifiable markers of pathological peripheral immune changes, deleterious circulating factors, ongoing astrocyte disruption, and amyloid pathology in AD animal models exposed to O₃ with those in AD, asthma, and COPD patient data.

This study is the first to identify astrocytes as part of the lung–brain axis and explore how trafficking immune cells can modify astrocytes and, potentially, amyloid plaque pathology in response to air pollution. Together, these findings provide much-needed insight into the underlying mechanisms driving how exposure to high levels of air pollutants, such as O₃, increase AD risk, highlighting the need to investigate this complex mechanistic pathway further to deepen our understanding of AD etiology, identify targets for the prevention and treatment of this disease, and guide the development of policies regulating air pollution.

Figures

Figure 2.1: Ozone exposure increases astrocyte density in the cortex of 5xFAD mice.

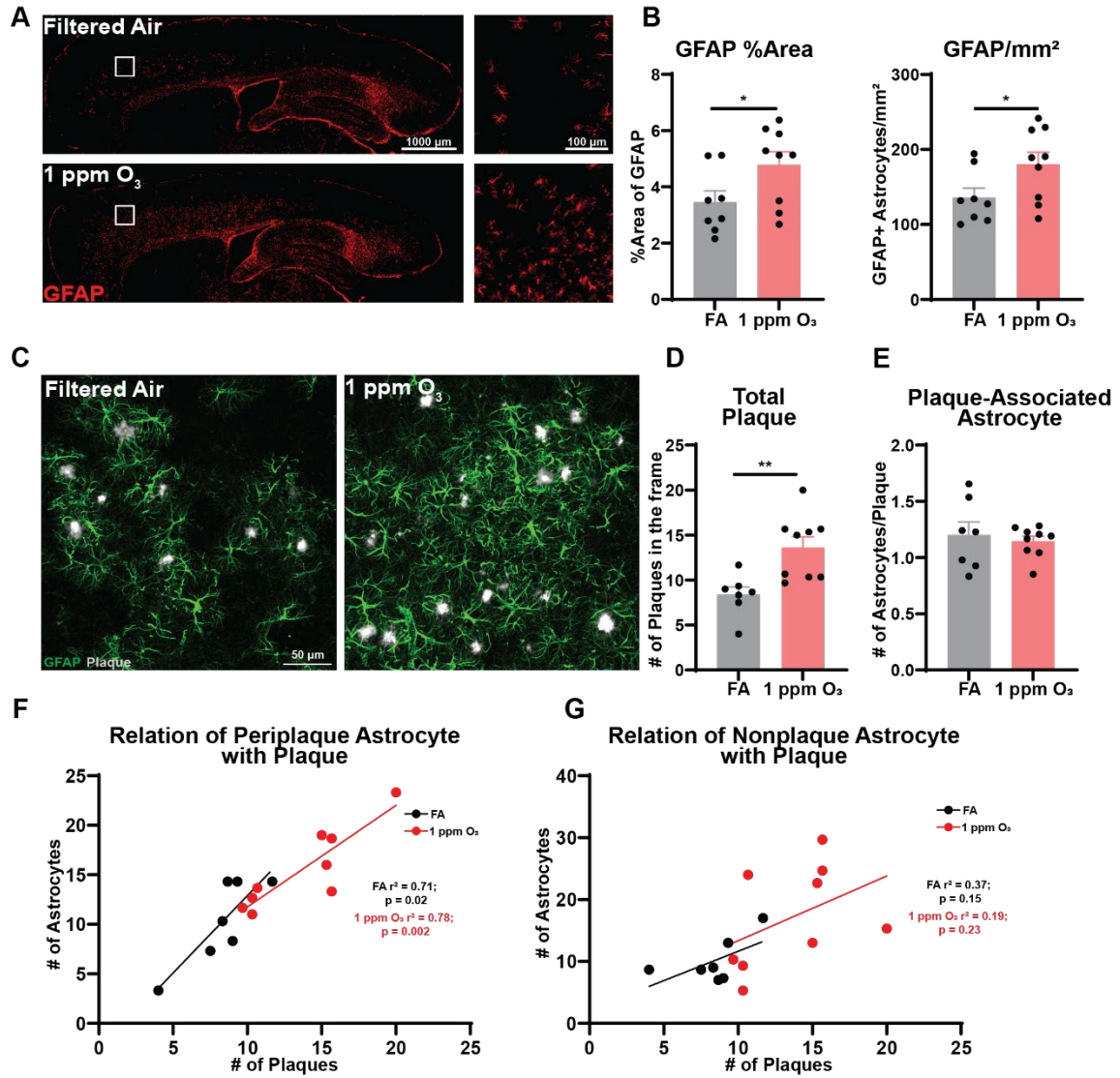


Figure 2.1: Male 5xFAD mice (10–11 weeks old) were exposed to either FA or 1.0 ppm ozone (O₃) for 3 consecutive days each week for 4 hours/day for 13 weeks. (A) Representative 10× images depicting cortical astrocyte density (GFAP, red) in FA- and O₃-exposed mice. Scale bar: 1000 μm or 100 μm. (B) Quantification of the number of GFAP-positive areas and GFAP-positive cells in the entire cortex (layers I–VI). (C) Representative maximum intensity projection images taken at 40× in the cortex, staining for plaques (Methoxy-X34, gray) and astrocytes (GFAP, green). Scale bar: 50 μm. (D) Quantification of plaque number in the 40× confocal images. (E) Quantification of plaque-associated astrocytes normalized to plaque number. Correlation of the number of plaques with the number of (F) periplaque and (G) nonplaque astrocytes in the cortex. Astrocytes were considered periplaque if their cell bodies or branches reached within the circular periplaque region of interest drawn at 50 μm diameter around the plaque center; if not, they were considered nonplaque. Data are represented as the mean ± SEM, n = 8–9 mice/exposure group. * = p <.05; Welch's t test.

Figure 2.2: Ozone exposure increases astrocyte density in the cortex in 5xFAD mice, which is associated with increased plaque number and independent of plaque localization.

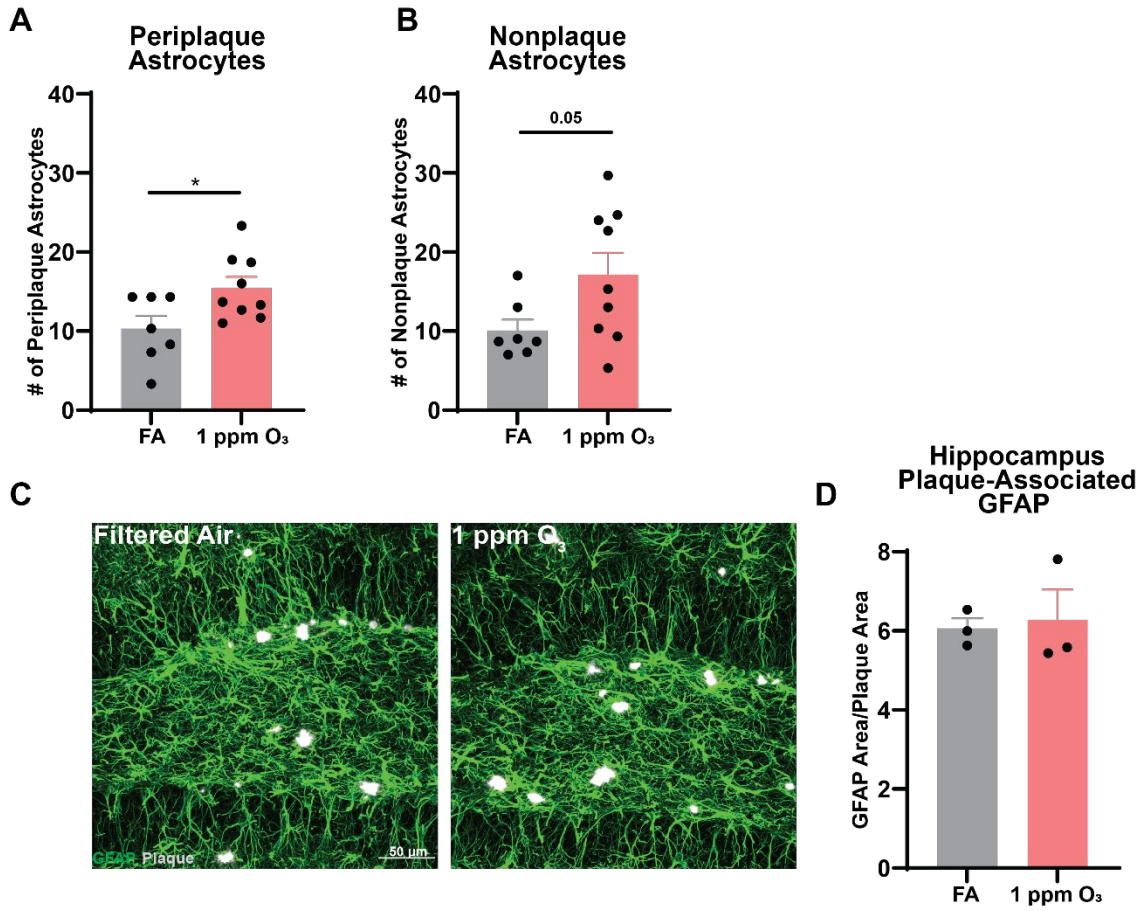


Figure 2.2: Male 5xFAD mice (10–11-week-old) were exposed to either FA or 1.0 ppm of O₃ for 3 consecutive days each week for 4h/d, for 13 weeks. Quantification of (A) periplaque and (B) non-plaque astrocytes. Astrocytes were considered periplaque if their cell bodies or branches reached within the circular periplaque region of interest drawn at 50 μm diameter around plaque center, if not they were considered non-plaque. Data are represented as mean ±SEM, n = 8-9 mice/exposure group. * = p < 0.05; Welch's t-test.

(C) Representative maximum intensity projection images taken at 40x in the hippocampus, staining for plaque (Methoxy-X34, gray) and astrocytes (GFAP, green). Scale bar, 50 μm. (D) Quantification of plaque associated astrocyte. Data are represented as mean ±SEM, n = 3 mice/exposure group. * = p < 0.05; Welch's t-test.

Figure 2.3: Ozone altered the astrocytic protein expression pattern, dependent on spatial localization with plaques.

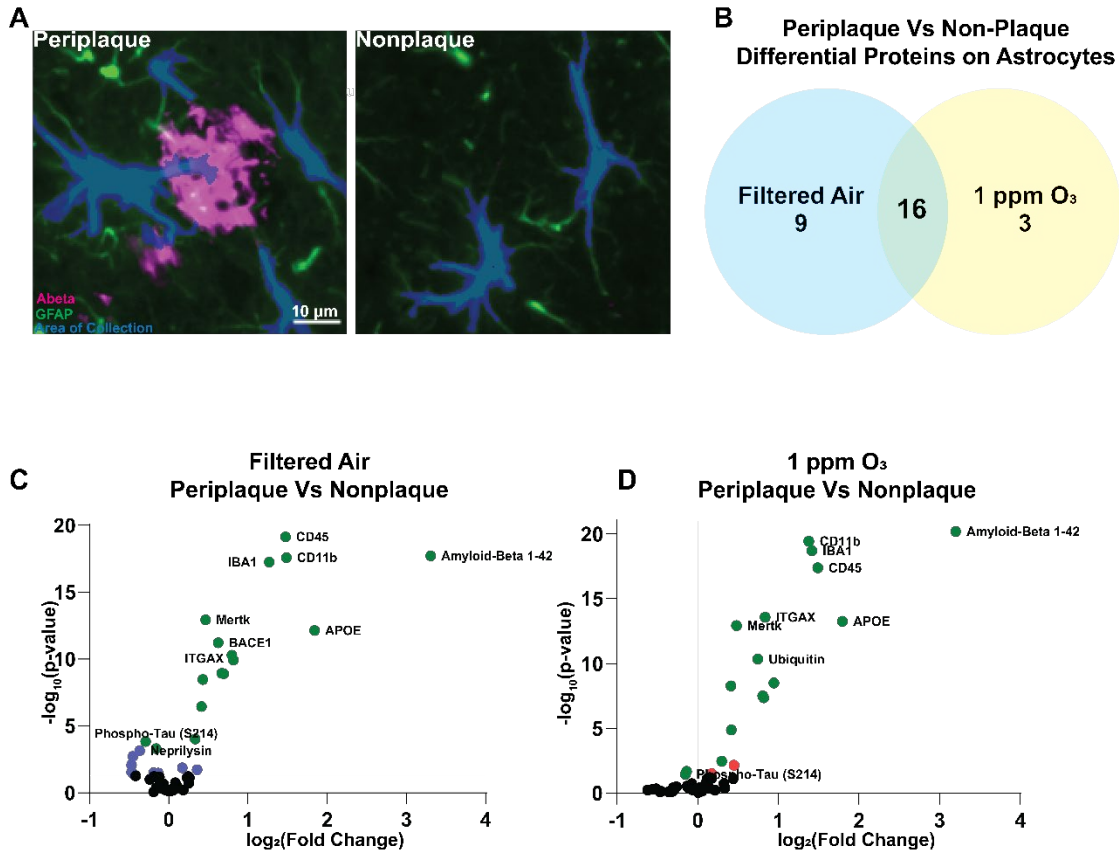


Figure 2.3: Male 5xFAD mice (10–11 weeks old) were exposed to FA or 1.0 ppm ozone (O_3) for 3 consecutive days each week for 4 hours/day for 13 weeks. (A) Representative images from the NanoString GeoMX DSP platform illustrating periplaque (left) and nonplaque astrocytes (right), as defined by plaque staining ($A\beta$, magenta), astrocyte (GFAP, green) staining, and the area from which samples were collected for analysis (blue). Scale bar: 10 μ m. (B) Venn diagram showing the number of plaque environment-induced changes in the astrocyte proteomic profile in FA and O_3 groups, indicating protein changes shared between the two groups. Volcano plots representing differentially expressed proteins on periplaque versus plaque-distant astrocytes in the (C) FA and (D) O_3 groups. n = 68–72 ROIs/region per exposure group (n = 4 mice/exposure group). p <.05.

Figure 2.4: Ozone increased astrocyte–microglia cell contacts in the plaque microenvironment.

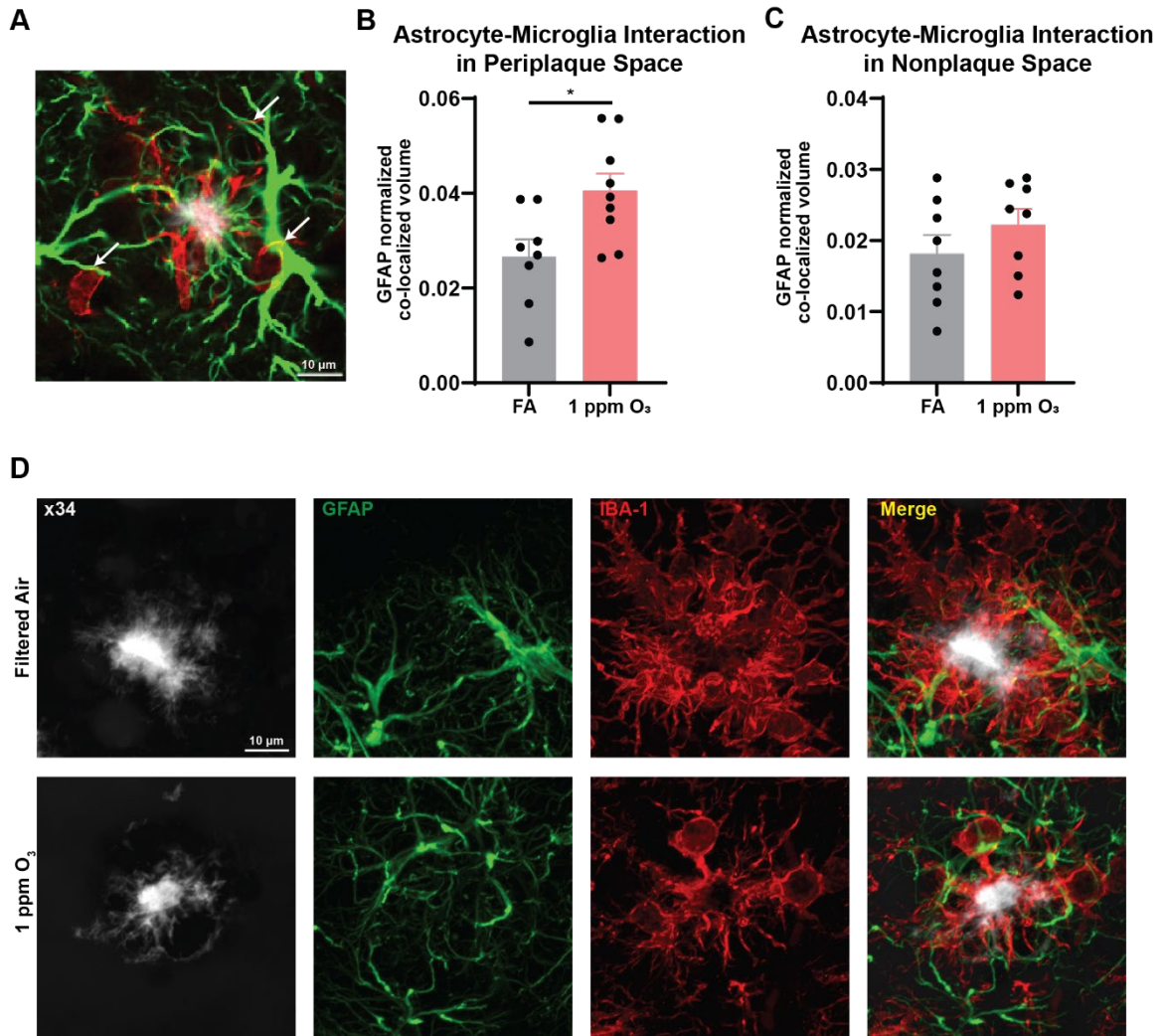


Figure 2.4. Male 5xFAD mice (10–11 weeks old) were exposed to either FA or 1.0 ppm ozone (O₃) for 3 consecutive days each week for 4 hours/day for 13 weeks. (A) Representative image showing colocalized areas (yellow) of cell–cell contact, as indicated by white arrows in a single image from a set of confocal Z-stack images taken at 40×. Scale bar: 10 μm. Quantification of astrocyte–microglia colocalization in the (B) periplaque and (C) nonplaque (right) space from confocal Z-stacks taken at 40× in the cortex. Data are represented as the mean ±SEM, n = 8–9 mice/exposure group. * = $p < .05$; Welch’s t test. (D) Representative maximum intensity images taken at 60× showing plaques (Methoxy-X34, gray), astrocytes (GFAP, green), and microglia (IBA-1, red) in the O₃ and FA groups. Scale bar: 10 μm.

Figure 2.5: Ozone increased astrocyte-microglia cell-contact in plaque microenvironment.

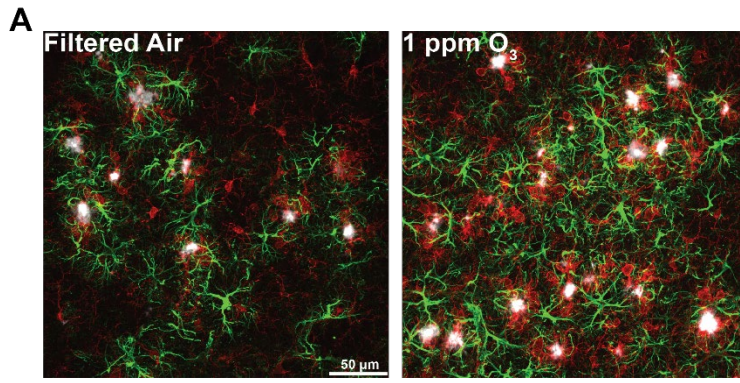


Figure 2.5. Male 5xFAD mice (10–11-week-old) were exposed to either FA or 1.0 ppm of O₃ for 3 consecutive days each week for 4h/d, for 13 weeks. (A) Representative maximum intensity projection images taken at 40x in the hippocampus, staining for plaque (Methoxy-X34, gray), astrocytes (GFAP, green) and microglia (IBA-1, red). Scale bar, 50 µm.

Figure 2.6: Ozone alters the astrocytic transcriptional profile in the plaque microenvironment.

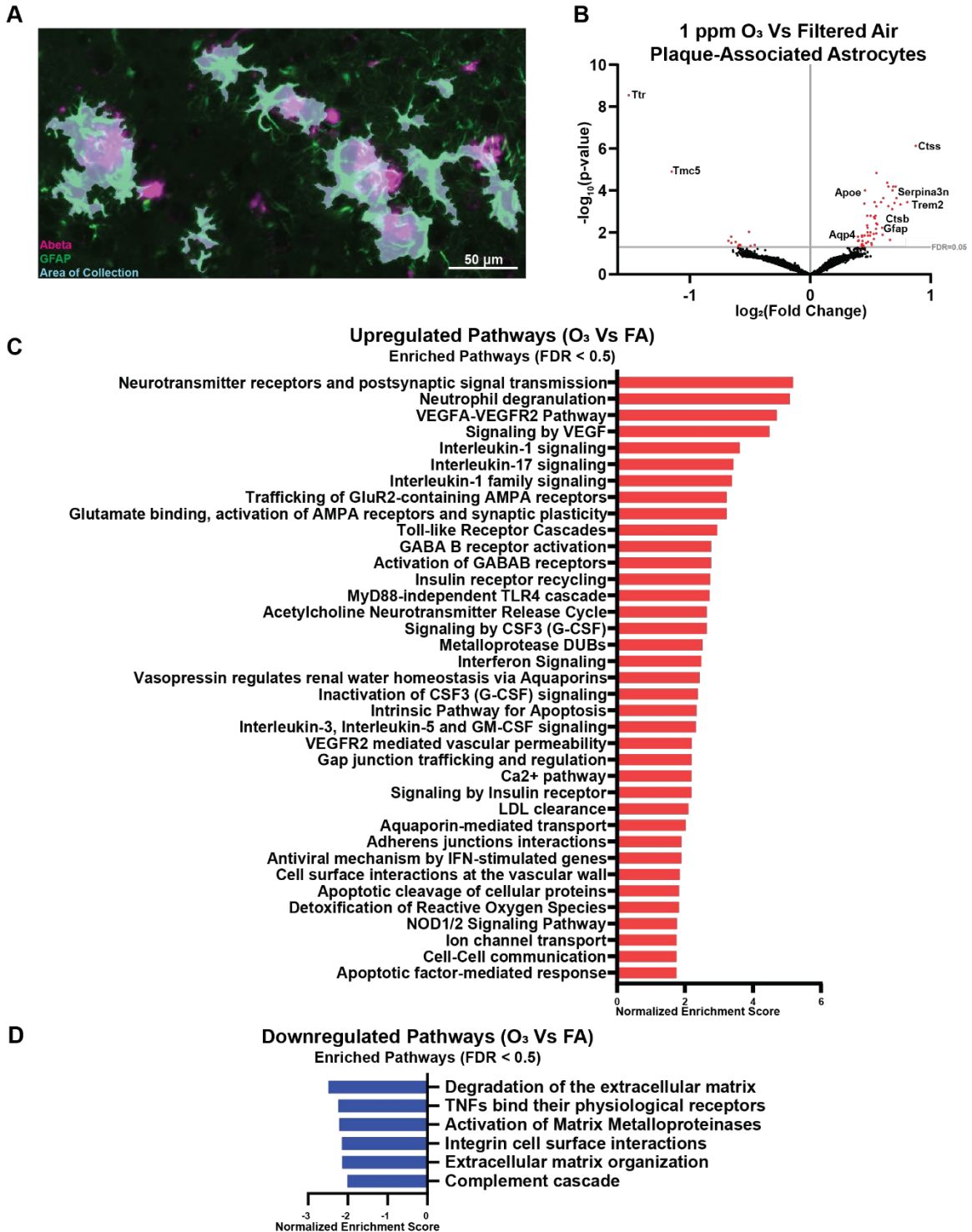


Figure 2.6. Male 5xFAD mice (10–11 weeks old) were exposed to either FA or 1.0 ppm ozone (O₃) for 3 consecutive days each week for 4 hours/day for 13 weeks. (A) Representative image showing the digital spatial profiler scan for regions of interest containing astrocytes localized in the periplaque space, as defined by plaque staining (6e10, magenta), astrocyte staining (GFAP, green), and the area from which GFAP-positive cells were collected for mRNA analysis (blue). Scale bar, 50 μm. (B) Volcano plot showing O₃-induced gene expression in plaque-associated astrocytes compared to that in the FA group. Highlighted genes represent a subset of significantly changed genes (red dots) after FDR correction (Benjamini–Hochberg, $p < .05$). Pathway analysis of O₃ vs. FA cortical astrocyte gene expression in plaque-associated astrocytes depicting significantly (C) increased and (D) decreased pathways of interest (Benjamini–Hochberg, $p < .05$. n = 96 ROIs/region per exposure group (n = 3 mice/exposure group).

Figure 2.7: Peripheral HMGB1 modulates ozone-induced astrocytic dysregulation.

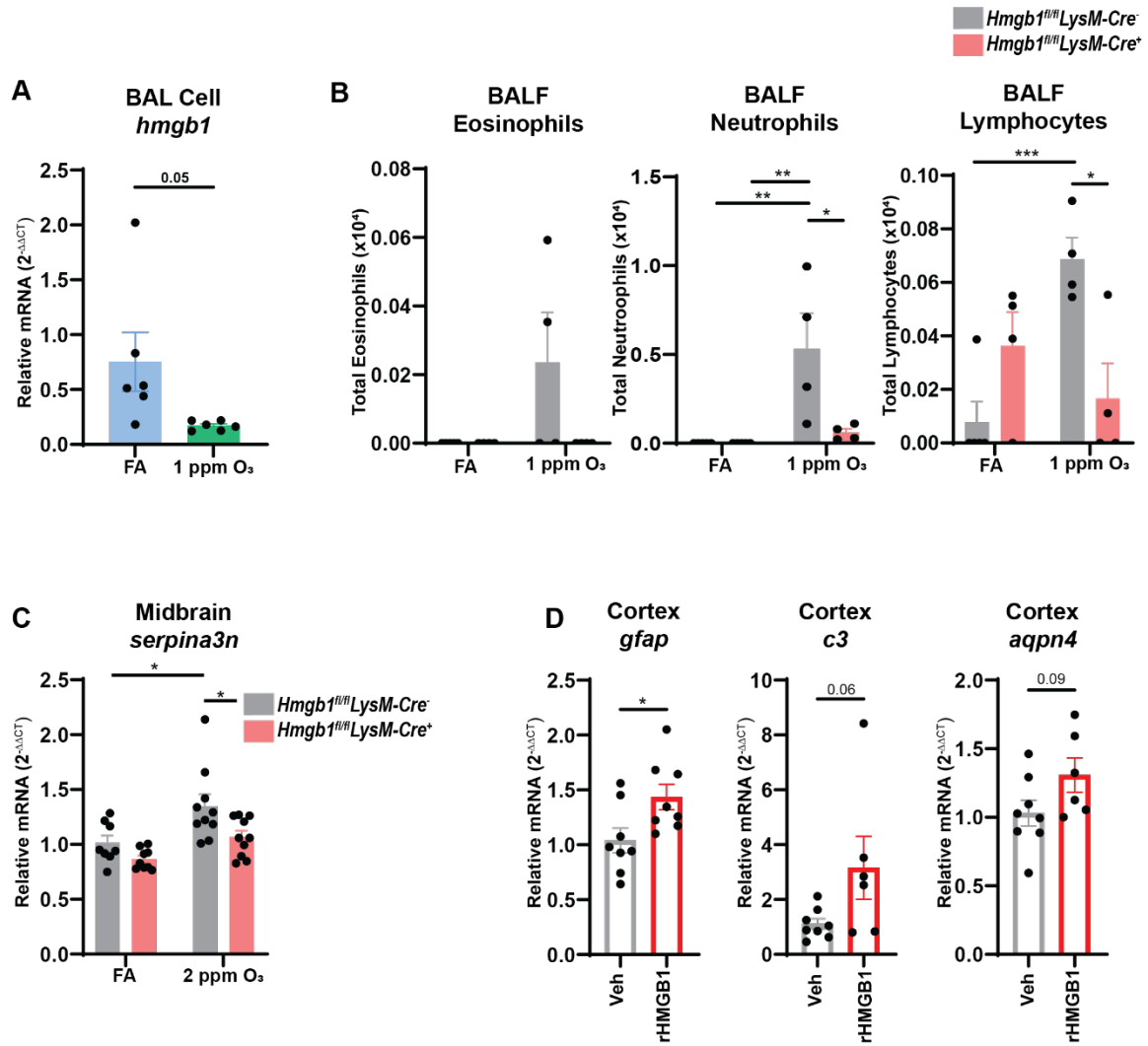


Figure 2.7: (A) Subchronic (13-week) O₃ (1 ppm) exposure reduced HMGB1 mRNA expression in the BAL cells of 5xFAD mice. Data are represented as the mean ± SEM, n = 6 mice/exposure group. Welch's t test.

(B) Hmgb1fl/fl.LysM-Cre⁺ mice have Hmgb1 genetically ablated in peripheral myeloid cells (comprising a substantial component of BAL fluid cells) but not microglia.

Hmgb1fl/fl.LysM-Cre⁻ and Hmgb1fl/fl.LysM-Cre⁺ mice were exposed to O₃ (1.0 ppm) or FA once for 4 hours. Cell counts of eosinophils, neutrophils, and lymphocytes infiltrating the BAL are shown. Data are represented as the mean ± SEM, n = 3–5 mice/group. * = p <.05, ** = p <.01, *** = p <.001; Welch's t test. (C)

Hmgb1fl/fl.LysM-Cre⁻ and Hmgb1fl/fl.LysM-Cre⁺ mice were exposed to O₃ (2.0 ppm) or FA once for 4 hours. Serpina3n mRNA levels in the midbrain after a single 2 ppm O₃ exposure are shown. Data are represented as the mean ± SEM, n = 9–10 mice/exposure group. * = p <.05, †† = p <.01 (D) Gfap, C3 and Aqp4 mRNA levels were assessed 3 hours after a tail vein injection of rHMGB1 (32.5 µg). Data are represented as the mean ± SEM, n = 6–8 mice/exposure group. * = p <.05; Welch's t test.

Figure 2.8: Plaque-associated astrocytes and peripheral myeloid cells interact in the O₃-dysregulated lung–brain axis: Implications for Alzheimer’s disease.

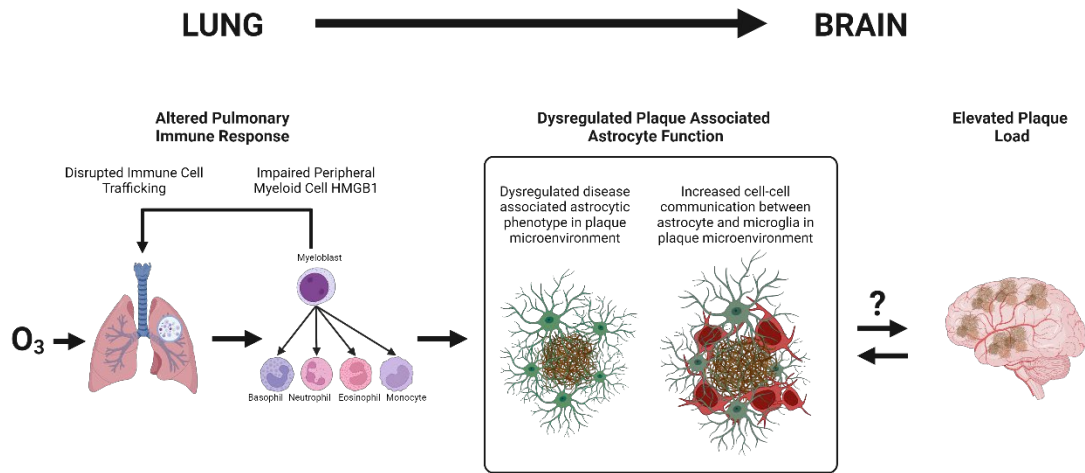


Figure 2.8: O₃, a reactive gas component of urban air pollution that cannot reach the brain, increased astrocyte density in the 5xFAD mouse cortex, concomitant with decreased bronchoalveolar lavage fluid cell (predominantly myeloid) HMGB1 expression and an exacerbated plaque burden. O₃-induced astrocyte effects (transcriptomic and proteomic) were dependent on the localization of astrocytes relative to plaques, indicating that this air pollution exposure selectively and qualitatively changes astrocytes in the plaque microenvironment, accelerates the astrocyte transcriptomic shift to a disease-associated astrocyte phenotype, and increases astrocyte contact with microglia but not plaques. Mechanistically, O₃-exposed mice with HMGB1 deleted from the peripheral myeloid cells but not microglia exhibited a perturbed pulmonary immune response to O₃ and disrupted DAA markers in the brain, indicating that peripheral myeloid cells and HMGB1 regulate the astrocyte DAA response to O₃. These findings provide much-needed insight into how urban air pollution may dysregulate the lung–brain axis, disrupt astrocytic function, and increase the amyloid burden.

Tables

Table 2.1: Antibodies and chemical stains used in specific applications.

Primary Antibodies	Secondary Antibodies	Application
Rabbit anti-GFAP (Agilent DAKO, Z0334; RRID AB_10013382)	Donkey anti-Rabbit-647 (Invitrogen A-31573; RRID AB_2536183)	GFAP-positive astrocyte number and area quantification in whole cortex and periplaque region in Figure 2.1. Astrocyte–microglia colocalization quantification in Figure 2.4.
Goat anti-IBA-1 (Novus biologicals, NB100-10280)	Donkey anti-Goat-488 (Invitrogen A11055; RRID AB_2534102)	Astrocyte–microglia colocalization quantification in Figure 2.4.
Alexa Fluor 647 conjugated mouse anti-GFAP antibody (BioLegend, 837512; RRID AB_2734611)	N/A	Periplaque and nonplaque astrocyte staining for GeoMx spatial protein profiling in Figure 2.3.
Alexa Fluor 594 conjugated mouse anti-Abeta antibody (BioLegend 803019; RRID AB_2734552)	N/A	GeoMx spatial whole transcriptome analysis of periplaque astrocytes in Figure 2.6. Plaque staining for GeoMx spatial whole transcriptome analysis of periplaque astrocytes in Figure 2.6.
Chemical stains		
Methoxy x34 (SL 1954, Millipore Sigma, St Louis, MO)	N/A	Chemical staining of dense core plaques in Figure 2.6.

Table 2.2: Primer sequences for qPCR.

Primer Name	Sequence
Aquaporin-4 (<i>Aqpn4</i>)	Forward 5'-ATTGGGAGTCACCACGGTTC-3' Reverse 5'-CGTTTGGAATCACAGCTGGC-3'
Apolipoprotein E (<i>ApoE</i>)	Forward 5'-AGATGGGGTTCTCTGGGTGG-3' Reverse 5'-TAGGCATCCTGTCAGCAATGT-3'
Complement factor 3 (<i>C3</i>)	Forward 5'-AAGCATCAACACACCCAACA-3' Reverse 5'-CTTGAGCTCCATTCGTGACA-3'
Glyceraldehyde 3-phosphate dehydrogenase (<i>Gapdh</i>)	Forward 5'-GAACATCATCCATGCATCCA-3' Reverse 5'-CCAGTGAGCTTCCCGTTCA-3'

Table 2.3: TaqMan probes.

Probe	Catalog Number
Glial fibrillar acidic protein (<i>Gfap</i>)	Mm01253033_m1
Serine (or cysteine) peptidase inhibitor, clade A, member 3N (<i>Serpina3n</i>)	Mm00776439_m1
Glyceraldehyde 3-phosphate dehydrogenase (<i>Gapdh</i>)	Mm99999915_gI
High mobility group box 1 (<i>Hmgbl</i>)	Mm04205650_gH

Table 2.4: Other reagents used in Methods.

Reagent	Application
Paraformaldehyde (PFA) (1921, Electron Microscopy Sciences)	Brain fixation
Optimal cutting temperature compound (OCT) (4583, Sakura Finetec)	Fixed brain sectioning
Hanks Balanced Saline Solution (HBSS) (21-622CV, Corning)	Broncho alveolar lavage fluid (BALF) collection
Prolong gold (P36930, Life Technologies, Eugene, OR)	Immunofluorescent staining
Tissue Protein Extraction Reagent (T-PER) (78510, ThermoScientific)	RNA extraction
Protease inhibitor (78429, Thermo Scientific)	Used in tissue homogenizing solution with T- PER at 1:100 dilution
Phosphatase inhibitor (1862495, Thermo Scientific)	Used in tissue homogenizing solution with T- PER at 1:100 dilution
TRIzol (15596018, Invitrogen)	RNA extraction
Choloroform (BP-1145-1, Fisher BioReagents)	RNA extraction
Molecular grade ethanol (BP2818-500, Fisher BioReagents)	RNA extraction
Ambion Nuclease free water (AM9932, Invitrogen)	RNA extraction
Ambion DNA-free kit (AM1906, Invitrogen)	RNA extraction
Maxima First Strand cDNA synthesis kit (K1641, Invitrogen)	RNA reverse transcription
PoweUp SYBR Green Master Mix (100029284, Thermo Fisher)	qPCR
TaqMan Fast Advnced Master Mix (4444557, Thermo Fisher)	qPCR

Table 2.5: Reagents used in GeoMx DSP.

Reagent	Application
DEPC treated water (AM9922, ThermoFisher)	Slide preparation for protein expression assay and whole transcriptomic assay
Tris buffered saline (TBS) (12498S, Cell Signaling Technologies)	Slide preparation for protein expression assay
TBS with tween 20 (TBS-T) (9997S, Cell Signaling Technologies)	Slide preparation for protein expression assay
Fluoromount-G (0100-01, SouthernBiotech)	Slide storage
Citrate buffer (AP-9003-125, Richard-Allan Scientific)	Slide preparation for protein expression assay
GeoMx Protein Slide Prep Kit (121300312, NanoString)	Slide preparation for protein expression profiling
GeoMx Neural Cell Profiling Panel (121300120, NanoString)	Slide preparation for protein expression assay
GeoMx Glial Cell Profiling Panel (121300125, NanoString)	Slide preparation for protein expression assay
GeoMx AD pathology panel (121300109, NanoString)	Slide preparation for protein expression assay
GeoMx AD pathology Extend panel (121300114, NanoString)	Slide preparation for protein expression assay
GeoMx probe R (121302135; 121302140; 121302136; 121302152, NanoString)	Collection plate preparation for readout
GeoMx Alzheimer's Morphology Kit (121300306, NanoString)	Slide preparation for protein expression assay
GeoMx Nuclear Stain Morphology Kit (121300303, NanoString)	Slide preparation for protein expression assay
GeoMx Instrument Buffer Kit (100474, NanoString)	DSP instrument run
GeoMx Hybridization Code Pack (121300401, NanoString)	Collection plate preparation for readout
GeoMx Hybridization buffer (121300401, NanoString)	Collection plate preparation for readout
Proteinase K (AM2548, Thermo Fisher)	Slide preparation for whole transcriptomic assay
Antigen Retrieval Solution (00-4956-58, Ebioscience)	Slide preparation for whole transcriptomic assay
20x SSC (S6639, Sigma-Aldrich)	Slide preparation for whole transcriptomic assay
Phosphate buffered solution (PBS) (P5368-10PAK, Sigma-Aldrich)	Slide preparation for whole transcriptomic assay
Geomx RNA Slide Prep Kit (121300313, NanoString)	Slide preparation for whole transcriptomic assay
GeoMx Whole Transcriptome Assay (121401103, NanoString)	Slide preparation for whole transcriptomic assay
100% deionized formamide (AM9342, Thermo Fisher)	Slide preparation for whole transcriptomic assay

10% Tween-20 (T0710, Teknova)	Slide preparation for whole transcriptomic assay
Agencount AMPure XP (A63880, Beckman Coulter)	NGS readout preparation
Elution buffer (T1485, Teknova)	NGS readout preparation

Table 2.6: Pathogen Exclusion List in Indiana University Mouse Colony.

Pathogen
<i>Aspiculunis tetraptera</i>
<i>Syphacia muris</i>
<i>Syphacia obvelata</i>
<i>Myocoptes</i>
<i>Radfordia/Myobia</i>
EDIM
MHV
MPV 1-5
MVM
TMEV
<i>Mycoplasma pulmonis</i>
<i>Clostridium piliforme</i>
LCMV
PVM
REO3
Sendai
Ectromelia
MAV1 (MAD)
MAV2 (MAD)
K virus
Polyoma virus
CAR baillus
<i>Clostridium difficile</i> Toxins A&B

Table 2.7: List of altered proteins in GeoMx DSP assay.

Filtered Air		
Upregulated targets	Fold Change	p-value
CD45	2.78	7E-20
CD11b	2.81	2E-18
Amyloid-Beta 1-42	9.92	3E-18
IBA1	2.41	6E-18
Mertk	1.38	1E-13
APOE	3.59	7E-13
BACE1	1.54	6E-12
ITGAX	1.74	5E-11
CD39	1.76	1E-10
Ubiquitin	1.59	1E-09
Amyloid Precursor Protein	1.62	1E-09
CD9	1.35	3E-09
S100B	1.33	3E-07
Ctsd	1.26	9E-05
Ki-67	1.13	1E-02
P2RX7	1.28	2E-02
Downregulated targets		
Phospho-Tau (S214)	-1.22	1E-04
NeuN	-1.12	5E-04
Neprilysin	-1.29	7E-04
MHC II	-1.37	2E-03
Amyloid-Beta 1-40.2	-1.38	8E-03
Phospho-Tdp-43 (S409/S410).1	-1.38	3E-02
NRGN	-1.14	3E-02
CD31	-1.09	3E-02
SPP1	-1.36	4E-02
O₃ (1PPM)		
Upregulated targets		
Amyloid-Beta 1-42	9.19	7E-21
CD11b	2.60	4E-20
IBA1	2.67	2E-19
CD45	2.81	4E-18
ITGAX	1.79	3E-14
APOE	3.47	6E-14
Mertk	1.40	1E-13
Ubiquitin	1.68	5E-11
CD39	1.93	3E-09
CD9	1.33	5E-09
BACE1	1.75	3E-08

Amyloid Precursor Protein	1.77	4E-08
S100B	1.34	1E-05
Ctsd	1.23	3E-03
Myelin basic protein	1.37	7E-03
CSF1R	1.13	3E-02
Clec7a	1.13	4E-02
<hr/>		
Downregulated targets		
<hr/>		
NeuN	-1.10	2E-02
Phospho-Tau (S214)	-1.11	4E-02
<hr/>		

Table 2.8: List of Altered targets from GeoMx Whole Transcriptomic Assay.

Upregulated targets	Fold Change	Adjusted p-value
Ctss	1.84	7E-07
Sparc	1.46	1E-05
Fcgr3	1.56	4E-05
Cx3cr1	1.57	7E-05
Mpeg1	1.61	7E-05
Serpina3n	1.64	7E-05
Laptn5	1.61	1E-04
Apoe	1.37	1E-04
Csf1r	1.52	2E-04
C1qb	1.64	2E-04
Itgb5	1.45	4E-04
Tyrobp	1.75	4E-04
Lag3	1.50	4E-04
C1qa	1.62	4E-04
Cd63	1.36	4E-04
Trem2	1.68	5E-04
Egr3	1.57	6E-04
Ctsb	1.46	6E-04
C1qc	1.60	8E-04
Ctsl	1.39	2E-03
Ly86	1.46	2E-03
Hexa	1.42	2E-03
Man2b1	1.44	2E-03
Ctsz	1.45	2E-03
Selplg	1.46	4E-03
Ccl3	1.47	4E-03
Cotl1	1.39	5E-03
Hexb	1.51	6E-03
Cd9	1.39	6E-03
Fcgr2b	1.46	7E-03
Gfap	1.39	1E-02
Csf3r	1.41	1E-02
Grn	1.46	1E-02
Itgam	1.44	1E-02
Ctsd	1.52	1E-02
Tmem176b	1.35	1E-02
Fscn1	1.37	1E-02
Cd68	1.41	1E-02
Fcrls	1.39	1E-02
Aqp4	1.32	2E-02

Vsir	1.35	2E-02
Cd52	1.44	2E-02
Cst7	1.58	2E-02
Npc2	1.32	2E-02
Ly6e	1.35	3E-02
Ctsa	1.32	3E-02
B2m	1.39	3E-02
Etv5	1.38	3E-02
Enc1	1.42	3E-02
P2ry12	1.35	4E-02
Itgb2	1.42	4E-02
Btbd3	1.35	4E-02
Zfp3612	1.34	4E-02
Ctsh	1.36	4E-02
Lgals3bp	1.34	5E-02
Cck	1.35	5E-02
<hr/> Downregulated targets		
Ttr	-2.84	3E-09
Tmc5	-2.22	1E-05
Sgk1	-1.42	9E-03
Ogn	-1.58	2E-02
Prr32	-1.60	2E-02
Mia	-1.54	3E-02
Olf1388	-1.57	3E-02
Sult6b1	-1.50	4E-02
Pltp	-1.38	4E-02
Fmo2	-1.49	4E-02
Plat	-1.41	4E-02
Olf301	-1.51	4E-02

Table 2.9: Selected Upregulated Pathways from GeoMx Whole Transcriptomic Assay.

Reactome pathway ID	Pathway description	Normalized enrichment score	Adjusted pValue	Targets
R-MMU-112314	Neurotransmitter receptors and postsynaptic signal transmission	5E+00	9.5E-04	Gng11,Gabbr3,Chrna9,Ap2s1,Adecy3,Adecy4,Ap2b1,Adecy1,Arhgef9,Gla2,Grip1,Chrn4,Chrn3,Camk2d,Camkk2,Chrna1,Chrna4,Chrna6,Chrna7,Chrn2,Chrn2,Chrnd,Chrne,Actn2,Adecy6,Adecy7,Adecy8,Adecy9,Ap2a1,Ap2a2,Ap2m1,Glra3,Calm1,Calm2,Calm3,Camk2a,Camk2b,Camk2g,Grik4,Chrna5,Chrna3,Gabra5,Chrna2,Lrrc7,Gabbr2,Grin3a,Dlg1,Dlg4,Gnat3,Grip2,Gabra1,Gabra2,Gabra3,Gabra4,Gabra6,Gabbr1,Gabbr2,Gabbr3,Gabrg2,Gabrg3,Gabbr1,Gabbr2,Glra1,Glrb,Gnai1,Gnai2,Gnai3,Gnal,Gnb1,Gnb2,Gnb3,Gnb4,Gnb5,Gngt1,Gng10,Gng2,Gng3,Gng4,Gng5,Gng8,Gngt2,Gria1,Gria4,Grik3,Grik5,Grin1,Grin2a,Grin2b,Grin2c,Grin2d,Htr3a,Kcnj10,Kcnj12,Kcnj15,Kcnj16,Kcnj2,Kcnj3,Kcnj5,Kcnj6,Kcnj9,Nefl,Nsf,Prkaca,Prkacb,Prkca,Prkcb,Prkcg,Plcb1,Plcb2,Plcb3,Prkar1a,Prkar1b,Prkar2b,Camk1,Ncald,Dlg3,Gria3,Gabbr1,Tspan7,Camkk1,Htr3b,Gabrq,Adecy5,Gng13
R-MMU-6798695	Neutrophil degranulation	5E+00	1.3E-03	Flg2,Defa34,Defa40,Defa41,Serp1b1a,Psm6,Lamtor1,Serp1b3d,Ormdl3,Pgm2,Actr2,Pycard,Fuca2,Dsn1,Psm12,Magt1,Cmtm6,Bpi,Snap29,Agpat2,Plac8,Aldh3b1,Tmem179b,Arpe5,Ilf2,Slc15a4,2310033P09Rik,1600012H06Rik,Npc2,Cxcl3,Pdap1,Ndufc2,Rab14,Clec12a,Dera,Slc4a2,Arl8a,Mgam,Cd177,Oscar,Lilra5,Psm11,Ubr4,Gsdmd,Mcemp1,Siglec7,Dnase111,Bst2,Cdk13,Tmbim1,Plekhoe2,Tmem30a,Cpne1,Mettl7a1,Psm1,Copb1,Unc13d,Atp6ap2,Qpct,Cpne3,Arhgap45,AY761185,Qsox1,Acly,Vps351,H2-M10.2,Fuca1,Stk11ip,Cd59b,Ppia,Apeh,Abca13,Dync111,Acaa1b,H2-M10.6,Serp1b12,Chit1,Cand1,Ist1,Cot1,Rap2c,Pgm1,Cda,Dynl1a,Prep,Txndc5,Nfasc,Ms4a3,Sting1,Vcp,Creg1,Ano6,Nckap1,Glipr1,Rab31,Atp6v1d,Rap2b,Nfam1,Hvcn1,Armc8,Atg7,Kcmf1,Serpina3f,Cd300c2,Scamp1,Chrn4,Olr1,Gns,Svip,Cant1,Atad3a,Mmp25,Tbcd10c,H2-M5,Atp11b,Erp44,Mlec,Commd9,Faf2,Mospd2,Dsp,Cyb5r3,Adam10,Adam8,Cfd,Aga,Rap1a,Ahsg,Aldoa,Aldoc,Alox5,Gusb,Ampd3,Prdx6,Ap1m1,Ap2a2,Pygb,Apaf1,Pygl,Aprr,Arg1,Rhoa,Manba,Arsb,Arsa,Asah1,Rab27a,Atp6v0a1,Atp8a1,Atp6v0c,B2m,Agl,Glb1,Bst1,Tmem63a,Commd3,H2-Q6,Atp8b4,C3,C3ar1,C5ar1,Cab39,Anxa2,Cap1,Capn1,Cat,H2-M10.3,Cct2,Cct8,Cd14,Cd36,Cd44,Cd53,Cd63,Cd68,Gm8909,Chil1,Cxcr2,Camp,Cnn2,Mvp,Lrrc7,Csnk2b,Dnajc5,Cst3,Cstb,Ctsb,Ctsc,Ctsd,Ctsg,Ctsh,Ctss,Cyba,Cybb,Dbn1,Ddost,Ddx3x,Dege1,Dgat1,Crispld2,Diaph1,Dync1h1,Dsc1,Dsg1a,Ear1,Eef2,Stom,Epx,Fcer1g,Fcgr2b,Fcna,Fcnb,Fgl2,Fgr,Folr2,Fpr2,Fpr1,Frk,Fth1,Xrcc6,Lpcat1,Gaa,Gdi2,Ggh,B4galt1,Gm2a,Lilrb4b,Gpi1,Grn,Cxcl1,Gstp1,H2-K1,H2-M10.1,H2-M2,H2-M3,H2-M9,H2-Q1,H2-Q10,H2-T23,H2-T24,Ptpn6,Hexb,Calm4,Hmgb1,Ghdc,Hmox2,Gpr84,Hk3,Hp,Hpse,Hspa8,Nhlrc3,Hsp90ab1,Hsp90aa1,Tarm1,Idh1,Igf2r,Kpnb1,Frmpd3,Itgav,Itgax,Itgb2,Cd47,Trappc1,Jup,Kcnab2,Fabp5,Krt1,Lamp1,Lamp2,Anpep,Lcn2,Rab44,Lta4h,Ltf,Alad,Cd93,Lyz2,Man2b1,Mif,Mme,Mmp8,Mmp9,Psm7,Clec4d,Mpo,Siglece,Lamtor2,Elane,Atp11a,Neu1,Nfkb1,Nme2,Galns,Slc11a1,Dpp7,Orm1,Orm2,P2rx1,Pafah1b2,Padi2,Pecam1,Cfp,Pfkl,Pgam1,Pigr,Pkm,Prkcd,Pkp1,Plau,Plaur,Pa2g4,Rap1b,Pnp,Ctsa,Prp2,Prtn3,Psap,Psma2,Psm1b1,Psmb7,Psmc2,Psmc3,Ptafr,Sirpa,Ptprb,Ptprc,Ptprj,Ptprn2,A1bg,Ptx3,Rab10,Rab18,Rab24,Rab3a,Rab3d,Rab4b,Rab5b,Rab5c,Rab6a,Rab7,Hgsnat,Rac1,Pdxk,St

				bd1,Ckap4,Cep290,Tspan14,Arhgap9,Nit2,Rock1,Lair1,S100a11,S100a8,S100a9,Serpib3a,Cxcl2,Sell,Ostf1,Cyfp1,Slc2a3,Pgrmc1,Slpi,Sdcbp,Prdx4,Snapt25,Snapt23,Iqgap2,Cd300a,Serpina3g,Serpib6a,Tmc6,Srp14,Serpib3c,Ifi211,Stk10,Surf4,Syng1,Gm5150,Prg3,Rnase2b,Tollip,Psmd2,Adgrg3,Tnfaip6,Tnfrsf1b,Pglyrp1,Tom1,Psmd3,Ttr,Tubb5,Tyrobp,Vamp8,Vcl,Vnn1,Xrcc5,Ypel5,Bri3,Hebp2,Ppie,Rhog,Acpp,Actr10,Dynll1,Slc2a5,Clec5a,Mgst1,Clec4n,Defa17,Rhof,Impdh1,Impdh2,Lamtor3,Psmd13,Tlr2,Retn,Pbbp,Golga7,Rab9b,Rab37,Huwe1,Psmd14,Adgre5,Ceacam1,Mapk1,Mapk14,Psma5,Slc27a2,Ncstn,Vat1,Naprt,Tcigr1,Dok3,Gyg,Cpped1,H2-M10.4,H2-M1,H2-M10.5,Ear6,Enpp4,Ear10,Rnase2a,Trpm2,Dock2,Iqgap1,Hspa1a,Ifi205,Gm1127,Actr1b,Rnaset2a,Dnajc3,Cxcr1,Slco4c1,Vapa,Gm9733,Tubb4b,Gsn,Gmfg,Gca,Ctsz,Ptges2,Mndal
R-MMU-4420097	VEGFA-VEGFR2 Pathway	5E+00	9.5E-04	Shb,Abi2,Dock1,Brk1,Mapkapk3,Nckap11,Pik3cb,Elmo2,Elmo1,Baiap2,Them4,Prr5,Abi1,Cyfp2,Actb,Actg1,Akt1,Act2,Rhoa,Calm1,Calm2,Calm3,Ctnna1,Ctnnb1,Ctnnd1,Cav1,Cdc42,Cdh5,Bcar1,Crk,Cyba,Cybb,Rictor,Wasf2,Ptk2,Fyn,Hras,Hspb1,Hsp90aa1,Itgav,Itgb3,Jup,Wasf3,Kdr,Kras,Mapkapk2,Ncf1,Ncf2,Ncf4,Nck1,Nck2,Nckap1,Nos3,Wasf1,Pak3,Pdpk1,Pik3ca,Pik3r1,Pik3r2,Prkaca,Prkacb,Prkca,Prkcb,Prkcd,Prkcz,Pleg1,Mapk11,Ptk2b,Pxn,Rac1,Shc2,Rock1,Rock2,Cyfp1,Sphk1,Src,Rasa1,Vav1,Vav2,Vegfa,Akt3,Mlst8,Mtor,Vav3,Axl,Mapk13,Mapk14,Sh2d2a,Pak2,Mapk12,Mapkap1,Trib3
R-MMU-194138	Signaling by VEGF	4E+00	9.5E-04	Shb,Abi2,Dock1,Brk1,Mapkapk3,Nckap11,Pik3cb,Elmo2,Elmo1,Baiap2,Them4,Prr5,Abi1,Cyfp2,Actb,Actg1,Akt1,Act2,Rhoa,Calm1,Calm2,Calm3,Ctnna1,Ctnnb1,Ctnnd1,Cav1,Cdc42,Cdh5,Bcar1,Crk,Cyba,Cybb,Rictor,Wasf2,Ptk2,Vegfd,Flt1,Flt4,Fyn,Hras,Hspb1,Hsp90aa1,Itgav,Itgb3,Jup,Wasf3,Kdr,Kras,Mapkapk2,Ncf1,Ncf2,Ncf4,Nck1,Nck2,Nckap1,Nos3,Nrp1,Nrp2,Wasf1,Pak3,Pdpk1,Pgf,Pik3ca,Pik3r1,Pik3r2,Prkaca,Prkacb,Prkca,Prkcb,Prkcd,Prkcz,Pleg1,Mapk11,Ptk2b,Pxn,Rac1,Shc2,Rock1,Rock2,Cyfp1,Sphk1,Src,Rasa1,Vav1,Vav2,Vegfa,Vegfb,Vegfc,Akt3,Mlst8,Mtor,Vav3,Axl,Mapk13,Mapk14,Sh2d2a,Pak2,Mapk12,Mapkap1,Trib3
R-MMU-9020702	Interleukin-1 signaling	4E+00	9.5E-04	Psmd6,Tab1,Ube2v1,Tab3,Psmd12,Psmd5,Psmc6,Psmd9,Peli1,Tnip2,Tab2,Psmd11,Nkiras1,Irak4,Psmd1,Psme4,Fbxw11,Nkiras2,Psma8,Psmb11,Irak3,Nod1,Irak2,Peli3,Ager,App,Rps27a,Hmgb1,Ikbkb,Ikbkg,Ill1a,Ill1b,Ill1r1,Ill1r2,Irak1,Ill1rap,Ill1rn,Psmb9,Psmb8,Psmd7,Myd88,Nfkb1,Nfkb2,Nfkbia,Nfkbib,Sqstm1,Psma2,Psma3,Psmb1,Psmb10,Psmb4,Psmb5,Psmb6,Psmb7,Psmc1,Psmc2,Psmc3,Psmc5,Psmd4,Psmc1,Psmc2,Psmc3,Rela,S100b,Psmd10,Skp1,Tollip,Psmd2,Traf6,Psmd3,Uba52,Ubb,Rbx1,Psmc4,Psmd13,Psmd8,Psmd14,Map2k6,Map3k3,Map3k7,Map3k8,Psma1,Psma4,Psma5,Psma6,Psma7,Psmb2,Psmb3,Cull1,Ube2n,Peli2,Ripk2,Psmf1
R-MMU-448424	Interleukin-17 signaling	3E+00	9.5E-04	Tab1,Ube2v1,Tab3,Tnip2,Dusp6,Tab2,Vrk3,Mapkapk3,Fbxw11,Dusp7,Dusp3,Rps6ka5,Ppp2r1b,Nod1,Irak2,Atf1,Atf2,Rps27a,Creb1,Fos,Ikbkb,Ikbkg,Irak1,Jun,Mapkapk2,Nfkb1,Ppp2r1a,Ppp2ca,Ppp2cb,Mapk11,Skp1,Traf6,Uba52,Ubb,Mapk7,Dusp4,Map2k3,Map2k4,Map2k6,Map2k7,Map3k7,Map3k8,Mapk1,Mapk10,Mapk14,Mapk3,Mapk8,Mapk9,Cul1,Ube2n,Ripk2
R-MMU-446652	Interleukin-1 family signaling	3E+00	9.5E-04	Psmd6,Tab1,Ube2v1,Tab3,Psmd12,Psmd5,Psmc6,Psmd9,Peli1,Tnip2,Tab2,Psmd11,Gsdmd,Ill36b,Nkiras1,Irak4,Psmd1,Psme4,Fbxw11,Nkiras2,Psma8,Psmb11,Irak3,Ill1r2,Nod1,Irak2,Peli3,Ill33,Ager,App,Casp1,Rps27a,Ctsg,Hmgb1,Ikbkb,Ikbkg,Ill1a,Ill1b,Ill1r1,Ill1r2,Irak1,Ill1rap,Ill1rn,Psmb9,Psmb8,Ill1r1,Psmd7,Myd88,Nfkb1,Nfkb2,Nfkbia,Nfkbib,Sqstm1,Ill1f10,Psma2,Psma3,Psmb1,Psmb10,Psmb4,

				Psmb5,Psmb6,Psmb7,Psmc1,Psmc2,Psmc3,Psmc5,Psmc4,Psmc1,Psmc2,Psmc3,Rela,S100b,Psmc10,Stat3,Skp1,Ii36a,Ii36m,Tollip,Psmc2,Traf6,Psmc3,Uba52,Ubb,Rbx1,Tbk1,Psmc4,Psmc13,Psmc8,Psmc14,Map2k6,Map3k3,Map3k7,Map3k8,Mapk8,Psmc1,Psmc4,Psmc5,Psmc6,Psmc7,Psmc2,Psmc3,Cul1,Ube2n,Peli2,Ripk2,Psmf1
R-MMU-399721	Glutamate binding, activation of AMPA receptors and synaptic plasticity	3E+00	9.5E-04	Ap2s1,Ap2b1,Grip1,Ap2a1,Ap2a2,Ap2m1,Grip2,Gria1,Gria4,Nsf,Prkca,Prkcb,Prkcg,Gria3,Tspan7
R-MMU-416993	Trafficking of GluR2-containing AMPA receptors	3E+00	9.5E-04	Ap2s1,Ap2b1,Grip1,Ap2a1,Ap2a2,Ap2m1,Grip2,Gria1,Gria4,Nsf,Prkca,Prkcb,Prkcg,Gria3,Tspan7
R-MMU-168898	Toll-like Receptor Cascades	3E+00	9.5E-04	Ube2d3,Tab1,Ube2v1,Tab3,Fgg,Peli1,Tnip2,Bpi,Dusp6,Tab2,Vrk3,Gsdmd,Nkiras1,Mapkapk3,Fbxw11,Plcg2,Dnm3,Dusp7,Nkiras2,Cnpy3,Dusp3,Tlr7,Tlr8,Rps6ka5,Ppp2r1b,Ticam1,Sarm1,Apob,Nod1,Pik3r4,Irak2,Peli3,Ager,Birc3,Birc2,App,Fgb,Atf1,Atf2,Casp8,Cd14,Cd36,Rbsn,Rps27a,Creb1,Ctsb,Ctsk,Ctsl,Ctss,Dnm1,Dnm2,Fadd,Fga,Fos,Hmgb1,Ikbbk,Ikkg,Irak1,Tlr9,Itgb2,Jun,Lbp,Cd180,Ly86,Ly96,Mapkapk2,4930486L24Rik,Nfkb1,Nfkb2,Nfkbia,Nfkbib,Tirap,Ppp2r1a,Ppp2ca,Ppp2cb,Mapk11,Lgmn,Ptpn11,Ube2d1,Eea1,Rela,Ripk1,S100a1,S100a8,S100a9,S100b,Sftpd,Tank,Irf7,Irf3,Skp1,Unc93b1,Tlr1,Tlr4,Tlr6,Gsdme,Hsp90b1,Traf3,Traf6,Uba52,Ubb,Tbk1,Ikbe,Ripk3,Ube2d2a,Mapk7,Tlr2,Dusp4,Map2k3,Map2k4,Map2k6,Map2k7,Map3k7,Map3k8,Mapk1,Mapk10,Mapk14,Mapk3,Mapk8,Mapk9,Ecsit,Cul1,Ube2n,Peli2,Ripk2
R-MMU-991365	Activation of GABAB receptors	3E+00	9.5E-04	Gng11,Adcy3,Adcy4,Adcy1,Adcy6,Adcy7,Adcy8,Adcy9,Gabbr2,Gnat3,Gnai1,Gnai2,Gnai3,Gnal,Gnb1,Gnb2,Gnb3,Gnb4,Gnb5,Gngt1,Gng10,Gng2,Gng3,Gng4,Gng5,Gng8,Gngt2,Kcnj10,Kcnj12,Kcnj15,Kcnj16,Kcnj2,Kcnj3,Kcnj5,Kcnj6,Kcnj9,Gabbr1,Adcy5,Gng13
R-MMU-977444	GABA B receptor activation	3E+00	9.5E-04	Gng11,Adcy3,Adcy4,Adcy1,Adcy6,Adcy7,Adcy8,Adcy9,Gabbr2,Gnat3,Gnai1,Gnai2,Gnai3,Gnal,Gnb1,Gnb2,Gnb3,Gnb4,Gnb5,Gngt1,Gng10,Gng2,Gng3,Gng4,Gng5,Gng8,Gngt2,Kcnj10,Kcnj12,Kcnj15,Kcnj16,Kcnj2,Kcnj3,Kcnj5,Kcnj6,Kcnj9,Gabbr1,Adcy5,Gng13
R-MMU-77387	Insulin receptor recycling	3E+00	9.5E-04	Atp6v1f,Atp6v1g2,Atp6v1g1,Atp6v1c1,Atp6v1c2,Atp6v1d,Atp6v1e2,Atp6v0a4,Atp6v1h,Atp6v1g3,Atp6v0e2,Atp6v1a,Atp6v1b2,Atp6v0d1,Atp6v1e1,Atp6v0e,Atp6v0a1,Atp6v0c,Atp6v1b1,Atp6v0d2,Atp6v0b,Ins2,Insr,Atp6ap1,Atp6v0a2,Tcirg1
R-MMU-166166	MyD88-independent TLR4 cascade	3E+00	1.3E-03	Ube2d3,Tab1,Ube2v1,Tab3,Tnip2,Dusp6,Tab2,Vrk3,Nkiras1,Mapkapk3,Fbxw11,Dusp7,Nkiras2,Dusp3,Rps6ka5,Ppp2r1b,Ticam1,Sarm1,Nod1,Irak2,Ager,Birc3,Birc2,App,Atf1,Atf2,Casp8,Cd14,Rps27a,Creb1,Fadd,Fos,Hmgb1,Ikbbk,Ikkg,Irak1,Jun,Ly96,Mapkapk2,Nfkb1,Nfkb2,Nfkbia,Nfkbib,Ppp2r1a,Ppp2ca,Ppp2cb,Mapk11,Ptpn11,Ube2d1,Rela,Ripk1,S100b,Tank,Irf7,Irf3,Skp1,Tlr4,Traf3,Traf6,Uba52,Ubb,Tbk1,Ikbe,Ripk3,Ube2d2a,Mapk7,Dusp4,Map2k3,Map2k4,Map2k6,Map2k7,Map3k7,Map3k8,Mapk1,Mapk10,Mapk14,Mapk3,Mapk8,Mapk9,Cul1,Ube2n,Ripk2

R-MMU-264642	Acetylcholine Neurotransmitter Release Cycle	3E+00	9.5E-04	Ppfia2,Ppfia4,Ppfia1,Tspoap1,Ppfia3,Cplx1,Rims1,Rab3a, Snap25,Stx1a,Stxbp1,Syt1,Unc13b,Vamp2,Slc5a7
R-MMU-9674555	Signaling by CSF3 (G-CSF)	3E+00	9.5E-04	Ube2d3,Elob,Eloc,Cul5,Socs3,Socs1,Rps27a,Csf3,Csf3r, Grb2,Hck,Jak2,Kras,Lyn,Ptpn11,Ube2d1,Rnf7,Shc1,Syk, Tyk2,Uba52,Ubb,Ube2d2a
R-MMU-5689901	Metalloprotease DUBs	3E+00	9.5E-04	Ep300,Babam1,H2aj,Stampb,Abraxas1,Babam2,Abraxas2, Stampb1,Rps27a,Brec3,H2ac18,Kat2b,Uimc1,Nlrp3,St am,Uba52,Ubb,H2aw,H2ac10,Mysm1,Psm14,H2ac21
R-MMU-913531	Interferon Signaling	2E+00	9.5E-04	Ddx58,Ifna13,Eif4e3,Eif4g3,Oasl1,Uba7,Camk2d,Eif4g1, Camk2a,Camk2b,Camk2g,Socs3,Socs1,Ifna12,Eif4a1,Eif4a2,Eif4e,Eif4g2,Ifit1bl2,Ptpn6,Pde12,Ifna1,Ifna4,Ifnar1, Ifnar2,Ifnb1,Ifng,Ifngr1,Ifngr2,Irf9,Jak2,Mx2,Nedd4,Prkc d,Plcg1,Ppm1b,Eif2ak2,Ptpn1,Ptpn11,Ptpn2,Trim25,Irf3, Tyk2,Ube2e1,Sumo1,Pias1,Arih1,Rnasel,Abce1,Ube2l6, Usp18,Flnb,Mapk3,Eif4e2,Ube2n,Eif4a3,Isg15
R-MMU-432040	Vasopressin regulates renal water homeostasis via Aquaporins	2E+00	1.5E-03	Gng11,Rab11fip2,Aqp1,Aqp2,Aqp3,Aqp4,Avp,Avpr2,Gn as,Gnb1,Gnb2,Gnb3,Gnb4,Gnb5,Gngt1,Gng10,Gng2,Gng3, Gng4,Gng5,Gng8,Gngt2,Prkaca,Prkacb,Prkar1a,Prkar1 b,Prkar2b,Rab11a,Gng13
R-MMU-9705462	Inactivation of CSF3 (G-CSF) signaling	2E+00	1.1E-03	Ube2d3,Elob,Eloc,Cul5,Socs3,Socs1,Rps27a,Csf3,Csf3r, Hck,Jak2,Lyn,Ube2d1,Rnf7,Syk,Tyk2,Uba52,Ubb,Ube2d2a
R-MMU-109606	Intrinsic Pathway for Apoptosis	2E+00	2.5E-03	Diablo,Dynl12,Gsdmd,Bmf,Aven,Apaf1,Xiap,Bad,Bak1, Bax,Bcl2,Bcl2l1,Bid,Bcl2l11,Casp3,Casp7,Casp8,Casp9, Cycs,Gzmb,Nmt1,Septin4,Ppp3cc,Ppp3r1,Ywhab,Gsdme, Ywhae,Ywhag,Ywhah,Ywhaq,Ywhaz,Sfn,Apip,Dynl11,P maip1,Mapk1,Mapk3,Mapk8
R-MMU-512988	Interleukin-3, Interleukin-5 and GM-CSF signaling	2E+00	2.0E-03	Pik3cb,Rapgef1,Cbl,Rps27a,Crk,Crkl,Csf2,Csf2ra,Csf2rb2, Fyn,Grb2,Hck,Ptpn6,Il2ra,Il2rb,Il2rg,Il5ra,Inpp5d,Inpp11, Jak2,Jak3,Lyn,Pik3ca,Pik3cd,Pik3r1,Pik3r2,Pik3r3,Prka ca,Ptpn11,Shc1,Sos1,Stat5a,Stat5b,Syk,Tec,Uba52,Ubb, Vav1,Yes1,Ywhaz
R-MMU-5218920	VEGFR2 mediated vascular permeability	2E+00	1.9E-03	Them4,Prr5,Akt1,Akt2,Calm1,Calm2,Calm3,Ctnna1,Ctn nb1,Ctnnd1,Cav1,Cdh5,Rictor,Hsp90aa1,Jup,Nos3,Pak3, Pdpk1,Rac1,Vav1,Vav2,Akt3,Mlst8,Mtor,Vav3,Pak2,Map kap1,Trib3
R-MMU-157858	Gap junction trafficking and regulation	2E+00	4.1E-03	Cltc,Tubb6,Tubb2b,Cltb,Tuba3,Actb,Actg1,Ap2m1,Dab2, Dnm1,Dnm2,Gja1,Gja10,Gja3,Gja4,Gja5,Gjc1,Gja8,Gj d2,Gjb1,Gjb2,Gjb3,Gjb4,Gjb5,Gjb6,Gjc2,Src,Tuba8,Tub b1,Tjp1,Tuba1a,Tuba1b,Tuba4a,Tuba3b,Tubb3,Tubb4a, Gjd3,Gjd4,Tubb4b
R-MMU-4086398	Ca ²⁺ pathway	2E+00	3.4E-03	Gng11,Calm1,Calm2,Calm3,Camk2a,Ctnnb1,Fzd3,Fzd4, Fzd5,Fzd6,Gnao1,Gnat2,Gnb1,Gnb2,Gnb3,Gnb4,Gnb5,G ng1,Gng10,Gng2,Gng3,Gng4,Gng5,Gng8,Gngt2,Kras,Le fl,Nlk,Pde6b,Pde6g,Plcb1,Plcb2,Plcb3,Ppp3ca,Ppp3cb,P pp3r1,Tcf7l2,Wnt11,Wnt5a,Fzd2,Map3k7,Gng13

R-MMU-74752	Signaling by Insulin receptor	2E+00	3.2E-03	Frs2,Atp6v1f,Atp6v1g2,Atp6v1g1,Atp6v1c1,Fgf22,Atp6v1c2,Atp6v1d,Pik3cb,Atp6v1e2,Atp6v0a4,Pik3r4,Them4,Atp6v1h,Atp6v1g3,Atp6v0e2,Akt2,Atp6v1a,Atp6v1b2,Atp6v0d1,Atp6v1e1,Atp6v0e,Atp6v0a1,Atp6v0c,Atp6v1b1,Atp6v0d2,Fgf1,Fgf10,Fgf15,Fgf17,Fgf18,Fgf2,Fgf4,Fgf5,Fgf6,Fgf7,Fgf8,Fgf9,Fgfr1,Fgfr2,Fgfr4,Flt3,Flt3l,Gab1,Grb10,Grb2,Fgf20,Fgf16,Atp6v0b,Ins2,Insr,Tlr9,Irs1,Kl,Klb,Pde3b,Pdpk1,Pik3ca,Pik3r1,Pik3r2,Ptpn11,Shc1,Sos1,Atp6ap1,Atp6v0a2,Irs2,Mapk1,Mapk3,Tcirg1,Fgf23,Trtb3
R-MMU-8964038	LDL clearance	2E+00	5.2E-03	Ldlrap1,Cltc,Pcsk9,Npc2,Ap2s1,Ap2b1,Apob,Ap2a1,Ap2a2,Ap2m1,Ces3b,Ldlr,Lipa,Npc1,Soat1,Nceh1,Soat2
R-MMU-445717	Aquaporin-mediated transport	2E+00	7.6E-03	Gng11,Aqp11,Rab11fip2,Aqp1,Aqp2,Aqp3,Aqp4,Aqp5,Aqp7,Aqp8,Avp,Avpr2,Aqp12,Gnas,Gnb1,Gnb2,Gnb3,Gnb4,Gnb5,Gngt1,Gng10,Gng2,Gng3,Gng4,Gng5,Gng8,Gngt2,Mip,Prkaca,Prkacb,Prkar1a,Prkar1b,Prkar2b,Rab11a,Aqp9,Gng13
R-MMU-418990	Adherens junctions interactions	2E+00	1.3E-02	Nectin4,Cdh24,Cadm2,Actb,Actg1,Ang,Cdh7,Ctnna1,Ctnnb1,Ctnnd1,Cdh1,Cdh11,Cdh13,Cdh15,Cdh17,Cdh2,Cdh3,Cdh4,Cdh5,Cdh6,Cdh8,Jup,Afdn,Cdh12,Nectin2,Pvr,Cadm1,Nectin1,Cdh18,Cdh10,Nectin3
R-MMU-1169410	Antiviral mechanism by IFN-stimulated genes	2E+00	1.4E-02	Ddx58,Eif4e3,Eif4g3,Oasl1,Uba7,Eif4g1,Eif4a1,Eif4a2,Eif4e,Eif4g2,Ifit1bl2,Pde12,Mx2,Nedd4,Plcg1,Ppm1b,Eif2ak2,Trim25,Irf3,Ube2e1,Arih1,Rnasel,Abce1,Ube2l6,Usp18,Flnb,Mapk3,Eif4e2,Ube2n,Eif4a3,Isg15
R-MMU-202733	Cell surface interactions at the vascular wall	2E+00	2.1E-02	Ppil2,Jam2,Slc7a6,Cd177,Esam,Ppia,Jaml,Apob,Pik3cb,Olr1,Angpt1,Angpt2,Angpt4,Atp1b1,Atp1b2,Atp1b3,Bsg,Cav1,Cd44,Cd48,Cd84,Col1a1,Col1a2,Cxadr,Dok2,F2,Fcer1g,Fn1,Fyn,Gp6,Gas6,Gpc1,Grb2,Grb7,Ptpn6,Slc16a3,Hras,Sdc2,Jchain,Cd74,Inpp5d,Itga3,Itga4,Itga5,Itga6,Itgav,Itgax,Itgb1,Itgb2,Itgb3,Cd47,F11r,Psg29,Kras,Lck,Epcam,Lyn,Mag,Slc3a2,Mertk,Mif,Cd244a,Grb14,Slc7a8,Jam3,Pecam1,Pik3ca,Pik3r1,Pik3r2,Plcg1,Proc,Procr,Prosl,Ptpn11,Sirpa,Sele,Glg1,Sell,Selp,Shc1,Slc16a1,Slc7a5,Slc7a7,Sos1,Spn,Src,Sdc1,Sdc3,Sdc4,Gm5150,Slc7a10,Tek,Tgfb1,Thbd,Tnfrsf10b,Yes1,Pf4,Slc16a8,Trem1,Ceacam1,Ceacam2,Psg18,Slc7a11,Slc7a9,Gm9733,Fcamr
R-MMU-111465	Apoptotic cleavage of cellular proteins	2E+00	2.0E-02	Stk26,Clspn,Dsp,Add1,Birc2,Bmx,Casp3,Casp6,Casp7,Casp8,Ctnnb1,Cdh1,Dbnl,Dsg1a,Dsg2,Dsg3,Plk2,Fnta,Gas2,Lmna,Lmnb1,Mapt,Ocln,Prkcd,Prkcg,Pkp1,Plec,Rock1,Satb1,Tjp1,Tjp2,Vim,Acin1,Stk24,Bcap31,Gsn
R-MMU-3299685	Detoxification of Reactive Oxygen Species	2E+00	1.9E-02	Nudt2,Gpx7,Gpx8,Gpx6,Prdx3,Prdx6,Cat,Ccs,Cyba,Cybb,Cyca,Gpx1,Gpx2,Gpx3,Gpx5,Gsr,Gstp1,Nox4,Txnrd1,Ero1a,Ncf1,Ncf2,Ncf4,P4hb,Prdx1,Sod1,Sod2,Sod3,Prdx2,Prdx5,Txn1,Txn2,Txnrd2
R-MMU-168638	NOD1/2 Signaling Pathway	2E+00	2.3E-02	Tab1,Ube2v1,Tab3,Tab2,Cyld,Nod1,Irak2,Birc3,Birc2,Casp1,Casp4,Casp2,Casp8,Casp9,Rps27a,Ikkbk,Ikkbg,Irak1,Itch,Mapk11,Tnfaip3,Traf6,Uba52,Ubb,Map2k6,Map3k7,Mapk13,Mapk14,Ube2n,Ripk2,Mapk12,Aamp

R-MMU-983712	Ion channel transport	2E+00	2.4E-02	Atp1a2,Asph,Clea2,Atp6v1f,Atp6v1g2,Atp6v1g1,Atp6v1c1,Clea4b,Unc80,Atp8b3,Atp10d,Atp2b1,Mcoln2,Wnk1,Trpm4,Atp6v1c2,Ano1,Atp2c2,Atp1a3,Ano5,Ano10,Wnk4,Tpcn2,Ano9,Atp2c1,Atp13a5,Sgk3,Atp13a1,Slc17a3,Pdzd11,Mcoln3,Asic3,Ano6,Trpm8,Atp6v1d,Mlkl,Atp13a2,Wwp1,Atp6v1e2,Bsnd,Atp6v0a4,Fxyd4,Camk2d,Wnk2,Atp6v1h,Atp6v1g3,Nalcn,Atp6v0e2,Atp11b,Trdn,Sri,Ano7,Asic2,Asic1,Asic4,Raf1,Atp1a1,Atp1b1,Atp1b2,Atp1b3,Fxyd2,Atp2a1,Atp2a2,Atp2b2,Atp4b,Atp6v1a,Atp6v1b2,Atp6v0d1,Atp6v1e1,Atp6v0e,Atp6v0a1,Atp7a,Atp7b,Atp8a1,Atp9a,Atp10a,Atp6v0c,Atp8b4,Calm1,Calm2,Calm3,Camk2a,Camk2b,Camk2g,Casq1,Casq2,Atp6v1b1,Cln1,Cln2,Cln4,Cln5,Clnka,Rps27a,Ttyh3,Atp6v0d2,Stom,Fkbp1b,Ano2,Tsc22d3,Ostm1,Trpa1,Atp6v0b,Best2,Fxyd3,Trpm1,Trpv3,Wnk3,Atp8a2,Atp11a,Atp9b,Pln,Ttyh2,Ripk1,Ryr1,Ryr2,Ryr3,Scnn1a,Scnn1b,Scnn1g,Sgk1,Atp2a3,Atp2b4,Unc79,Ano8,Atp6ap1,Atp6v0a2,Atp8b1,Best3,Trpc1,Trpc4,Trpc5,Trpc6,Uba52,Ubb,Trpv2,Fxyd1,Clnkb,Tpcn1,Trpc4ap,Ripk3,Clea1,Trpm5,Best1,Atp10b,Ttyh1,Fxyd7,Ano4,Asic5,Atp2b3,Atp11c,Trpm7,Fxyd6,Cln6,Cln7,Trpc7,Tcigr1,Sgk2,Atp1a4,Atp13a4,Trpm2,Atp12a,Mcoln1,Trpv1,Trpm6,Trpv5,Trpv4,Trpv6,Slc9b2,Ano3,Stoml3
R-MMU-1500931	Cell-Cell communication	2E+00	2.6E-02	Kirrel3,Sdk1,Flnc,Nectin4,Nphs2,Kirrel,Parvb,Wasl,Arhgef6,Sdk2,Fblim1,Cdh24,Cadm2,Actn1,Actb,Actg1,Ang,Cdh7,Krt5,Ctnna1,Ctnnb1,Ctnnd1,Cd151,Lims1,Cdh1,Cdh11,Cdh13,Cdh15,Cdh17,Cdh2,Cdh3,Cdh4,Cdh5,Cdh6,Cdh8,Col17a1,Dst,Fyn,Kirrel2,Grb2,Ilk,Itga6,Itgb1,Cd47,F1lr,Jup,Krt14,Lama3,Lamb3,Afdn,Nck1,Nck2,Prkci,Plec,Cdh12,Ptk2b,Sirpa,Nectin2,Pxn,Pvr,Sftpd,Gm5150,Skap2,Tesk1,Nphs1,Cadm1,Tyrobp,Vasp,Fermt2,Pard6a,Fyb,Parva,Pard6b,Nectin1,Cdh18,Cdh10,Nectin3,Pard6g,Pard3,Flna,Lims2,Itgb4,Iqgap1,Gm9733
R-MMU-111471	Apoptotic factor-mediated response	2E+00	3.0E-02	Diablo,Gsdmd,Aven,Apaf1,Xiap,Bak1,Bax,Casp3,Casp7,Casp9,Cyts,Septin4,Gsdme,Apip,Mapk1,Mapk3

Table 2.10: Selected Downregulated Pathways from GeoMx Whole Transcriptomic

Assay.

Reactome pathway ID	Pathway description	Normalized enrichment score	Adjusted pValue	Targets
R-MMU-1474228	Degradation of the extracellular matrix	-2E+00	9.5E-04	Ctrb1,Col8a2,A2m,Capns2,Tmprss6,Scube3,Capn11,Capn8,Optc,Spock3,Phykpl,Capn9,Col6a5,Mmp25,Adam10,Adam15,Adam8,Adamts4,Acan,Bcan,Bmp1,Bsg,Capn1,Capn2,Capn3,Capns1,Capn5,Capn6,Capn7,Cast,Cd44,Cdh1,Col10a1,Col11a1,Col11a2,Col12a1,Col13a1,Col15a1,Col18a1,Col19a1,Col2a1,Col3a1,Col4a1,Col4a2,Col4a3,Col4a4,Col4a5,Col5a1,Col5a2,Col6a1,Col6a2,Col7a1,Col8a1,Col1a1,Col1a2,Ctsb,Ctsd,Ctsg,Ctsk,Ctsl,Ctss,Dcn,Klk1b22,Klk1b9,Eln,Fbn1,Fbn2,Fn1,Hspg2,Col6a6,Klk1b11,Klk1b16,Klk1b21,Klk1b26,Klkb1,Klk1b1,Lama3,Lamb3,Cma1,Mmp12,Mmp10,Mmp11,Mmp13,Mmp14,Mmp15,Mmp16,Mmp2,Mmp24,Mmp3,Mmp8,Mmp9,Elane,4930486L24Rik,Capn15,Klk1b3,Nid1,Furin,Plg,Capn13,Spp1,Col5a3,Timp1,Htra1,Adamts5,Capn10,Mmp17,Klk7,Tll2,Mmp19,Capn12,Col4a6,Mmp20,Scubel
R-MMU-5669034	TNFs bind their physiological receptors	-2E+00	1.4E-03	Tnfrsf14,Tnfsf13,Tnfsf18,Eda,Edar,Eda2r,Lta,Tnfrsf11b,Tnfrsf25,Tnfrsf17,Tnfrsf18,Tnfrsf1a,Tnfrsf1b,Cd27,Tnfrsf8,Tnfrsf9,Tnfsf11,Cd70,Tnfsf8,Tnfsf9,Tnfrsf4,Tnfsf4,Tnfsf13b,Tnfrsf13b,Tnfsf15
R-MMU-1592389	Activation of Matrix Metalloprotein ases	-2E+00	3.1E-03	Ctrb1,Spock3,Mmp25,Col18a1,Ctsg,Ctsk,Klk1b22,Klk1b9,Klk1b11,Klk1b16,Klk1b21,Klk1b26,Klkb1,Klk1b1,Cma1,Mmp10,Mmp11,Mmp13,Mmp14,Mmp15,Mmp16,Mmp2,Mmp24,Mmp3,Mmp8,Mmp9,Elane,4930486L24Rik,Klk1b3,Furin,Plg,Timp1,Mmp17
R-MMU-216083	Integrin cell surface interactions	-2E+00	4.5E-03	Fgg,Jam2,Col8a2,Itga9,Col16a1,Col6a5,Itga1,Fgb,Itga8,Bsg,Cd44,Cdh1,Col13a1,Col18a1,Col2a1,Col3a1,Col4a1,Col4a2,Col4a3,Col4a4,Col4a5,Col5a1,Icam4,Col5a2,Col6a1,Col6a2,Col7a1,Col8a1,Col9a1,Col9a3,Col1a1,Col1a2,Comp,Fbn1,Fga,Fn1,Hspg2,Col6a6,Ibsp,Icam1,Icam2,Icam5,Itga2,Itga2b,Itga3,Itga4,Itga5,Itga6,Itgae,Itgav,Itgax,Itgb1,Itgb2,Itgb3,Itgb5,Itgb6,Itgb7,Cd47,F11r,Kdr,Lum,Jam3,Pecam1,Spp1,Col5a3,Tnc,Vtn,Vwf,Itgb8,Col4a6
R-MMU-1474244	Extracellular matrix organization	-2E+00	3.1E-03	Ctrb1,Fgg,Tnn,Jam2,Mfap1a,Loxl4,Col8a2,Adamts3,Emilin1,A2m,Capns2,Pxdn,Col22a1,Colgalt1,Itga9,Col24a1,Tmprss6,Scube3,Capn11,Ltbp1,Capn8,Optc,Colgalt2,Spock3,Phykpl,Col20a1,Capn9,Col23a1,Col16a1,Col26a1,Col6a5,Ltbp4,Mmp25,Mfap4,Pcolce2,Itga1,Adam10,Adam12,Adam15,Adam19,Adam8,Adamts4,Acan,App,Fgb,Itga8,Bcan,Bgn,Bmp1,Bmp10,Bmp2,Bmp4,Bmp7,Bsg,Ddr1,Capn1,Capn2,Capn3,Capns1,Capn5,Capn6,Capn7,Cast,Serpinh1,Cd151,Cd44,Cdh1,Col10a1,Col11a1,Col11a2,Col12a1,Col13a1,Col14a1,Col15a1,Col17a1,Col18a1,Col19a1,Col2a1,Col3a1,Col4a1,Col4a2,Col4a3,Col4a4,Col4a5,Col5a1,Icam4,Col5a2,Col6a1,Col6a2,Col7a1,Col8a1,Col9a1,Col9a3,Col1a1,Col1a2,Comp,Hapln1,Ncan,Ctsb,Ctsd,Ctsg,Ctsk,Ctsl,Ctss,Dag1,Dcn,Dmp1,Col27a1,Dst,Klk1b22,Klk1b9,Eln,P3h2,Fbln2,Fbn1,Fbn2,Fga,Fgf2,Sh3pxd2a,Fn1,Gdf5,P3h3,Sdc2,Hspg2,Col6a6,Ibsp,Icam1,Icam2,Icam5,Tnxb,Itga2,Itga2b,Itga3,Itga4,Itga5,Itgae,Itgav,Itgax,Itgb1,Itgb2,Itgb3,Itgb5,Itgb6,Itgb7,Cd47,F11r,Kdr,Klk1b11,Klk1b16,Klk1b21,Klk1b26,Klkb1,Klk1b1,Lama1,Lama2,Lama3,Lama4,Lama5,Lamb1,Lamb2,Lamb3,Lox,Loxl1,Loxl3,Ltbp2,Ltbp3,

				Lum,Mfap2,Matn1,Matn3,Matn4,Cma1,Emilin2,Col28a1,Mmp12,Mmp10,Mmp11,Mmp13,Mmp14,Mmp15,Mmp16,Mmp2,Mmp24,Mmp3,Mmp8,Mmp9,Mfap5,Elane,4930486L24Rik,Capn15,Klk1b3,Nid1,Nid2,Ddr2,Jam3,P4ha1,P4ha2,P4hb,Emilin3,Peolce,Furin,Pdgfa,Pdgfb,Pecam1,Prkca,Plec,Plg,Plod1,Ppib,Adams2,Mfap3,Capn13,Sparc,Spp1,Sdc1,Sdc3,Sdc4,Col5a3,Tgfb1,Tgfb2,Timp1,Tnc,Tnr,Ttr,Vtn,Vwf,Htra1,P3h1,Adams5,Capn10,Fbln5,Crtap,Lamc3,Mmp17,Klk7,Tll2,Mmp19,Itgb8,Efemp2,Ceacam1,Plod2,Plod3,Capn12,Col4a6,Loxl2,Itgb4,Mmp20,Scube1
R-MMU-166658	Complement cascade	-2E+00	8.2E-03	C8a,C8g,Colec11,Cd59b,Cpn2,Colec10,C7,Cfd,C8b,Serping1,C1qa,C1qb,C1qc,C2,C3,C3ar1,C4b,C5ar1,C9,Cd19,Cd81,Cfh,Cfi,Clu,Crp,F2,Fcna,Fcnb,Hc,Gzmm,Masp1,Masp2,Cd46,Elane,C1ra,Cfp,Vtn,C1s2,Cpb2,C5ar2,Cpn1

CHAPTER THREE

ROLE OF VEGF IN O₃ INDUCED ALTERED VASCULAR PHENOTYPE

Introduction

Vascular abnormalities, including leaky blood brain barrier (BBB) and reduced cerebral blood flow (CBF), are commonly observed in Alzheimer's disease (AD) [56]. Studies show vascular dysregulation starts early in the pathology progression [56,238–240] and a complex mixture of pathways are involved in mediating its dysregulation [56,60,61,90]. Even though a number of mechanisms behind dysregulated vascular phenotype in AD have been determined [57,61,95,96,241–244], a clear understanding of it is still lacking. An increasing body of epidemiologic studies have associated air pollution, including ozone (O₃), with higher risk of dementia and AD [16,19,20,141]. O₃ has long been linked to cerebral vascular effects such as stroke [9,158,245–248], which itself has been associated with increased dementia risk [249,250]. However, how O₃ may affect the vasculature characteristics in AD pathology is largely unknown.

The neurovascular unit (NVU) regulates CBF and modulates BBB integrity, maintaining central nervous system (CNS) health and homeostasis [56]. These functions are carried out by a combination of cells, that form the NVU, and their mutual communication [56,60,61,65,95,251]. Neurovascular coupling regulating CBF is mediated by mutual communication between neurons, astrocytes, pericytes with the capillary wall [56,65,252–254]. Reduced CBF, a well-established feature in AD [56,60,65,240,255–257], contributes to increased amyloid-beta (A β) generation [56,258–262] and dysfunctional vascular clearance increases its accumulation [39,56,263,264]. On the other hand, A β accumulation promote further neurovascular dysregulation and CBF

reduction [244,265–267]. A number dysregulations in these NVU components caused by A β accumulation have been noted [244,265,268–274], including altered cellular communication [273,275,276] among them. However, how their phenotypes and hence their functions and cell to cell communications are altered in the plaque microenvironment is not clearly understood.

Animal studies demonstrate deleterious effects of air pollution on CNS vasculature encompassing reduced tight junction protein levels, increased BBB permeability [29,277–279], artery narrowing and thickening, vascular inflammation [280], upregulated p-glycoprotein via oxidative stress [281], dysregulated vessel-microglia association [27]. O₃ exposure itself has been associated with increased BBB permeability [150,186,187]. However, how O₃ alters NVU cellular component phenotype and their mutual communication, particularly in the plaque microenvironment, is unknown.

Consistent with prior reports from other labs, Figure 2.6 demonstrates pathways involving astrocyte-vascular wall communication being dysregulated in periplaque region from O₃ exposure implicating dysregulated cellular communication in mediating O₃ induced BBB damage. Our findings also suggested involvement of multiple VEGFA-VEGFR2 signaling pathways (Figure 2.6). VEGFA is a well-studied angiogenic factor [100,101,282,283], responsible for vascular growth and maintenance [101,283], mediated by signaling via its specific receptor VEGFR2 [283], with both beneficial [107,284] and detrimental [97,98,104] observed roles in pathological conditions. In AD as well it has been attributed to attenuation [106,107] and exacerbation [102,104,285] of pathology, possibly owing to the differing sites of VEGFA upregulation [103]. However, nothing is

known about its role in air pollution mediated neurovascular damage. While we have previously shown increased circulating VEGF from subchronic O₃ exposure in AD mouse model [22], how it modulates O₃'s effect on amyloid pathology and associated neurovascular phenotype is not known.

Hence, in this study we aimed to examine: a) how ozone alters vascular phenotype in plaque microenvironment along with vascular amyloid deposition, and b) the potential role of VEGFA in mediating dysregulated vascular phenotype from O₃ exposure.

Methods

Animals

Male transgenic 5xFAD mice hemizygous for five familial AD mutations (APP K670N/M671L, Swedish; I716V, Florida; V717,I London; PSEN1 M146L; and PSEN1, L286V) [61], littermate controls on a C57Bl/6J background (B6. Cg-Tg(APP^{Sw}FIL^{on},PSEN1*^{M146L}*^{L286V})6799^{Vas}/Mmjax; RRID:MMRRC_034848-JAX), C57Bl/6J (RRID:IMSR_JAX:000664), and *LysM*-Cre (B6.129P2-Lyz2^{tm1}(cre)Ifo/J; RRID:IMSR_JAX:004781) mice were obtained from the Jackson Laboratory. Female 5xFAD mice exhibit markedly exacerbated amyloid pathology that increases rapidly over time [62,63], risking a ceiling effect when combined with O₃ exposure; thus, to prevent potentially confounding analyses, only male mice were employed in the current study.

The mice were acclimated to the housing facility for at least 1 week before all studies. All mice were maintained on a 12-hour light/dark cycle (7:00 AM–7:00 PM) in a

specific pathogen-free environment. Experimental mice were individually housed in HEPA-filtered ventilated polycarbonate cages with food and acidic water (pH 2.2–2.7) provided *ad libitum*. All experiments were completed in strict accordance with the IUSM IACUC protocols (29002 and 27001) and NIH guidelines for housing, breeding, and experimental use. All mice were treated humanely to alleviate suffering.

O₃ Exposure

Mice were exposed to O₃ in full-body Hinner's inhalation chambers [65] as previously described [29]. Briefly, O₃ was produced with an HFL-10 O₃ generator (Ozonology, Northfield, IL, USA). The O₃ concentration was continuously monitored using a UV photometric O₃ analyzer (465L, Teledyne API, San Diego, CA), and the temperature was maintained at 21 ± 2°C. Rodents have lower sensitivity to O₃ toxicity than primates [66,67] due to their complex nasal turbinates, lung morphological differences, and unique airway surfactant [67,68]. Thus, increasing exposure by a factor of 3 is traditionally accepted for extrapolating to environmentally relevant human exposures [66]. O₃ concentrations of 0.2–0.3 ppm is frequent in areas of high air pollution, similar to 1 ppm O₃ exposure in rodents [41,69]. The mice were placed in wire mesh individual housing cages that were transferred to the chambers for exposure. Before the experiment, mice were habituated to the exposure chambers for 5 consecutive days (4 hours/day).

For each study, animals were assigned to experimental groups using a randomized block design. Random numbers were generated using <http://www.jerrydallal.com/random/randomize.htm>.

For the subchronic O₃ exposure experiments exploring how astrocytes are modified during O₃-augmented amyloid plaque pathology, one hundred twenty 10- to 11-week-old male 5xFAD mice and littermate controls were exposed in two separate experiments (60 for CNS and 60 for pulmonary measures) to filtered air (FA), 0.3 ppm, or 1.0 ppm O₃ for 4 hours/day, 3 consecutive days/week, for 13 weeks (n = 10 per group). The mice were then euthanized, and samples were collected 18–24 hours after the last exposure, as reported previously [29]. Because the purpose of the study was to determine how O₃ modified the neurovascular phenotype during ongoing O₃-augmented amyloid pathology, the littermate control strain (no plaques) and the mice exposed to 0.3 ppm O₃ (no O₃-induced change in plaque pathology [29]) were excluded from processing and analysis.

For VEGFR2 inhibition experiments, forty male 5xFAD mice (10-11 weeks) were intraperitoneally injected with 100 µl of VEGFR2 antibody (BioXCell, BP0060, RRID AB_1107766, Lebanon, NH) or IgG1 (BioXCell, BP0088, RRID AB_1107775, Lebanon, NH) for controls. 30 minutes after injection mice were exposed to FA or 1.0 ppm O₃ for 4 hours/day, 3 consecutive days/week, for 10 weeks (n = 10 per group). While we have previously seen exacerbated amyloid pathology from a 13 week long O₃ exposure [22], owing to increasing sickness and mortality in VEGFR2 ab treated groups the experiment was stopped at 10 weeks and tissue samples were collected 24 hours after the last exposure.

Sample Collection

Mice were euthanized with isoflurane. One brain hemisphere was microdissected (cortex, hippocampus, and midbrain), flash-frozen in liquid nitrogen, and stored at

-80°C. The other half of the brain was fixed in 4% paraformaldehyde (PFA, Electron Microscopy Sciences, 1921) by immersion for 2 days, followed by cryopreservation in 30% sucrose in phosphate-buffered saline (PBS) for another 2 days. Then, the entire hemisphere was embedded with optimal cutting temperature compound (OCT, 4583, Sakura Finetec, Terrance, CA) in cryomolds (Tissue-Tek, 4557, Sakura Finetec, Terrance, CA).

Fluorescent Immunohistochemistry (IHC)

Sagittal sections (40 µM) were collected using a freezing stage microtome (Microm HM 450, Thermo Scientific, Waltham, MA). For all following IHC endpoints, three evenly spaced sections approximately 0.24 mm apart spanning the motor cortex starting at the sagittal plane ~0.6 mm lateral to the midline [70] were stained per brain. All sections were washed for 10 minutes in 0.1% PBST prior to antigen retrieval. Antigen retrieval was performed in 1 M sodium citrate solution at 85°C for 15 minutes with subsequent cooling to room temperature for 30 minutes. Blocking was performed with normal donkey serum containing mouse on mouse (1:1000, MKB-2213-1, Vector Laboratories) blocking solution for 1 hour, followed by overnight incubation in primary antibody diluted (1: 500) in blocking serum. Rabbit anti-Laminin (Novus Biologicals, NB300-144), mouse anti-Aqp4 (Abcam, ab9512) and mouse anti-6e10 (BioLegend, 803001; RRID AB_2564653) were used to stain vessels and A β , respectively. Sections were washed three times in 0.1% PBST and incubated with secondary Alexa Fluor antibodies diluted (1: 1000) in blocking serum at room temperature for 1 hour, followed by three washes with 0.1% PBST. Donkey anti-rabbit 647 (Invitrogen A-31573; RRID AB_2536183) and donkey anti-mouse 568 (Invitrogen A10037; RRID AB_2534013)

were used as secondary antibodies (1:1000) for Laminin and 6e10 staining, respectively. For select experiments, sections were incubated with Dylight-488 conjugated lectin (DL-1174-1, Vector Laboratories) for 1 hour for vessel visualizations. Sections were mounted on slides with Prolong Gold (P36930, Life Technologies, Eugene, OR), coverslipped, and dried overnight in the dark. Slides were stored at -20°C before imaging.

To stain for $\text{A}\beta$ plaques, sections were washed in 0.1% PBST for 5 minutes and Methoxy x34 (SL 1954, Millipore Sigma, St Louis, MO) solution (0.04 g X34 in 400 mL 100% ETOH and 600 mL DI H_2O) for 10 minutes. The slides were then sequentially washed five times with DDH_2O and 0.1% PBST for 5 minutes before the addition of Prolong Gold and coverslipping. For Thioflavin S (ThioS, T1892, Sigma-Aldrich, St Louis, MO) staining was done by incubating slides with ThioS solution (1g ThioS in 500 ml 100% EtOH and 500 ml ddH_2O) for 10 min followed by subsequent washes in 80% EtOH twice, 95% EtOH and ddH_2O three times for 3 minutes each.

Imaging

Vessel Associated Plaque Quantification

To assess $\text{A}\beta$ deposition in and around vessels, 1 μm spaced Z-stacks were acquired from the primary motor region of the cortex at $40\times$ with oil immersion with a Nikon A1R confocal microscope. Images were analyzed in NIS Elements AR using the General Analysis 3 Module. Image stacks were thresholded using criteria maintained across the entire analysis. Areas double-positive for Laminin and 6e10 were quantified per stack. The total colocalized volume was obtained by adding the colocalized area of all the stacks in the image and normalized by the total Laminin volume. A sample size of 8 mice per group was analyzed per endpoint. Statistical outliers were excluded.

Plaque Microenvironment Vessel Density Quantification

For vessel density quantification, 1 μm Z-stacks were acquired at 40 \times with oil immersion with a Nikon A1R confocal microscope (Nikon, Tokyo, Japan) in the primary motor region of the cortex. Images were analyzed in ImageJ (FIJI, version 2.9.0, NIH). To consistently define the plaque microenvironment, 5 similar sized plaques were selected in each sample and a 50 μm diameter circle was drawn around a plaque-positive area of this specific size, defining the periplate ROI. Image stacks were thresholded and denoised and laminin positive area within the ROI was measured in all the stacks. The total volume was obtained by adding the area of all the stacks in the image and normalized by the total ROI volume. A sample size of 8 mice per group was analyzed per endpoint. Statistical outliers were excluded.

Astrocytic Endfeet Quantification

To assess aqp4-positive astrocytic endfeet association with vessels, 1 μm spaced Z-stacks were acquired from the primary motor region of the cortex at 40 \times with oil immersion with a Nikon A1R confocal microscope. Images were analyzed in ImageJ (FIJI, version 2.9.0, NIH). Image stacks were thresholded and denoised and aqp4-positive area was quantified per stack. The total volume was obtained by adding the area of all the stacks in the image and normalized by the total vessel volume. A sample size of 7 mice per group was analyzed per endpoint. Statistical outliers were excluded.

NanoString GeoMx Digital Spatial Profiling: Protein Expression

Fixed frozen 10 μm coronal sections were acquired with a cryostat (CM1900, Leica) and stored at $-20\text{ }^{\circ}\text{C}$ before processing. Slides were processed per the NanoString Slide Prep manual for protein analysis. Briefly, slices were incubated with

the NanoString GeoMx Alzheimer's Morphology kit, which contains the A β antibody for plaque visualization and Alexa Fluor 647-conjugated mouse anti-Laminin antibody (Novus Biologicals, NB300-144AF647) for vessel identification, along with NanoString panels (Neural Cell Profiling Core, Alzheimer's Disease Panel, Alzheimer's Disease Extended Panel, Glial Subtyping Panel) containing approximately 60 antibodies with unique photo-cleavable oligonucleotide tags. Slices were scanned in the NanoString Digital Spatial Profiler, and polygonal ROIs were drawn around plaque-associated and non-plaque-associated astrocytes in the cortex. The Laminin-positive area within each ROI was delineated for photocleavable oligonucleotides collection. The collected oligonucleotides were hybridized with NanoString codeset, per the NanoString user manual, to map the counts to corresponding antibodies and region from where the oligonucleotides was collected. Digital counts were generated on an nCounter Max/Flex system (NanoString Technologies, Seattle, WA). The differential protein expression analysis was performed using the NanoString GeoMx Digital Spatial Profiling (DSP) Analysis Suite. The digital counts were tested for quality control and normalized to the CD31 counts. Three sections were scanned per brain from a sample size of 4 animals per exposure group (FA or 1.0 ppm O₃) for the analysis, resulting in 96 ROIs analyzed per experimental group. ROIs that did not pass the quality control checks were excluded.

Statistical Analysis

Experimenters were blinded to the experimental groups. The sample size was determined according to prior reports, and power analyses were calculated for 80% power. Data were analyzed in GraphPad Prism 8.0 (GraphPad Prism, San Diego, CA, USA). Outliers were determined using the ROUT method with Q = 1% and removed

from all analyses. Normal distribution was tested using the Shapiro–Wilk test. Welch’s t test was performed for data that passed the normality test. A 2-way ANOVA with Bonferroni’s post hoc analysis was performed when applicable. Linear mixed model (LMM) was used for GeoMx DSP protein profiling. Data are expressed as the mean \pm standard error of the mean (SEM). A P value $<.05$ was considered to indicate significance.

Result

O₃ Increases Vessel Associated A β

Vascular A β accumulation [56,90,93,276,286,287] is commonly seen in AD and studies have shown reduced vascular density [56,90,288–292]. To explore the role of air pollution in mediating vascular amyloid pathology, overlapping laminin-positive and A β -positive volume was calculated in the cortex. We demonstrated, along with aggravated amyloid plaque burden (Figure 2.1D), O₃ exposure elevates A β deposition in and around vessels (Figure 3.1A, 3.1 B and 3.1D), implicating potential role of air pollution in reduced A β clearance and increased accumulation. We also quantified vessel density in plaque microenvironment and observed reduced periplaque vascular volume from O₃ exposure (Figure 3.1C and 3.1D).

O₃ Alters Vasculature Associated Protein Expression in Plaque Microenvironment

To begin to understand how O₃ exposure affects vascular phenotype in the plaque microenvironment we spatially profiled protein expression on vessels that were present near plaques (periplaque) and away from plaque (nonplaque). We analyzed differential protein expression between periplaque and nonplaque vessels in both FA and O₃ exposed

mice and compared how O₃ exposure alters that differential expression pattern, thereby changing vascular response to plaque deposition. As expected, our analysis showed a baseline change in expression of 14 proteins on periplaque vessels compared to the nonplaque ones (Figure 3.2B and C and Table 3.1), While 8 of those were also changed in O₃ exposure, 6 protein were only differentially expressed in FA exposed mice (Figure 3.2B and C) and not in O₃ exposed mice (Figure 3.2B and D), implying O₃ impedes the baseline vascular response to plaque deposition. Notably, one of the proteins upregulated in FA exposed mice, IDE (Figure 3.2C and Table 3.1) an A β degradation enzyme [293], is not upregulated in O₃ exposed periplaque vessels, revealing obstructed A β degradation and clearance from O₃ exposure. On the other hand, only O₃ exposed periplaque vessels show upregulation of several proteins including CD9 and CD11b (Figure 3.2B and Table 3.1). In particular, CD9 is associated with cell to cell interaction and communication [294,295] and important for migration and adhesion [295–297], suggesting increased cell to cell communication along periplaque vessels from O₃ exposure and upregulated CD11b, implicating increased microglial association falls in line with that. A common marker of exosome and extracellular vesicle mediated communication [298,299], CD9 has also been associated with increased A β transfer and accumulation across BBB into the parenchyma [300–302]. While APOE was upregulated in both FA and O₃ exposed periplaque vessels, a greater upregulation was seen in the FA samples and reduced upregulation in O₃ (Table 3.1), fortifying O₃ induced dysregulated A β processing.

A direct comparison between FA and O₃ exposed mice, however, showed minimal differences in periplaque vessels (Figure 3.2E) and no significant difference in nonplaque vessels (Figure 3.2F). The use of such an aggressive disease model as 5xFAD

[33,303], potentially have muted the subtle O₃ induced dysregulation that more likely precede the pathology onset.

Role of VEGFA in O₃ Induced Exacerbated Amyloid Pathology

We have previously found increased circulating VEGF in 5xFAD from subchronic O₃ exposure [22]. While studies have shown beneficial roles of increased brain VEGF in AD [106,107], circulating VEGF-A has been shown to cause BBB damage and stalls [103,104] and inhibiting VEGF receptor demonstrated reduced A β deposition [102]. To understand the role of VEGF-A in O₃ induced exacerbated amyloid pathology we inhibited its action by blocking VEGFR2, receptor specific for VEGF-A signaling [283]. Even though we did not achieve statistical significance, possibly owing to inter-experimental differences, our results show a trend towards increased plaque deposition from O₃ exposure, supporting our previously reported observation [22]. Similarly, VEGFR2 inhibition show only a trend towards decreased plaque deposition (Figure 3.3A and B).

O₃ Potentially Alters Vascular Wall-Astrocytic Association

Vascular amyloid accumulation has previously been shown to cause reduced AQP4 and loss of astrocytic endfeet association with vasculature [274]. Our findings from astrocytic transcriptomic analysis in O₃ exposed mice demonstrated upregulated astrocytic communication with vascular wall (Figure 2.6). We assessed astrocytic endfeet coverage changes from O₃ by quantifying AQP4 positive area on vessels and found, though not statistically significant, a decreasing trend of AQP4 positive area in O₃ exposed mice (Figure 3.4A and B). VEGFR2 inhibition however did not change the trend.

Discussion

Air pollution has been associated with increased risk of AD. Studies show air pollution cause vascular damage including increased BBB permeability. Impact of O₃ on neurovasculature is well established [245–247]. However, the mechanistic underpinnings of its vascular effects in AD pathology are obscure. In the current study we explored how vascular phenotype changes with O₃ exposure in an AD mouse model, 5xFAD, uncovering important insight into its functional dysregulation.

Here we demonstrate O₃ increases vascular amyloid (Figure 3.1), suggesting a greater deterioration of clearance mechanism leading to increased accumulation. This could be one of the causes driving exacerbated disease progression observed previously from subchronic O₃ exposure in these mice [22]. Along with increased accumulation we also observed reduced vascular density in plaque microenvironment (Figure 3.1), a classic AD feature [56], that leads to reduced CBF and hypoxia [56] resulting in neuronal damage and further A β accumulation [56].

O₃ also qualitatively altered these vessels in the plaque microenvironment (Figure 3.2). These periplaque vessels from O₃ exposed mice had an altered proteomic response to plaque deposition and the change in periplaque versus nonplaque vessel associated protein expression pattern with O₃ exposure signified important loss of function. Particularly, loss of IDE upregulation on periplaque vessels from O₃ exposure potentially is a contributor to increased A β accumulation.

Similar to our previous observation from O₃ induced astrocytic proteomic response to plaque (Figure 2.3), altered cell-cell communication from O₃ exposure was evident from vasculature phenotyping in plaque microenvironment. Upregulated CD9 in

these samples suggests an increase in cell-cell communication with vasculature in plaque microenvironment. In line with this premise, upregulated CD11b reflects an increase in microglial association with vessels in plaque microenvironment from O₃ exposure. Further, more detailed, experiments need to be carried out to verify the nature of this altered inter-cellular interaction and their effects on amyloid pathology.

Vascular dysregulation precedes amyloid accumulation. Vascular two-hit hypothesis posits an initial systemic insult dysregulates neurovasculature, triggering a cascading loop of hypoxia leading to neuronal damage resulting in increasing A β accumulation [56]. This in turn furthers the neuronal damage and degeneration as well as neurovascular dysfunction and A β clearance disruption augmenting the accumulation and pathology [56]. While pre-existing cardiovascular disorders being an AD risk factor [56] provide substantial support to the vascular 2 hit hypothesis, no clear evidence of what causes the initial vascular hit is present. Lung–brain axis has been implicated in mediating air pollution induced CNS pathology [22,26,142], particularly with O₃ [22,26,28], an air pollutant that cannot translocate to the brain [34]. It defines a mechanistic pathway where circulating factors resulting from the lung response to O₃ exposure triggers BBB damage and subsequent CNS pathology [22,26]. In support of lung–brain axis we previously found circulating factors such as HMGB1, VEGF, that have been previously associated with AD, elevated from subchronic O₃ exposure [22].

Our data (increased A β accumulation on vessels and decreased clearance) potentially support the early vascular two-hit theory. However, our current experimental paradigm, with pathology already setting in and use of such an aggressive AD mouse model as 5xFAD, pinpointing the pre-amyloid pathology vascular changes would be

challenging. No changes in protein expression profile on nonplaque vessels from O₃ exposure (Figure 3.2F) suggests investigations at earlier stages of the pathology are required to uncover the initial subtle vascular effects of O₃ exposure preceding plaque development.

We next sought to explore the role of VEGFA in mediating O₃ induced vascular damage and exacerbated amyloid. Our astrocytic analysis highlighted multiple VEGFA-VEGFR2 signaling pathways being altered from O₃ exposure and more importantly we previously found increased circulating VEGF [22] which has been shown to cause detrimental vascular effects [97,98,103,104]. However, our analysis for parenchymal amyloid plaque, on VEGFR2 inhibition, did not show statistically significant difference possibly owing to several study limitations. Both VEGFR2 antibody and IgG treatment for controls seemed to increase the variance of observed pathology markers, which we did not anticipate before, affecting our analysis. But more importantly, VEGFR2 inhibition seemed to affect multiple organ systems, evidenced by antibody treated mice presenting with different sickness symptoms. Because of increasing mortality in the antibody treated group, irrespective of O₃ exposure, we decided to stop the exposure earlier, at 10 weeks, than our subchronic exposure paradigm (13 weeks) possibly resulting in reduced pathology than was previously observed.

Interestingly, FA exposed antibody treated mice started becoming sick earlier in the experimental timeline, whereas the O₃ exposed mice that were treated with antibody only started showing sickness very late in the process. Suggesting effects of O₃ exposure was initially counteracting effects of VEGFR2 inhibition. However, our parenchymal plaque deposition analysis show a decreasing trend, while not significantly so, of O₃

induced amyloid pathology from VEGFR2 inhibition in 5xFAD mice, reflecting a potential beneficial role of VEGFR2 inhibition in O₃ induced amyloid pathology. Even though studies show beneficial effect of VEGF inhibition in AD [102–104] with implications for potential therapeutic target, our data shows no changes in plaque deposition from VEGFR2 inhibition alone and while our experiment demonstrates its potential for counteracting the O₃ induced exacerbated pathology, it will be extremely important to consider its long term treatment effects on other organs systems.

Taken together, our findings suggest O₃ dysregulates neurovasculature, potentially contributing to increased A β plaque burden. O₃ induced vascular dysregulation reflected altered cell-cell communication strengthening the need to investigate intercellular interaction in AD pathology. Finally, in my opinion, our data does not strongly reject the potential for VEGFR2 inhibition as a therapeutic target but highlights the importance of better understanding its role in physiological and pathological conditions.

Figures

Figure 3.1: O₃ increases vessel associated A β and decreases vascular density in plaque microenvironment.

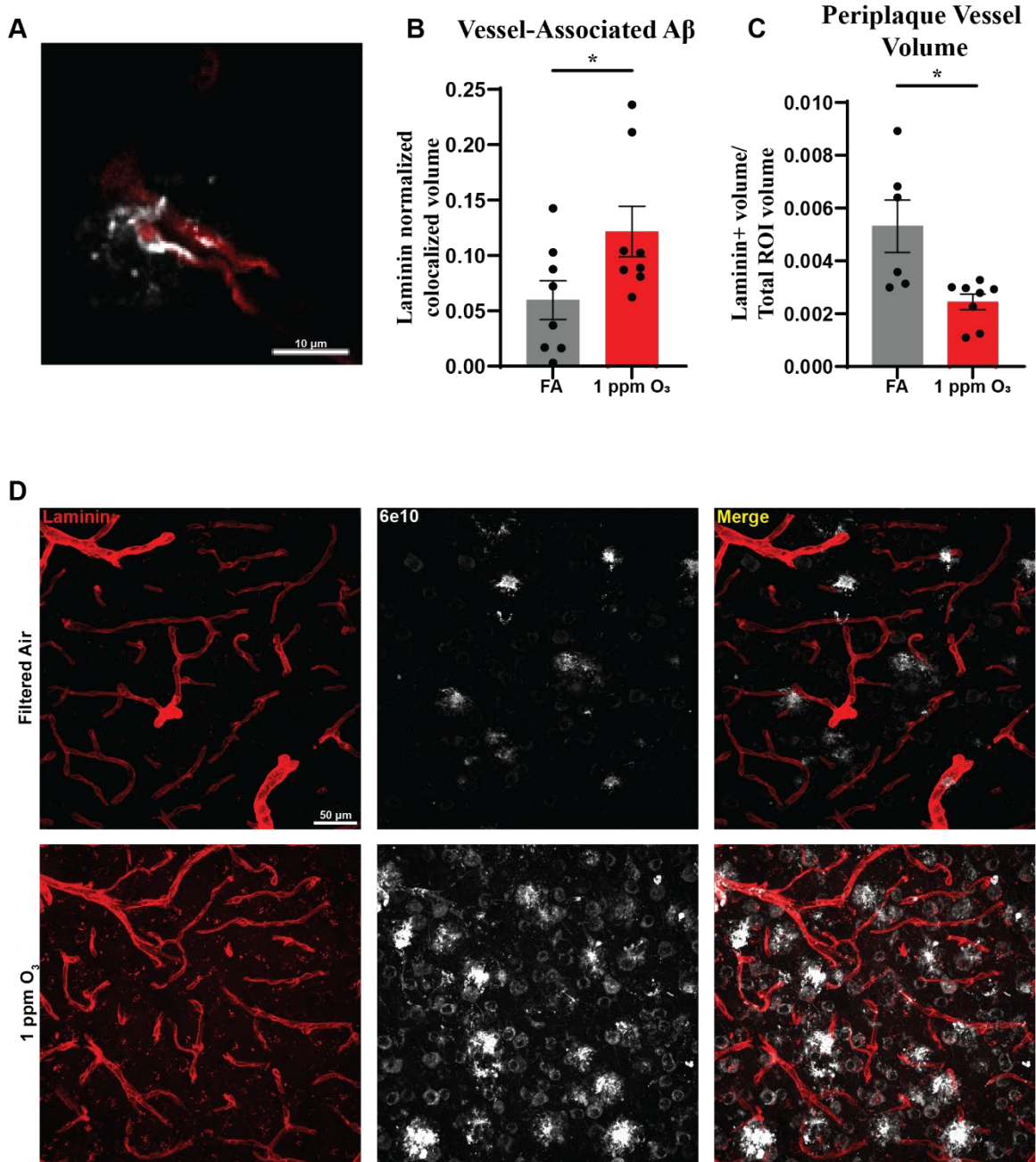


Figure 3.1: Male 5xFAD mice (10–11 weeks old) were exposed to either FA or 1.0 ppm O₃ for 3 consecutive days each week for 4 hours/day for 13 weeks. (A) Representative image showing vascular A β in a single image from a set of confocal Z-stack images taken at 40 \times . Scale bar: 10 μ m. (B) Quantification of A β -vessel colocalization in the periplaque and (C) Quantification of periplaque vessel density from confocal Z-stacks taken at 40 \times in the cortex. Data are represented as the mean \pm SEM, n = 8 mice/exposure group. * = p <.05; Welch's t test. (D) Representative maximum intensity images taken at 40 \times showing plaques (Methoxy-X34, gray), vessels (Laminin, red) in the O₃ and FA groups. Scale bar: 50 μ m.

Figure 3.2: O₃ alters vasculature associated protein expression in plaque microenvironment.

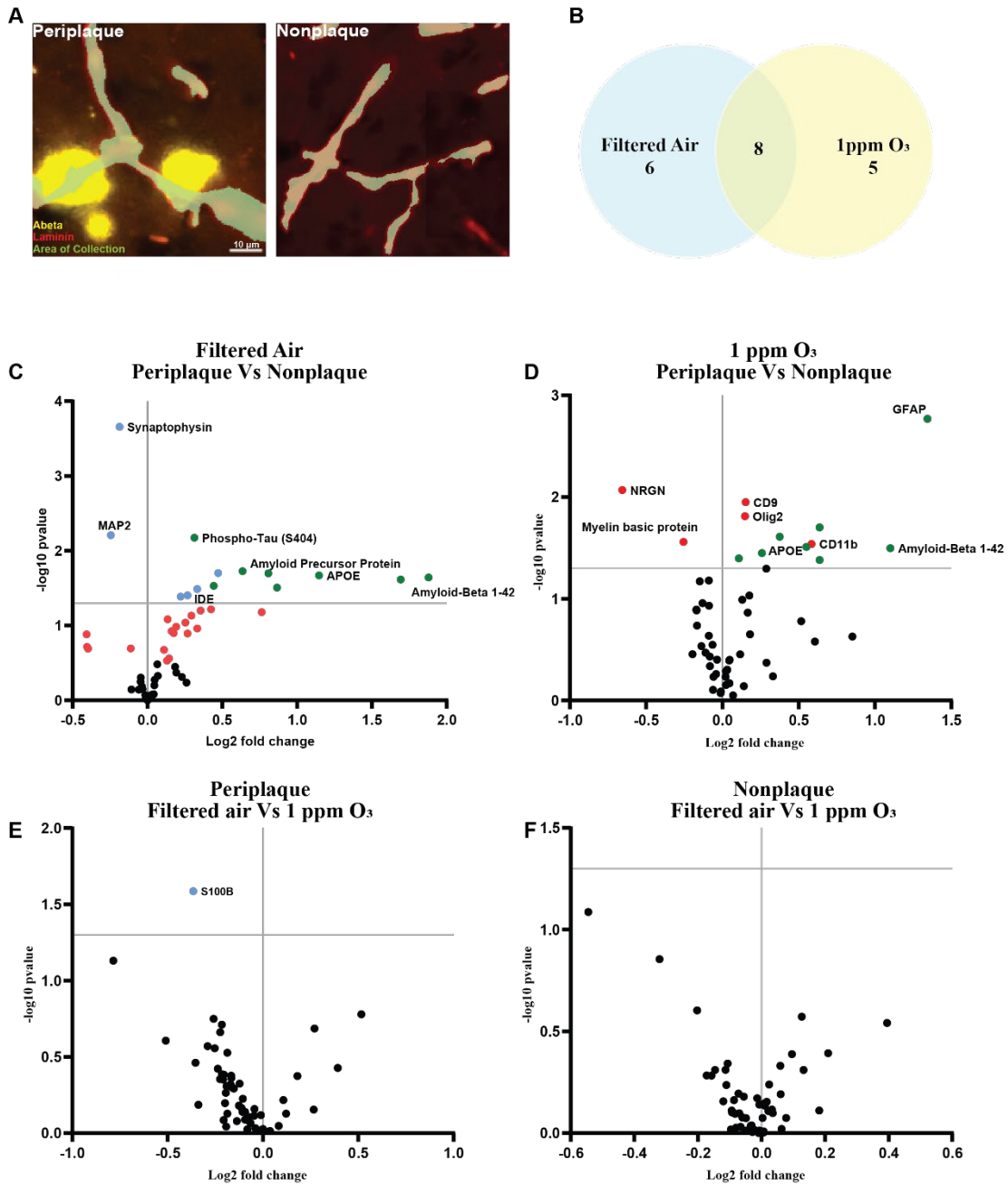


Figure 3.2: Male 5xFAD mice (10–11 weeks old) were exposed to FA or 1.0 ppm O₃ for 3 consecutive days each week for 4 hours/day for 13 weeks. (A) Representative images from the NanoString GeoMX DSP platform illustrating periplaque (left) and nonplaque vessels (right), as defined by plaque staining (A β , yellow), vessel (Laminin, red) staining, and the area from which samples were collected for analysis (green). Scale bar: 10 μ m. (B) Venn diagram showing the number of plaque environment-induced changes in the vascular proteomic profile in FA and O₃ groups, indicating protein changes shared between the two groups. Volcano plots representing differentially expressed proteins on periplaque versus plaque-distant vessels in the (C) FA and (D) O₃ groups. Volcano plots representing differentially expressed proteins on FA versus O₃ groups in the (C) periplaque and (D) nonplaque vessels. n = 96 ROIs/region per exposure group (n = 4 mice/exposure group). p < .05.

Figure 3.3: Role of VEGFA in O₃ Induced Exacerbated Amyloid Pathology.

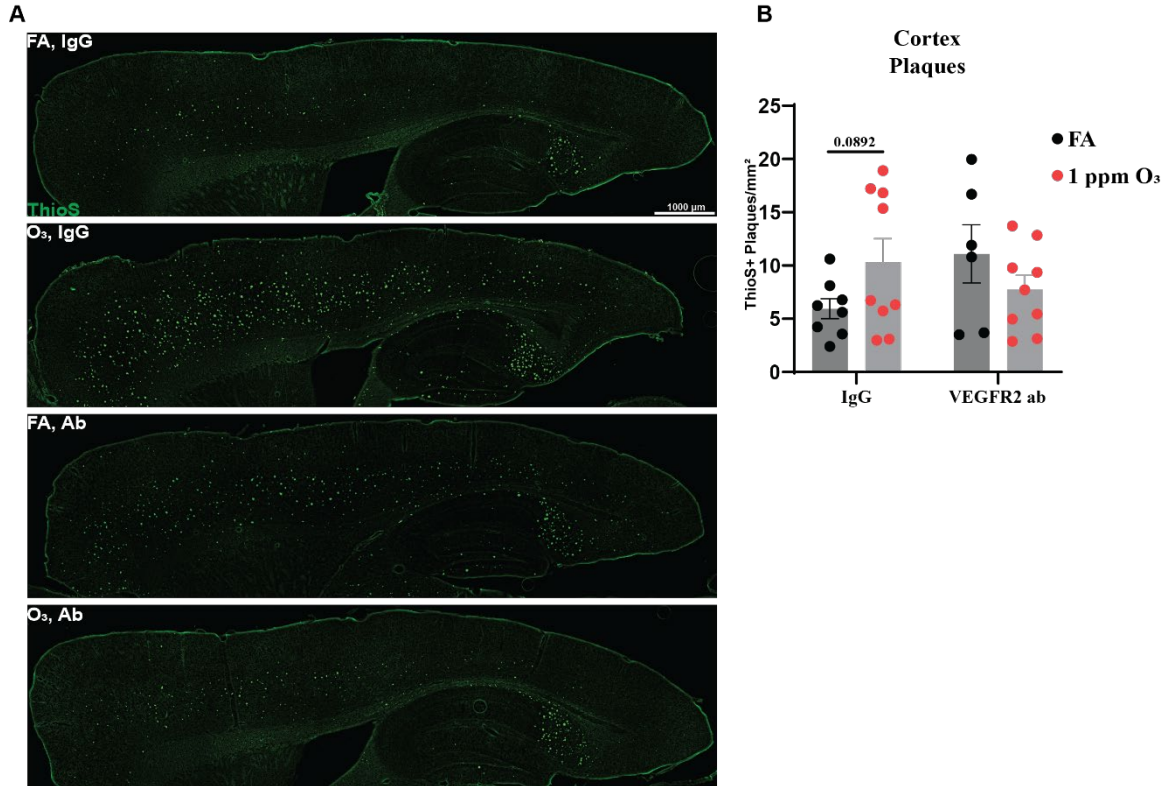


Figure 3.3: Male 5xFAD mice (10–11 weeks old) were exposed to either FA or 1.0 ppm O₃ and treated with VEGFR2ab or IgG control for 3 consecutive days each week for 4 hours/day for 10 weeks. (A) Representative 10× images depicting cortical plaques (ThioS, green). Scale bar: 1000 μm. (B) Quantification of the number of ThioS-positive plaques in the cortex. Data are represented as the mean ± SEM, n = 7–9 mice/exposure group. * = p < .05; Welch's t test.

Figure 3.4: O₃ Potentially Alters Vascular Wall-Astrocytic Association.

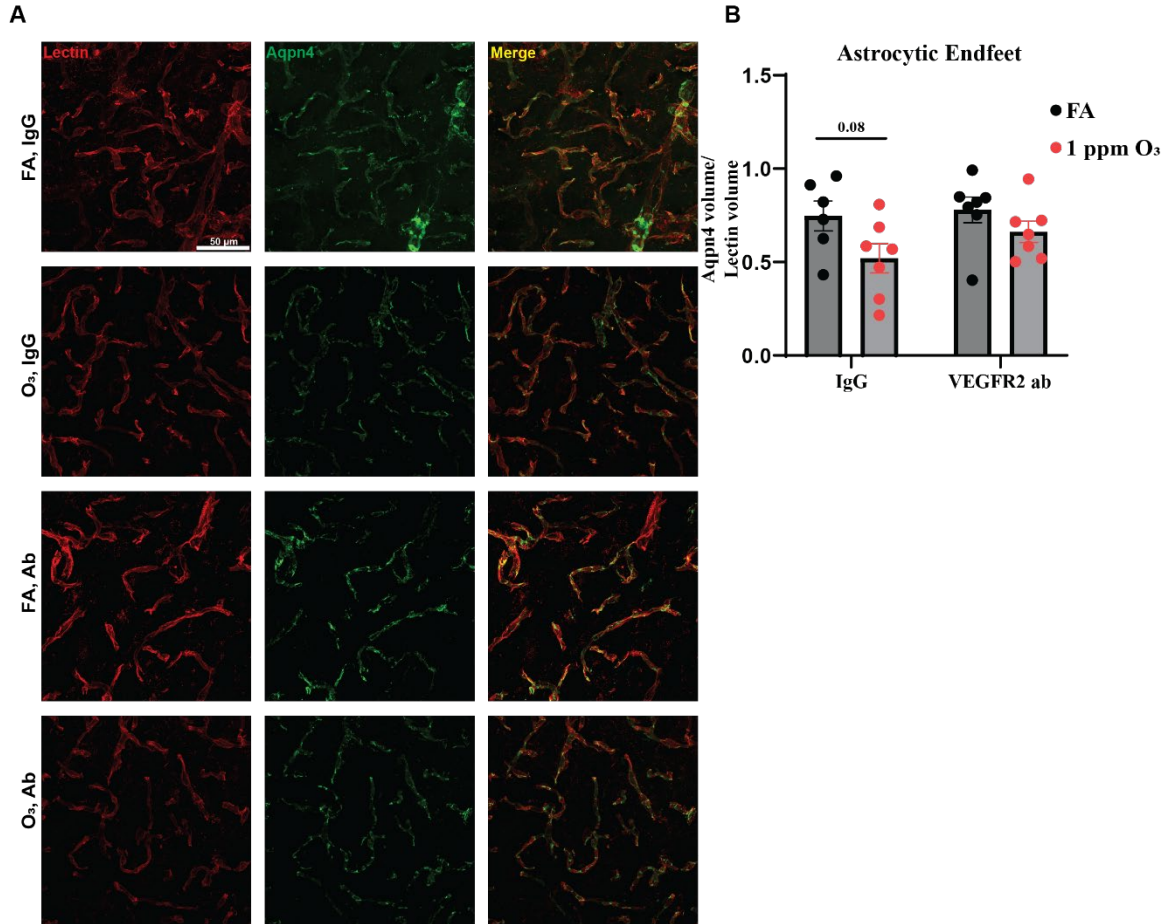


Figure 3.4: Figure 3.3: Male 5xFAD mice (10–11 weeks old) were exposed to either FA or 1.0 ppm O₃ and treated with VEGFR2ab or IgG control for 3 consecutive days each week for 4 hours/day for 10 weeks. (A) Representative 60 \times images depicting vessels (Lectin, red) and astrocytic endfeet (AQP4, green). Scale bar: 50 μ m. (B) Quantification of lectin normalized AQP4 positive area in the cortex. Data are represented as the mean \pm SEM, n = 6–8 mice/exposure group. * = p < .05; Welch's t test.

Tables

Table 3.1: List of altered proteins in GeoMx DSP assay.

Filtered Air		
Upregulated targets	Log ₂ fold change	p-value
Phospho-Tau (S404)	0.31	7E-03
Amyloid Precursor Protein	0.63	2E-02
Neurofilament light	0.47	2E-02
IBA1	0.81	2E-02
APOE	1.15	2E-02
Amyloid-Beta 1-42	1.88	2E-02
GFAP	1.69	2E-02
Ubiquitin	0.44	3E-02
CD45	0.87	3E-02
BACE1	0.33	3E-02
IDE	0.27	4E-02
Phospho-Tau (S396)	0.22	4E-02
Downregulated targets		
Synaptophysin	-0.19	2E-04
MAP2	-0.25	6E-03
O ₃ (1 ppm)		
Upregulated targets		
GFAP	1.34	2E-03
CD9	0.15	1E-02
Olig2	0.15	2E-02
CD45	0.64	2E-02

Amyloid Precursor Protein	0.38	2E-02
CD11b	0.58	3E-02
IBA1	0.55	3E-02
Amyloid-Beta 1-42	1.10	3E-02
Ubiquitin	0.26	4E-02
Phospho-Tau (S404)	0.11	4E-02
APOE	0.64	4E-02

Downregulated targets

NRGN	-0.66	9E-03
Myelin basic protein	-0.26	3E-02

CHAPTER FOUR

CONCLUSION

Alzheimer's disease (AD) pathology progression takes decades [86]. Even though considerable numbers of disease risk factors have been identified, its etiology is still largely unknown and likely involves a combinatory effect of multiple risk factors over time. Epidemiologic studies have associated air pollution with higher risk of AD incidences [8,11,12,15–17,19] and evidence from animal studies supports that air pollution exposure affects the central nervous system (CNS) [22–25,27]. However, not much is known about the mechanisms of how it affects the CNS. Rising global prevalence of air pollution [1,134,157], despite mitigation efforts, and an increasing number of population being exposed to some form of air pollution emphasizes the urgency to understand how it affects the brain.

Air pollution is a complex mixture of components, likely exerting mixed effects on human health [134,142,161]. However, to begin to understand how air pollution impact CNS physiology and influence ongoing pathology in AD we used ozone (O₃) exposure, a major component of air pollution [134,158]. Increased O₃ exposure has been implicated as a risk factor for dementia and AD [19,20]. However studies show, being a reactive gaseous element of air pollution, O₃ is unable to translocate to the CNS as it reacts in its entirety with the lung barrier lining right after inhalation [34]. Hence the lung–brain axis has been identified as a potential mechanistic pathway where it is hypothesized that the lung response to O₃ exposure modulates its CNS effects, potentially via circulating factors [22,26].

We have previously demonstrated subchronic O₃ exposure exacerbates amyloid pathology in 5xFAD mice along with dysregulating microglial association with A β plaque and promoting a differential proteomic profile in the plaque microenvironment [22]. Importantly, HMGB1, VEGF, and IL-9 were elevated in the circulation [22] providing us with potential mechanistic targets to explore as a part of the O₃ lung–brain axis.

In this dissertation, to advance our understanding of how O₃ impacts ongoing AD pathology we have identified several alterations in astrocytic and neurovascular responses to amyloid plaque deposition from O₃ exposure. We also investigated how the astrocytic dysregulation connects to the O₃ lung response and our findings show peripheral myeloid HMGB1 regulate lung immune response to O₃ exposure as well as brain disease associated astrocyte (DAA) signature gene expression, thereby implicating an important role in modulating the lung–brain axis in O₃ induced aggravated amyloid pathology. We briefly explored the potential role of VEGFA in regulating O₃ induced aggravated amyloid pathology and altered vascular phenotype and while we did not find a conclusive result, our findings demonstrate inhibiting circulating VEGFA has the potential to ameliorate some of the pathological effects.

In the first part of this project we demonstrated increased plaque burden from O₃ exposure promoted an increase in GFAP positive astrocyte density in the cortex. While this increase was equally present in periplaque and nonplaque regions, the astrocytes in the periplaque region proved to be phenotypically different as a consequence of O₃ exposure. Spatial proteomic analysis showed O₃ exposure caused a broad elimination of protein changes that occurred in response to plaque deposition in FA exposed mice in

periplaque region, thereby possibly impeding their function. Spatial transcriptomic profiling revealed an accelerated shift in the periplaque astrocytes towards a DAA phenotype, with a larger neurotoxic connotation [73]. Notably, *serpina3n*, a DAA signature gene was even further upregulated from O₃ exposure and has been implicated to impede plaque degradation [73,229]. Thus, while our data indicate increase in GFAP positive astrocyte density is potentially a consequence of the O₃ induced increased plaque number, the transcriptional shift in periplaque astrocyte implicate a contribution of these astrocytes towards increased plaque burden from O₃ exposure. Both the proteomic and transcriptomic analyses suggested O₃ increased cell-cell communication in the plaque microenvironment, an observation that has been reflected in most works throughout this project. In this case, we tested astrocyte-microglia overlap and observed O₃ increases their cell-cell overlap in periplaque region only and not in nonplaque space. While studies have shown paracrine communication between microglia and astrocyte promoted neurotoxic astrocytic phenotype [304], Rostami et. al. demonstrated physical crosstalk between astrocyte and microglia was beneficial for A β degradation [237] and hence we think suggest a compensatory role here.

The second part of the project focused on how O₃ exposure dysregulates vasculature and we demonstrated increased vascular A β deposition, similar to increased parenchymal plaque burden from O₃ exposure. This was accompanied by reduced vascular density in the plaque microenvironment, both of which (increased vascular A β , reduced vascular density) have been described in AD before [56,90]. While A β accumulation has been shown to cause to reduced vessel density and hypoxia [56], O₃ exposure aggravates the circumstance potentially exacerbating the resulting toxicity.

Which is supported by our previously reported neurite degeneration from O₃ exposure [22]. A similar pattern of functional impedance and increased cell-cell interaction with other cellular components as seen in astrocytic profiling was also reflected in vascular spatial proteomic profiling of O₃ exposed samples. Functional impedance was notable here because an increased periplaque vascular expression of IDE in the FA exposed samples was no longer visible in O₃ exposed samples. IDE being one of the important A β degradation enzymes [293], it suggests a hindrance of A β degradation and clearance mechanism.

Altered cell-cell interaction and thereby, potential communication alteration has been a common observation in this project. A large portion of physiological functions carried out by the CNS cells take place in concert with each other and on the other hand they have been shown to have deleterious effects on each other. Astrocytes and microglia have been shown to aid each other in A β degradation [237] whereas, microglia also have been shown to induce neurotoxic astrocytic phenotype [304]. Pericytes play important roles in endothelial tight junction maintenance [251], however in pathological condition, they have been shown to contribute to BBB breakdown in an APOE dependent pathway [96]. Microglia vasculature association has been shown to play a biphasic dual role, first protecting, and later diminishing the barrier function [305]. All these examples emphasize the importance of investigating the nature of altered cell-cell communication indicated in our analyses. In fact in a recent study, Sun et al reported a dynamic directional alteration of cell-cell communication between vascular and neuronal or glial cells, finding increased communication from pericyte and endothelial cells to neurons, microglia and astrocytes and decreased communication from astrocyte and neuron to

pericytes and endothelial cells [275] highlighting the need to further investigate the nature of altered cell-cell communication from O₃ exposure.

The spatial proteomic profiling provided us with valuable insight into how O₃ modifies the astrocytic and neurovascular phenotype and more importantly demonstrated it does so differentially depending on their localization with respect to plaque. However the spatial proteomic assays that shaped these insights were done with AD pathology focused panels, hence provided us with a partial and biased picture. A more comprehensive assessment of protein expression is required to gain a better understanding of O₃'s effects.

Previous data from our lab demonstrated O₃ exposure increased circulating HMGB1 in 5xFAD mice [22]. Even though we did not have any definitive proof for the source of this circulating HMGB1, we hypothesized it could be the lungs. HMGB1, being a DAMP, has been shown to be released in response to lung damage facilitating immune response supporting our hypothesis. To begin to understand the role of HMGB1 in O₃ lung–brain axis, we utilized *Hmgb1^{fl/fl}.LysM-Cre⁺* strain, with deletion of HMGB1 specifically in the peripheral myeloid cells. These myeloid cells are the dominant constituent of the infiltrating immune response in the lungs to O₃ and hence a potential source of HMGB1. O₃ exposure resulted in reduced lung immune infiltration in these mice. However, more importantly, deletion of HMGB1 specifically in the peripheral myeloid cells reduced *serpina3n* expression in the CNS. Implicating a role of HMGB1 and peripheral myeloid cells in regulating CNS response to O₃ exposure.

While this signifies a promising start in identifying HMGB1 as an important mechanistic component in lung–brain axis, and strengthens the case for lung as its

source, it does not yet provide definitive proof. In fact, it is possible for the CNS to be the source of circulating HMGB1, released from damaged neurons, since we found the significantly elevated HMGB1 only in 5xFAD and not in the non-carrier controls. We have previously shown that ongoing AD pathology enhances lung immune response to O₃ proposing a bidirectional lung–brain axis [22] and necrotic cells including neurons have been shown to release HMGB1 into extracellular space [131,306]. Cytokine like HMGB1 has been shown to stimulate macrophages to pro-inflammatory activation [116]. Hence, theoretically, CNS derived circulating HMGB1 could potentially be how ongoing AD pathology mediate enhanced lung immune response to O₃ exposure.

Regardless of the source of circulating HMGB1, deletion of HMGB1 in peripheral myeloid cells showed reduction of *serpina3n* in the brain in response to O₃ in this project, as well as *trem2* as has been previously reported [22]. In pathological condition HMGB1 has been classically considered as DAMP and its cytokine like activity has been studied [116]. However, we also need to consider HMGB1, as a transcriptional cofactor, has the potential to regulate myeloid cell behavior and thereby it can regulate the role of myeloid cells in AD pathology. More importantly, it signifies brain pathology does not always occur in isolation and it is crucial to investigate peripheral effects in a disease like AD, whose progression encompasses decades.

Transcriptional profiling of periplaque astrocytes revealed that O₃ affects many vasculature associated pathways, including pathways involved in VEGFA-VEGFR2 signaling. To test the role of VEGFA in O₃'s effect on amyloid pathology we inhibited its receptor VEGFR2 using antibody against it. Irrespective of O₃ exposure, few of these antibody treated 5xFAD mice became sick with varying symptoms. VEGFA and

VEGFR2 are both common targets in cancer research [100] and while we could not find any reports of sickness from this antibody applications, differences in treatment protocols and pre-existing tumor could have masked the antibody specific effects that we observed in 5xFAD mice. Ongoing amyloid pathology along with treatment length could also be a potential confounder.

Even though our parenchymal plaque deposition assessment from VEGFR2 inhibition did not reach statistical significance, I do not think the data conclusively invalidated a potential role of VEGFA mediated signaling in O₃ induced aggravated amyloid pathology. Further much deeper investigation is required to decipher how VEGFR2 inhibition may have caused these diverse sicknesses. However given that our data trend suggests a beneficial role of VEGFR2 inhibition, a milder and shorter treatment regimen might be worth evaluating.

Overall, our findings denote an aggravated pathology progression from O₃ exposure as evidenced by increased parenchymal and vascular A β accumulation, accelerated astrocytic transcriptional shift towards DAA phenotype, reduced vascular density in plaque microenvironment-possibly causing increased hypoxia. It suggest a worse outcome from O₃ exposure for an ongoing pathological condition. However the role of O₃ and by extension air pollution exposure in pathology initiation, how it affects astrocytic and vascular phenotype at an earlier stage of the disease before the onset of pathology needs to be explored.

This project, to our knowledge, for the first time demonstrated astrocytic dysregulation from O₃ exposure and identified astrocytes as a part of lung–brain axis, connecting peripheral myeloid modulation to brain expression of DAA signature target in

O₃ exposure. O₃ induced neurovascular damage has been shown before [150,186,187] but here we, for the first time, demonstrate the O₃ neurovascular proteomic alteration with the potential to contribute to reduced A β clearance and increased accumulation. Taken together, the findings of this project makes one important step towards fortifying our premise that air pollution increases AD risk and that lung–brain axis is an important mechanistic pathway driving this effect via identification of novel impacts of O₃ exposure on CNS cellular components. Along with detecting potential peripheral biomarkers and therapeutic targets, this project also recognizes a modifiable risk factor of AD, air pollution, and the importance of intensifying the execution of global policies curbing exposure to air pollution.

This project also highlights several gaps in our knowledge indicating much more investigations are required to further our understanding of how air pollution drives CNS pathology. However few of the future queries are highlighted below:

1. Does peripheral myeloid cell specific HMGB1 ameliorate O₃ induced aggravated amyloid pathology via crossing our existing *Hmgb1^{fl/fl}.LysM-Cre⁺* strain with 5xFAD and their subchronic O₃ exposure. Although we demonstrate peripheral HMGB1 can regulate CNS DAA specific mRNA expression, their role in continued subchronic exposure in amyloid pathology needs to be explored.
2. The nature of increased astrocyte-microglia interaction in plaque microenvironment from O₃ exposure and characterizing its role in A β accumulation or degradation.

3. Does O₃ induced neurovascular dysregulation facilitate CNS infiltration of circulating factors and peripheral myeloid cells such as neutrophils enhancing the continuing neurotoxic processes.
4. Our previous work have defined the lung–brain axis as bidirectional [22] and deep cervical lymph nodes (DCLN), where cerebrospinal fluid has been shown to drain carrying CNS antigens, is an important communicator facilitating peripheral and CNS immune crosstalk [307]. It would be interesting to explore how O₃ exposure modifies the DCLN cellular composition and its role in O₃ lung–brain axis.

REFERENCES

- [1] Murray CJL, Aravkin AY, Zheng P, Abbafati C, Abbas KM, Abbasi-Kangevari M, et al. Global burden of 87 risk factors in 204 countries and territories, 1990–2019: a systematic analysis for the Global Burden of Disease Study 2019. *The Lancet* 2020;396:1223–49. [https://doi.org/10.1016/S0140-6736\(20\)30752-2](https://doi.org/10.1016/S0140-6736(20)30752-2).
- [2] Krishna MT, Madden J, Teran LM, Biscione GL, Lau LCK, Withers NJ, et al. Effects of 0.2 ppm ozone on biomarkers of inflammation in bronchoalveolar lavage fluid and bronchial mucosa of healthy subjects. *European Respiratory Journal* 1998;11:1294–300. <https://doi.org/10.1183/09031936.98.11061294>.
- [3] Bhalla DK. OZONE-INDUCED LUNG INFLAMMATION AND MUCOSAL BARRIER DISRUPTION: TOXICOLOGY, MECHANISMS, AND IMPLICATIONS. *Journal of Toxicology and Environmental Health, Part B* 1999;2:31–86. <https://doi.org/10.1080/109374099281232>.
- [4] Lee B-J, Kim B, Lee K. Air Pollution Exposure and Cardiovascular Disease. *Toxicological Research* 2014;30:71–5. <https://doi.org/10.5487/TR.2014.30.2.071>.
- [5] Mills NL, Donaldson K, Hadoke PW, Boon NA, MacNee W, Cassee FR, et al. Adverse cardiovascular effects of air pollution. *Nat Rev Cardiol* 2009;6:36–44. <https://doi.org/10.1038/ncpcardio1399>.
- [6] Miller KA, Siscovick DS, Sheppard L, Shepherd K, Sullivan JH, Anderson GL, et al. Long-Term Exposure to Air Pollution and Incidence of Cardiovascular Events in Women. *N Engl J Med* 2007;356:447–58. <https://doi.org/10.1056/NEJMoa054409>.
- [7] Peters A, Dockery DW, Muller JE, Mittleman MA. Increased Particulate Air Pollution and the Triggering of Myocardial Infarction. *Circulation* 2001;103:2810–5. <https://doi.org/10.1161/01.CIR.103.23.2810>.
- [8] Peters R, Ee N, Peters J, Booth A, Mudway I, Anstey KJ. Air Pollution and Dementia: A Systematic Review. *JAD* 2019;70:S145–63. <https://doi.org/10.3233/JAD-180631>.
- [9] Wilker EH, Osman M, Weisskopf MG. Ambient air pollution and clinical dementia: systematic review and meta-analysis. *BMJ* 2023:e071620. <https://doi.org/10.1136/bmj-2022-071620>.
- [10] Abolhasani E, Hachinski V, Ghazaleh N, Azarpazhooh MR, Mokhber N, Martin J. Air Pollution and Incidence of Dementia: A Systematic Review and Meta-analysis. *Neurology* 2023;100. <https://doi.org/10.1212/WNL.0000000000201419>.
- [11] Shi L, Steenland K, Li H, Liu P, Zhang Y, Lyles RH, et al. A national cohort study (2000–2018) of long-term air pollution exposure and incident dementia in older

adults in the United States. *Nat Commun* 2021;12:6754.
<https://doi.org/10.1038/s41467-021-27049-2>.

- [12] Mork D, Braun D, Zanobetti A. Time-lagged relationships between a decade of air pollution exposure and first hospitalization with Alzheimer's disease and related dementias. *Environment International* 2023;171:107694.
<https://doi.org/10.1016/j.envint.2022.107694>.
- [13] Reilly AM, Tsai AP, Lin PB, Ericsson AC, Oblak AL, Ren H. Metabolic Defects Caused by High-Fat Diet Modify Disease Risk through Inflammatory and Amyloidogenic Pathways in a Mouse Model of Alzheimer's Disease. *Nutrients* 2020;12:2977. <https://doi.org/10.3390/nu12102977>.
- [14] Oblak AL, Kotredes KP, Pandey RS, Reagan AM, Ingraham C, Perkins B, et al. Plcg2M28L Interacts With High Fat/High Sugar Diet to Accelerate Alzheimer's Disease-Relevant Phenotypes in Mice. *Front Aging Neurosci* 2022;14:886575.
<https://doi.org/10.3389/fnagi.2022.886575>.
- [15] Chen H, Kwong JC, Copes R, Tu K, Villeneuve PJ, van Donkelaar A, et al. Living near major roads and the incidence of dementia, Parkinson's disease, and multiple sclerosis: a population-based cohort study. *The Lancet* 2017;389:718–26.
[https://doi.org/10.1016/S0140-6736\(16\)32399-6](https://doi.org/10.1016/S0140-6736(16)32399-6).
- [16] Gao Q, Zang E, Bi J, Dubrow R, Lowe SR, Chen H, et al. Long-term ozone exposure and cognitive impairment among Chinese older adults: A cohort study. *Environment International* 2022;160:107072.
<https://doi.org/10.1016/j.envint.2021.107072>.
- [17] Cerza F, Renzi M, Gariazzo C, Davoli M, Michelozzi P, Forastiere F, et al. Long-term exposure to air pollution and hospitalization for dementia in the Rome longitudinal study. *Environ Health* 2019;18:72. <https://doi.org/10.1186/s12940-019-0511-5>.
- [18] Morales E, Julvez J, Torrent M, De Cid R, Guxens M, Bustamante M, et al. Association of Early-life Exposure to Household Gas Appliances and Indoor Nitrogen Dioxide With Cognition and Attention Behavior in Preschoolers. *American Journal of Epidemiology* 2009;169:1327–36.
<https://doi.org/10.1093/aje/kwp067>.
- [19] Jung C-R, Lin Y-T, Hwang B-F. Ozone, Particulate Matter, and Newly Diagnosed Alzheimer's Disease: A Population-Based Cohort Study in Taiwan. *JAD* 2015;44:573–84. <https://doi.org/10.3233/JAD-140855>.
- [20] Wu Y, Lin Y, Yu H, Chen J, Chen T, Sun Y, et al. Association between air pollutants and dementia risk in the elderly. *Alzheimer's & Dementia: Diagnosis, Assessment & Disease Monitoring* 2015;1:220–8. <https://doi.org/10.1016/j.dadm.2014.11.015>.

- [21] Knopman DS, Amieva H, Petersen RC, Chételat G, Holtzman DM, Hyman BT, et al. Alzheimer disease. *Nat Rev Dis Primers* 2021;7:33. <https://doi.org/10.1038/s41572-021-00269-y>.
- [22] Greve HJ, Dunbar AL, Lombo CG, Ahmed C, Thang M, Messenger EJ, et al. The bidirectional lung brain-axis of amyloid- β pathology: ozone dysregulates the periplaque microenvironment. *Brain* 2023;146:991–1005. <https://doi.org/10.1093/brain/awac113>.
- [23] Cacciottolo M, Morgan TE, Saffari AA, Shirmohammadi F, Forman HJ, Sioutas C, et al. Traffic-related air pollutants (TRAP-PM) promote neuronal amyloidogenesis through oxidative damage to lipid rafts. *Free Radical Biology and Medicine* 2020;147:242–51. <https://doi.org/10.1016/j.freeradbiomed.2019.12.023>.
- [24] Woodward NC, Pakbin P, Saffari A, Shirmohammadi F, Haghani A, Sioutas C, et al. Traffic-related air pollution impact on mouse brain accelerates myelin and neuritic aging changes with specificity for CA1 neurons. *Neurobiology of Aging* 2017;53:48–58. <https://doi.org/10.1016/j.neurobiolaging.2017.01.007>.
- [25] Cacciottolo M, Wang X, Driscoll I, Woodward N, Saffari A, Reyes J, et al. Particulate air pollutants, APOE alleles and their contributions to cognitive impairment in older women and to amyloidogenesis in experimental models. *Transl Psychiatry* 2017;7:e1022–e1022. <https://doi.org/10.1038/tp.2016.280>.
- [26] Mumaw CL, Levesque S, McGraw C, Robertson S, Lucas S, Stafflinger JE, et al. Microglial priming through the lung–brain axis: the role of air pollution–induced circulating factors. *The FASEB Journal* 2016;30:1880–91. <https://doi.org/10.1096/fj.201500047>.
- [27] Greve HJ, Mumaw CL, Messenger EJ, Kodavanti PRS, Royland JL, Kodavanti UP, et al. Diesel exhaust impairs TREM2 to dysregulate neuroinflammation. *J Neuroinflammation* 2020;17:351. <https://doi.org/10.1186/s12974-020-02017-7>.
- [28] Erickson MA, Jude J, Zhao H, Rhea EM, Salameh TS, Jester W, et al. Serum amyloid A: an ozone-induced circulating factor with potentially important functions in the lung-brain axis. *The FASEB Journal* 2017;31:3950–65. <https://doi.org/10.1096/fj.201600857RRR>.
- [29] Adivi A, Lucero J, Simpson N, McDonald JD, Lund AK. Exposure to traffic-generated air pollution promotes alterations in the integrity of the brain microvasculature and inflammation in female ApoE^{-/-} mice. *Toxicology Letters* 2021;339:39–50. <https://doi.org/10.1016/j.toxlet.2020.12.016>.
- [30] Condello C, Yuan P, Schain A, Grutzendler J. Microglia constitute a barrier that prevents neurotoxic protofibrillar A β 42 hotspots around plaques. *Nat Commun* 2015;6:6176. <https://doi.org/10.1038/ncomms7176>.

- [31] Chen W-T, Lu A, Craessaerts K, Pavie B, Sala Frigerio C, Corthout N, et al. Spatial Transcriptomics and In Situ Sequencing to Study Alzheimer's Disease. *Cell* 2020;182:976-991.e19. <https://doi.org/10.1016/j.cell.2020.06.038>.
- [32] Das S, Li Z, Wachter A, Alla S, Noori A, Abdourahman A, et al. Distinct transcriptomic responses to A β plaques, neurofibrillary tangles, and *APOE* in Alzheimer's disease. *Alzheimer's & Dementia* 2024;20:74-90. <https://doi.org/10.1002/alz.13387>.
- [33] Oakley H, Cole SL, Logan S, Maus E, Shao P, Craft J, et al. Intraneuronal beta-Amyloid Aggregates, Neurodegeneration, and Neuron Loss in Transgenic Mice with Five Familial Alzheimer's Disease Mutations: Potential Factors in Amyloid Plaque Formation. *Journal of Neuroscience* 2006;26:10129-40. <https://doi.org/10.1523/JNEUROSCI.1202-06.2006>.
- [34] Pryor WA. How far does ozone penetrate into the pulmonary air/tissue boundary before it reacts? *Free Radical Biology and Medicine* 1992;12:83-8. [https://doi.org/10.1016/0891-5849\(92\)90060-T](https://doi.org/10.1016/0891-5849(92)90060-T).
- [35] Gustavsson A, Norton N, Fast T, Frölich L, Georges J, Holzapfel D, et al. Global estimates on the number of persons across the Alzheimer's disease continuum. *Alzheimer's & Dementia* 2023;19:658-70. <https://doi.org/10.1002/alz.12694>.
- [36] Rajan KB, Weuve J, Barnes LL, McAninch EA, Wilson RS, Evans DA. Population estimate of people with clinical Alzheimer's disease and mild cognitive impairment in the United States (2020-2060). *Alzheimer's & Dementia* 2021;17:1966-75. <https://doi.org/10.1002/alz.12362>.
- [37] 2023 Alzheimer's disease facts and figures. *Alzheimer's & Dementia* 2023;19:1598-695. <https://doi.org/10.1002/alz.13016>.
- [38] Hippus H, Neundörfer G. The discovery of Alzheimer's disease. *Dialogues in Clinical Neuroscience* 2003;5:101-8. <https://doi.org/10.31887/DCNS.2003.5.1/hhippius>.
- [39] De Strooper B, Karran E. The Cellular Phase of Alzheimer's Disease. *Cell* 2016;164:603-15. <https://doi.org/10.1016/j.cell.2015.12.056>.
- [40] Perrin RJ, Fagan AM, Holtzman DM. Multimodal techniques for diagnosis and prognosis of Alzheimer's disease. *Nature* 2009;461:916-22. <https://doi.org/10.1038/nature08538>.
- [41] Therriault J, Zimmer ER, Benedet AL, Pascoal TA, Gauthier S, Rosa-Neto P. Staging of Alzheimer's disease: past, present, and future perspectives. *Trends in Molecular Medicine* 2022;28:726-41. <https://doi.org/10.1016/j.molmed.2022.05.008>.

- [42] Porsteinsson AP, Isaacson RS, Knox S, Sabbagh MN, Rubino I. Diagnosis of Early Alzheimer's Disease: Clinical Practice in 2021. *J Prev Alz Dis* 2021;1–16. <https://doi.org/10.14283/jpad.2021.23>.
- [43] Carter SF, Herholz K, Rosa-Neto P, Pellerin L, Nordberg A, Zimmer ER. Astrocyte Biomarkers in Alzheimer's Disease. *Trends in Molecular Medicine* 2019;25:77–95. <https://doi.org/10.1016/j.molmed.2018.11.006>.
- [44] Arranz AM, De Strooper B. The role of astroglia in Alzheimer's disease: pathophysiology and clinical implications. *The Lancet Neurology* 2019;18:406–14. [https://doi.org/10.1016/S1474-4422\(18\)30490-3](https://doi.org/10.1016/S1474-4422(18)30490-3).
- [45] Den Braber A, Verberk IMW, Tomassen J, Den Dulk B, Stoops E, Dage JL, et al. Plasma biomarkers predict amyloid pathology in cognitively normal monozygotic twins after 10 years. *Brain Communications* 2022;5:fcad024. <https://doi.org/10.1093/braincomms/fcad024>.
- [46] Wang S, Mustafa M, Yuede CM, Salazar SV, Kong P, Long H, et al. Anti-human TREM2 induces microglia proliferation and reduces pathology in an Alzheimer's disease model. *Journal of Experimental Medicine* 2020;217:e20200785. <https://doi.org/10.1084/jem.20200785>.
- [47] Althafar ZM. Targeting Microglia in Alzheimer's Disease: From Molecular Mechanisms to Potential Therapeutic Targets for Small Molecules. *Molecules* 2022;27:4124. <https://doi.org/10.3390/molecules27134124>.
- [48] Jiwaji Z, Tiwari SS, Avilés-Reyes RX, Hooley M, Hampton D, Torvell M, et al. Reactive astrocytes acquire neuroprotective as well as deleterious signatures in response to Tau and A β pathology. *Nat Commun* 2022;13:135. <https://doi.org/10.1038/s41467-021-27702-w>.
- [49] Keren-Shaul H, Spinrad A, Weiner A, Matcovitch-Natan O, Dvir-Szternfeld R, Ulland TK, et al. A Unique Microglia Type Associated with Restricting Development of Alzheimer's Disease. *Cell* 2017;169:1276-1290.e17. <https://doi.org/10.1016/j.cell.2017.05.018>.
- [50] Wang Y, Ulland TK, Ulrich JD, Song W, Tzaferis JA, Hole JT, et al. TREM2-mediated early microglial response limits diffusion and toxicity of amyloid plaques. *Journal of Experimental Medicine* 2016;213:667–75. <https://doi.org/10.1084/jem.20151948>.
- [51] Thal DR. The role of astrocytes in amyloid β -protein toxicity and clearance. *Experimental Neurology* 2012;236:1–5. <https://doi.org/10.1016/j.expneurol.2012.04.021>.
- [52] Chun H, Lee CJ. Reactive astrocytes in Alzheimer's disease: A double-edged sword. *Neuroscience Research* 2018;126:44–52. <https://doi.org/10.1016/j.neures.2017.11.012>.

- [53] Xie Z, Meng J, Wu Z, Nakanishi H, Hayashi Y, Kong W, et al. The Dual Nature of Microglia in Alzheimer's Disease: A Microglia-Neuron Crosstalk Perspective. *Neuroscientist* 2023;29:616–38. <https://doi.org/10.1177/10738584211070273>.
- [54] Hansen DV, Hanson JE, Sheng M. Microglia in Alzheimer's disease. *The Journal of Cell Biology* 2018;217:459–72. <https://doi.org/10.1083/jcb.201709069>.
- [55] Mosher KI, Wyss-Coray T. Microglial dysfunction in brain aging and Alzheimer's disease. *Biochemical Pharmacology* 2014;88:594–604. <https://doi.org/10.1016/j.bcp.2014.01.008>.
- [56] Zlokovic BV. Neurovascular pathways to neurodegeneration in Alzheimer's disease and other disorders. *Nat Rev Neurosci* 2011;12:723–38. <https://doi.org/10.1038/nrn3114>.
- [57] Bell RD, Zlokovic BV. Neurovascular mechanisms and blood–brain barrier disorder in Alzheimer's disease. *Acta Neuropathologica* 2009;118:103–13. <https://doi.org/10.1007/s00401-009-0522-3>.
- [58] Sarlus H, Heneka MT. Microglia in Alzheimer's disease. *Journal of Clinical Investigation* 2017;127:3240–9. <https://doi.org/10.1172/JCI90606>.
- [59] Kim J, Yoo ID, Lim J, Moon J-S. Pathological phenotypes of astrocytes in Alzheimer's disease. *Exp Mol Med* 2024;56:95–9. <https://doi.org/10.1038/s12276-023-01148-0>.
- [60] Sweeney MD, Kisler K, Montagne A, Toga AW, Zlokovic BV. The role of brain vasculature in neurodegenerative disorders. *Nat Neurosci* 2018;21:1318–31. <https://doi.org/10.1038/s41593-018-0234-x>.
- [61] Sweeney MD, Sagare AP, Zlokovic BV. Blood–brain barrier breakdown in Alzheimer disease and other neurodegenerative disorders. *Nature Reviews Neurology* 2018;14:133–50. <https://doi.org/10.1038/nrneurol.2017.188>.
- [62] Kim Y, Park J, Choi YK. The Role of Astrocytes in the Central Nervous System Focused on BK Channel and Heme Oxygenase Metabolites: A Review. *Antioxidants* 2019;8:121. <https://doi.org/10.3390/antiox8050121>.
- [63] Eroglu C, Barres BA. Regulation of synaptic connectivity by glia. *Nature* 2010;468:223–31. <https://doi.org/10.1038/nature09612>.
- [64] Lee H-G, Wheeler MA, Quintana FJ. Function and therapeutic value of astrocytes in neurological diseases. *Nat Rev Drug Discov* 2022;21:339–58. <https://doi.org/10.1038/s41573-022-00390-x>.
- [65] Kisler K, Nelson AR, Montagne A, Zlokovic BV. Cerebral blood flow regulation and neurovascular dysfunction in Alzheimer disease. *Nat Rev Neurosci* 2017;18:419–34. <https://doi.org/10.1038/nrn.2017.48>.

- [66] Hösli L, Zuend M, Bredell G, Zanker HS, Porto De Oliveira CE, Saab AS, et al. Direct vascular contact is a hallmark of cerebral astrocytes. *Cell Reports* 2022;39:110599. <https://doi.org/10.1016/j.celrep.2022.110599>.
- [67] Lee H-G, Lee J-H, Flausino LE, Quintana FJ. Neuroinflammation: An astrocyte perspective. *Sci Transl Med* 2023;15:eadi7828. <https://doi.org/10.1126/scitranslmed.adi7828>.
- [68] Langen UH, Ayloo S, Gu C. Development and Cell Biology of the Blood-Brain Barrier. *Annu Rev Cell Dev Biol* 2019;35:591–613. <https://doi.org/10.1146/annurev-cellbio-100617-062608>.
- [69] Iliff JJ, Wang M, Liao Y, Plogg BA, Peng W, Gundersen GA, et al. A Paravascular Pathway Facilitates CSF Flow Through the Brain Parenchyma and the Clearance of Interstitial Solutes, Including Amyloid β . *Sci Transl Med* 2012;4. <https://doi.org/10.1126/scitranslmed.3003748>.
- [70] Rasmussen MK, Mestre H, Nedergaard M. The glymphatic pathway in neurological disorders. *The Lancet Neurology* 2018;17:1016–24. [https://doi.org/10.1016/S1474-4422\(18\)30318-1](https://doi.org/10.1016/S1474-4422(18)30318-1).
- [71] Hussain R, Graham U, Elder A, Nedergaard M. Air pollution, glymphatic impairment, and Alzheimer’s disease. *Trends in Neurosciences* 2023;46:901–11. <https://doi.org/10.1016/j.tins.2023.08.010>.
- [72] Olsen M, Aguilar X, Sehlin D, Fang XT, Antoni G, Erlandsson A, et al. Astroglial Responses to Amyloid-Beta Progression in a Mouse Model of Alzheimer’s Disease. *Mol Imaging Biol* 2018;20:605–14. <https://doi.org/10.1007/s11307-017-1153-z>.
- [73] Habib N, McCabe C, Medina S, Varshavsky M, Kitsberg D, Dvir-Szternfeld R, et al. Disease-associated astrocytes in Alzheimer’s disease and aging. *Nat Neurosci* 2020;23:701–6. <https://doi.org/10.1038/s41593-020-0624-8>.
- [74] Apelt J, Ach K, Schliebs R. Aging-related down-regulation of neprilysin, a putative β -amyloid-degrading enzyme, in transgenic Tg2576 Alzheimer-like mouse brain is accompanied by an astroglial upregulation in the vicinity of β -amyloid plaques. *Neuroscience Letters* 2003;339:183–6. [https://doi.org/10.1016/S0304-3940\(03\)00030-2](https://doi.org/10.1016/S0304-3940(03)00030-2).
- [75] Leal MC, Dorfman VB, Gamba AF, Frangione B, Wisniewski T, Castaño EM, et al. Plaque-Associated Overexpression of Insulin-Degrading Enzyme in the Cerebral Cortex of Aged Transgenic Tg2576 Mice With Alzheimer Pathology: *Journal of Neuropathology and Experimental Neurology* 2006;65:976–87. <https://doi.org/10.1097/01.jnen.0000235853.70092.ba>.
- [76] Dorfman VB, Pasquini L, Riudavets M, López-Costa JJ, Villegas A, Troncoso JC, et al. Differential cerebral deposition of IDE and NEP in sporadic and familial

Alzheimer's disease. *Neurobiology of Aging* 2010;31:1743–57.
<https://doi.org/10.1016/j.neurobiolaging.2008.09.016>.

- [77] Abramov AY, Canevari L, Duchen MR. Changes in Intracellular Calcium and Glutathione in Astrocytes as the Primary Mechanism of Amyloid Neurotoxicity. *J Neurosci* 2003;23:5088–95. <https://doi.org/10.1523/JNEUROSCI.23-12-05088.2003>.
- [78] Alberdi E, Wyssenbach A, Alberdi M, Sánchez-Gómez MV, Cavaliere F, Rodríguez JJ, et al. Ca²⁺-dependent endoplasmic reticulum stress correlates with astrogliosis in oligomeric amyloid β -treated astrocytes and in a model of Alzheimer's disease. *Aging Cell* 2013;12:292–302.
<https://doi.org/10.1111/accel.12054>.
- [79] Zhao J, O'Connor T, Vassar R. The contribution of activated astrocytes to A β production: Implications for Alzheimer's disease pathogenesis. *J Neuroinflammation* 2011;8:150. <https://doi.org/10.1186/1742-2094-8-150>.
- [80] Matos M, Augusto E, Machado NJ, Dos Santos-Rodrigues A, Cunha RA, Agostinho P. Astrocytic Adenosine A2A Receptors Control the Amyloid- β Peptide-Induced Decrease of Glutamate Uptake. *JAD* 2012;31:555–67.
<https://doi.org/10.3233/JAD-2012-120469>.
- [81] Peters O, Schipke CG, Philipps A, Haas B, Pannasch U, Wang LP, et al. Astrocyte Function is Modified by Alzheimer's Disease-like Pathology in Aged Mice. *JAD* 2009;18:177–89. <https://doi.org/10.3233/JAD-2009-1140>.
- [82] Masliah E, Alford M, Mallory M, Rockenstein E, Moechars D, Van Leuven F. Abnormal Glutamate Transport Function in Mutant Amyloid Precursor Protein Transgenic Mice. *Experimental Neurology* 2000;163:381–7.
<https://doi.org/10.1006/exnr.2000.7386>.
- [83] Huang S, Tong H, Lei M, Zhou M, Guo W, Li G, et al. Astrocytic glutamatergic transporters are involved in A β -induced synaptic dysfunction. *Brain Research* 2018;1678:129–37. <https://doi.org/10.1016/j.brainres.2017.10.011>.
- [84] Koistinaho M, Lin S, Wu X, Esterman M, Koger D, Hanson J, et al. Apolipoprotein E promotes astrocyte colocalization and degradation of deposited amyloid- β peptides. *Nat Med* 2004;10:719–26. <https://doi.org/10.1038/nm1058>.
- [85] Wildsmith KR, Holley M, Savage JC, Skerrett R, Landreth GE. Evidence for impaired amyloid β clearance in Alzheimer's disease. *Alzheimers Res Ther* 2013;5:33. <https://doi.org/10.1186/alzrt187>.
- [86] Masters CL, Bateman R, Blennow K, Rowe CC, Sperling RA, Cummings JL. Alzheimer's disease. *Nat Rev Dis Primers* 2015;1:15056.
<https://doi.org/10.1038/nrdp.2015.56>.

- [87] Sadick JS, O’Dea MR, Hasel P, Dykstra T, Faustin A, Liddelw SA. Astrocytes and oligodendrocytes undergo subtype-specific transcriptional changes in Alzheimer’s disease. *Neuron* 2022;110:1788-1805.e10. <https://doi.org/10.1016/j.neuron.2022.03.008>.
- [88] Dai DL, Li M, Lee EB. Human Alzheimer’s disease reactive astrocytes exhibit a loss of homeostatic gene expression. *Acta Neuropathol Commun* 2023;11:127. <https://doi.org/10.1186/s40478-023-01624-8>.
- [89] Grubman A, Chew G, Ouyang JF, Sun G, Choo XY, McLean C, et al. A single-cell atlas of entorhinal cortex from individuals with Alzheimer’s disease reveals cell-type-specific gene expression regulation. *Nat Neurosci* 2019;22:2087–97. <https://doi.org/10.1038/s41593-019-0539-4>.
- [90] Fisher RA, Miners JS, Love S. Pathological changes within the cerebral vasculature in Alzheimer’s disease: New perspectives. *Brain Pathology* 2022;32:e13061. <https://doi.org/10.1111/bpa.13061>.
- [91] Park R, Kook S-Y, Park J-C, Mook-Jung I. A β 1–42 reduces P-glycoprotein in the blood–brain barrier through RAGE–NF- κ B signaling. *Cell Death Dis* 2014;5:e1299–e1299. <https://doi.org/10.1038/cddis.2014.258>.
- [92] Deane R, Du Yan S, Subramanian RK, LaRue B, Jovanovic S, Hogg E, et al. RAGE mediates amyloid- β peptide transport across the blood-brain barrier and accumulation in brain. *Nat Med* 2003;9:907–13. <https://doi.org/10.1038/nm890>.
- [93] Greenberg SM, Bacskai BJ, Hernandez-Guillamon M, Pruzin J, Sperling R, van Veluw SJ. Cerebral amyloid angiopathy and Alzheimer disease — one peptide, two pathways. *Nature Reviews Neurology* 2020;16:30–42. <https://doi.org/10.1038/s41582-019-0281-2>.
- [94] Yang AC, Vest RT, Kern F, Lee DP, Agam M, Maat CA, et al. A human brain vascular atlas reveals diverse mediators of Alzheimer’s risk. *Nature* 2022;603:885–92. <https://doi.org/10.1038/s41586-021-04369-3>.
- [95] Bell RD, Winkler EA, Sagare AP, Singh I, LaRue B, Deane R, et al. Pericytes Control Key Neurovascular Functions and Neuronal Phenotype in the Adult Brain and during Brain Aging. *Neuron* 2010;68:409–27. <https://doi.org/10.1016/j.neuron.2010.09.043>.
- [96] Bell RD, Winkler EA, Singh I, Sagare AP, Deane R, Wu Z, et al. Apolipoprotein E controls cerebrovascular integrity via cyclophilin A. *Nature* 2012;485:512–6. <https://doi.org/10.1038/nature11087>.
- [97] Argaw AT, Asp L, Zhang J, Navrazhina K, Pham T, Mariani JN, et al. Astrocyte-derived VEGF-A drives blood-brain barrier disruption in CNS inflammatory disease. *J Clin Invest* 2012;122:2454–68. <https://doi.org/10.1172/JCI60842>.

- [98] Li Y, Pan R, Qin X, Yang W, Qi Z, Liu W, et al. Ischemic neurons activate astrocytes to disrupt endothelial barrier via increasing VEGF expression. *Journal of Neurochemistry* 2014;129:120–9. <https://doi.org/10.1111/jnc.12611>.
- [99] Wang W, Dentler WL, Borchardt RT. VEGF increases BMEC monolayer permeability by affecting occludin expression and tight junction assembly. *American Journal of Physiology-Heart and Circulatory Physiology* 2001;280:H434–40. <https://doi.org/10.1152/ajpheart.2001.280.1.H434>.
- [100] Apte RS, Chen DS, Ferrara N. VEGF in Signaling and Disease: Beyond Discovery and Development. *Cell* 2019;176:1248–64. <https://doi.org/10.1016/j.cell.2019.01.021>.
- [101] Lange C, Storkebaum E, De Almodóvar CR, Dewerchin M, Carmeliet P. Vascular endothelial growth factor: a neurovascular target in neurological diseases. *Nat Rev Neurol* 2016;12:439–54. <https://doi.org/10.1038/nrneurol.2016.88>.
- [102] Jeon SG, Lee H, Park H, Han K-M, Hoe H-S. The VEGF inhibitor vatalanib regulates AD pathology in 5xFAD mice. *Mol Brain* 2020;13:131. <https://doi.org/10.1186/s13041-020-00673-7>.
- [103] Ali M, Bracko O. VEGF Paradoxically Reduces Cerebral Blood Flow in Alzheimer’s Disease Mice. *J Exp Neurosci* 2022;17:263310552211092. <https://doi.org/10.1177/26331055221109254>.
- [104] Ali M, Falkenhain K, Njiru BN, Murtaza-Ali M, Ruiz-Urbe NE, Haft-Javaherian M, et al. VEGF signalling causes stalls in brain capillaries and reduces cerebral blood flow in Alzheimer’s mice. *Brain* 2022;145:1449–63. <https://doi.org/10.1093/brain/awab387>.
- [105] Religa P, Cao R, Religa D, Xue Y, Bogdanovic N, Westaway D, et al. VEGF significantly restores impaired memory behavior in Alzheimer’s mice by improvement of vascular survival. *Sci Rep* 2013;3:2053. <https://doi.org/10.1038/srep02053>.
- [106] Herrán E, Pérez-González R, Igartua M, Pedraz JL, Carro E, Hernández RM. VEGF-releasing biodegradable nanospheres administered by craniotomy: A novel therapeutic approach in the APP/Ps1 mouse model of Alzheimer’s disease. *Journal of Controlled Release* 2013;170:111–9. <https://doi.org/10.1016/j.jconrel.2013.04.028>.
- [107] Hohman TJ, Bell SP, Jefferson AL. The Role of Vascular Endothelial Growth Factor in Neurodegeneration and Cognitive Decline: Exploring Interactions With Biomarkers of Alzheimer Disease. *JAMA Neurol* 2015;72:520. <https://doi.org/10.1001/jamaneurol.2014.4761>.

- [108] Hu Y, Zheng Y, Wang T, Jiao L, Luo Y. VEGF, a Key Factor for Blood Brain Barrier Injury After Cerebral Ischemic Stroke. *Aging and Disease* 2022;13:647. <https://doi.org/10.14336/AD.2021.1121>.
- [109] Muñoz-Castro C, Mejias-Ortega M, Sanchez-Mejias E, Navarro V, Trujillo-Estrada L, Jimenez S, et al. Monocyte-derived cells invade brain parenchyma and amyloid plaques in human Alzheimer's disease hippocampus. *Acta Neuropathol Commun* 2023;11:31. <https://doi.org/10.1186/s40478-023-01530-z>.
- [110] Reed-Geaghan EG, Croxford AL, Becher B, Landreth GE. Plaque-associated myeloid cells derive from resident microglia in an Alzheimer's disease model. *Journal of Experimental Medicine* 2020;217:e20191374. <https://doi.org/10.1084/jem.20191374>.
- [111] Fernández Zapata C, Giacomello G, Spruth EJ, Middeldorp J, Gallaccio G, Dehlinger A, et al. Differential compartmentalization of myeloid cell phenotypes and responses towards the CNS in Alzheimer's disease. *Nat Commun* 2022;13:7210. <https://doi.org/10.1038/s41467-022-34719-2>.
- [112] Thome AD, Faridar A, Beers DR, Thonhoff JR, Zhao W, Wen S, et al. Functional alterations of myeloid cells during the course of Alzheimer's disease. *Mol Neurodegeneration* 2018;13:61. <https://doi.org/10.1186/s13024-018-0293-1>.
- [113] Smyth LCD, Murray HC, Hill M, Van Leeuwen E, Highet B, Magon NJ, et al. Neutrophil-vascular interactions drive myeloperoxidase accumulation in the brain in Alzheimer's disease. *Acta Neuropathol Commun* 2022;10:38. <https://doi.org/10.1186/s40478-022-01347-2>.
- [114] Cruz Hernández JC, Bracko O, Kersbergen CJ, Muse V, Haft-Javaherian M, Berg M, et al. Neutrophil adhesion in brain capillaries reduces cortical blood flow and impairs memory function in Alzheimer's disease mouse models. *Nat Neurosci* 2019;22:413–20. <https://doi.org/10.1038/s41593-018-0329-4>.
- [115] Zenaro E, Pietronigro E, Bianca VD, Piacentino G, Marongiu L, Budui S, et al. Neutrophils promote Alzheimer's disease-like pathology and cognitive decline via LFA-1 integrin. *Nat Med* 2015;21:880–6. <https://doi.org/10.1038/nm.3913>.
- [116] Lotze MT, Tracey KJ. High-mobility group box 1 protein (HMGB1): nuclear weapon in the immune arsenal. *Nat Rev Immunol* 2005;5:331–42. <https://doi.org/10.1038/nri1594>.
- [117] Sims GP, Rowe DC, Rietdijk ST, Herbst R, Coyle AJ. HMGB1 and RAGE in Inflammation and Cancer. *Annu Rev Immunol* 2010;28:367–88. <https://doi.org/10.1146/annurev.immunol.021908.132603>.
- [118] Chen R, Kang R, Tang D. The mechanism of HMGB1 secretion and release. *Exp Mol Med* 2022;54:91–102. <https://doi.org/10.1038/s12276-022-00736-w>.

- [119] Yang H, Antoine DJ, Andersson U, Tracey KJ. The many faces of HMGB1: molecular structure-functional activity in inflammation, apoptosis, and chemotaxis. *Journal of Leukocyte Biology* 2013;93:865–73. <https://doi.org/10.1189/jlb.1212662>.
- [120] Paudel YN, Angelopoulou E, Piperi C, Othman I, Aamir K, Shaikh MohdF. Impact of HMGB1, RAGE, and TLR4 in Alzheimer’s Disease (AD): From Risk Factors to Therapeutic Targeting. *Cells* 2020;9:383. <https://doi.org/10.3390/cells9020383>.
- [121] Kazama H, Ricci J-E, Herndon JM, Hoppe G, Green DR, Ferguson TA. Induction of Immunological Tolerance by Apoptotic Cells Requires Caspase-Dependent Oxidation of High-Mobility Group Box-1 Protein. *Immunity* 2008;29:21–32. <https://doi.org/10.1016/j.immuni.2008.05.013>.
- [122] Bonaldi T. Monocytic cells hyperacetylate chromatin protein HMGB1 to redirect it towards secretion. *The EMBO Journal* 2003;22:5551–60. <https://doi.org/10.1093/emboj/cdg516>.
- [123] Chen G, Li J, Ochani M, Rendon-Mitchell B, Qiang X, Susarla S, et al. Bacterial endotoxin stimulates macrophages to release HMGB1 partly through CD14- and TNF-dependent mechanisms. *Journal of Leukocyte Biology* 2004;76:994–1001. <https://doi.org/10.1189/jlb.0404242>.
- [124] Lutz W, Stetkiewicz J. High mobility group box 1 protein as a late-acting mediator of acute lung inflammation. *Int J Occup Med Environ Health* 2004;17:245–54.
- [125] Ueno H, Matsuda T, Hashimoto S, Amaya F, Kitamura Y, Tanaka M, et al. Contributions of High Mobility Group Box Protein in Experimental and Clinical Acute Lung Injury. *Am J Respir Crit Care Med* 2004;170:1310–6. <https://doi.org/10.1164/rccm.200402-188OC>.
- [126] Abraham E, Arcaroli J, Carmody A, Wang H, Tracey KJ. Cutting Edge: HMG-1 as a Mediator of Acute Lung Inflammation. *The Journal of Immunology* 2000;165:2950–4. <https://doi.org/10.4049/jimmunol.165.6.2950>.
- [127] Festoff BW, Sajja RK, van Dreden P, Cucullo L. HMGB1 and thrombin mediate the blood-brain barrier dysfunction acting as biomarkers of neuroinflammation and progression to neurodegeneration in Alzheimer’s disease. *Journal of Neuroinflammation* 2016;13. <https://doi.org/10.1186/s12974-016-0670-z>.
- [128] Takata K, Kitamura Y, Tsuchiya D, Kawasaki T, Taniguchi T, Shimohama S. High mobility group box protein-1 inhibits microglial A β clearance and enhances A β neurotoxicity. *J of Neuroscience Research* 2004;78:880–91. <https://doi.org/10.1002/jnr.20340>.
- [129] Takata K, Takada T, Ito A, Asai M, Tawa M, Saito Y, et al. Microglial Amyloid- β 1-40 Phagocytosis Dysfunction Is Caused by High-Mobility Group Box Protein-1: Implications for the Pathological Progression of Alzheimer’s Disease. *International*

Journal of Alzheimer's Disease 2012;2012:1–11.
<https://doi.org/10.1155/2012/685739>.

- [130] Tanaka H, Kondo K, Fujita K, Homma H, Tagawa K, Jin X, et al. HMGB1 signaling phosphorylates Ku70 and impairs DNA damage repair in Alzheimer's disease pathology. *Commun Biol* 2021;4:1175. <https://doi.org/10.1038/s42003-021-02671-4>.
- [131] Fujita K, Motoki K, Tagawa K, Chen X, Hama H, Nakajima K, et al. HMGB1, a pathogenic molecule that induces neurite degeneration via TLR4-MARCKS, is a potential therapeutic target for Alzheimer's disease. *Scientific Reports* 2016;6. <https://doi.org/10.1038/srep31895>.
- [132] Gulmammadli N, Konukoğlu D, Merve Kurtuluş E, Tezen D, Ibrahim Erbay M, Bozluoğlu M. Serum Sirtuin-1, HMGB1-TLR4, NF-KB and IL-6 Levels in Alzheimer's: The Relation Between Neuroinflammatory Pathway and Severity of Dementia. *CAR* 2022;19:841–8. <https://doi.org/10.2174/1567205020666221226140721>.
- [133] Boogaard H, Walker K, Cohen AJ. Air pollution: the emergence of a major global health risk factor. *International Health* 2019;11:417–21. <https://doi.org/10.1093/inthealth/ihz078>.
- [134] WHO global air quality guidelines. Geneva: WHO; 2021.
- [135] Zhang B, Weuve J, Langa KM, D'Souza J, Szpiro A, Faul J, et al. Comparison of Particulate Air Pollution From Different Emission Sources and Incident Dementia in the US. *JAMA Intern Med* 2023;183:1080. <https://doi.org/10.1001/jamainternmed.2023.3300>.
- [136] Calderón-Garcidueñas L, Solt AC, Henríquez-Roldán C, Torres-Jardón R, Nuse B, Herritt L, et al. Long-term Air Pollution Exposure Is Associated with Neuroinflammation, an Altered Innate Immune Response, Disruption of the Blood-Brain Barrier, Ultrafine Particulate Deposition, and Accumulation of Amyloid β -42 and α -Synuclein in Children and Young Adults. *Toxicol Pathol* 2008;36:289–310. <https://doi.org/10.1177/0192623307313011>.
- [137] Calderón-Garcidueñas L, Kavanaugh M, Block M, D'Angiulli A, Delgado-Chávez R, Torres-Jardón R, et al. Neuroinflammation, Hyperphosphorylated Tau, Diffuse Amyloid Plaques, and Down-Regulation of the Cellular Prion Protein in Air Pollution Exposed Children and Young Adults. *JAD* 2012;28:93–107. <https://doi.org/10.3233/JAD-2011-110722>.
- [138] Kioumourtoglou M-A, Schwartz JD, Weisskopf MG, Melly SJ, Wang Y, Dominici F, et al. Long-term PM_{2.5} Exposure and Neurological Hospital Admissions in the Northeastern United States. *Environ Health Perspect* 2016;124:23–9. <https://doi.org/10.1289/ehp.1408973>.

- [139] Lee M, Schwartz J, Wang Y, Dominici F, Zanobetti A. Long-term effect of fine particulate matter on hospitalization with dementia. *Environmental Pollution* 2019;254:112926. <https://doi.org/10.1016/j.envpol.2019.07.094>.
- [140] Chen H, Kwong JC, Copes R, Hystad P, Van Donkelaar A, Tu K, et al. Exposure to ambient air pollution and the incidence of dementia: A population-based cohort study. *Environment International* 2017;108:271–7. <https://doi.org/10.1016/j.envint.2017.08.020>.
- [141] Cleary EG, Cifuentes M, Grinstein G, Brugge D, Shea TB. Association of Low-Level Ozone with Cognitive Decline in Older Adults. *Journal of Alzheimer's Disease* 2017;61:67–78. <https://doi.org/10.3233/JAD-170658>.
- [142] Haghani A, Morgan TE, Forman HJ, Finch CE. Air Pollution Neurotoxicity in the Adult Brain: Emerging Concepts from Experimental Findings. *JAD* 2020;76:773–97. <https://doi.org/10.3233/JAD-200377>.
- [143] Jiang C, Stewart LT, Kuo H-C, McGilberry W, Wall SB, Liang B, et al. Cyclic O₃ exposure synergizes with aging leading to memory impairment in male APOE ε₃, but not APOE ε₄, targeted replacement mice. *Neurobiology of Aging* 2019;81:9–21. <https://doi.org/10.1016/j.neurobiolaging.2019.05.006>.
- [144] Win-Shwe T-T, Fujitani Y, Kyi-Tha-Thu C, Furuyama A, Michikawa T, Tsukahara S, et al. Effects of Diesel Engine Exhaust Origin Secondary Organic Aerosols on Novel Object Recognition Ability and Maternal Behavior in BALB/C Mice. *IJERPH* 2014;11:11286–307. <https://doi.org/10.3390/ijerph111111286>.
- [145] Avila-Costa MR, Colín-Barenque L, Fortoul TI, Machado-Salas JP, Espinosa-Villanueva J, Rugerio-Vargas C, et al. Memory deterioration in an oxidative stress model and its correlation with cytological changes on rat hippocampus CA1. *Neuroscience Letters* 1999;270:107–9. [https://doi.org/10.1016/S0304-3940\(99\)00458-9](https://doi.org/10.1016/S0304-3940(99)00458-9).
- [146] Rivas-Arancibia S, Vazquez-Sandoval R, Gonzalez-Kladiano D, Schneider-Rivas S, Lechuga-Guerrero A. Effects of Ozone Exposure in Rats on Memory and Levels of Brain and Pulmonary Superoxide Dismutase. *Environmental Research* 1998;76:33–9. <https://doi.org/10.1006/enrs.1997.3784>.
- [147] Akhter H, Ballinger C, Liu N, van Groen T, Postlethwait EM, Liu R-M. Cyclic Ozone Exposure Induces Gender-Dependent Neuropathology and Memory Decline in an Animal Model of Alzheimer's Disease. *Toxicol Sci* 2015;147:222–34. <https://doi.org/10.1093/toxsci/kfv124>.
- [148] Sgourakis NG, Yan Y, McCallum SA, Wang C, Garcia AE. The Alzheimer's Peptides Aβ₄₀ and Aβ₄₂ Adopt Distinct Conformations in Water: A Combined MD / NMR Study. *Journal of Molecular Biology* 2007;368:1448–57. <https://doi.org/10.1016/j.jmb.2007.02.093>.

- [149] Kim SH, Knight EM, Saunders EL, Cuevas AK, Popovech M, Chen L-C, et al. Rapid doubling of Alzheimer’s amyloid- β 40 and 42 levels in brains of mice exposed to a nickel nanoparticle model of air pollution. *F1000Res* 2012;1:70. <https://doi.org/10.12688/f1000research.1-70.v1>.
- [150] Tyler CR, Noor S, Young TL, Rivero V, Sanchez B, Lucas S, et al. Aging Exacerbates Neuroinflammatory Outcomes Induced by Acute Ozone Exposure. *Toxicological Sciences* 2018;163:123–39. <https://doi.org/10.1093/toxsci/kfy014>.
- [151] Woodward NC, Levine MC, Haghani A, Shirmohammadi F, Saffari A, Sioutas C, et al. Toll-like receptor 4 in glial inflammatory responses to air pollution in vitro and in vivo. *J Neuroinflammation* 2017;14:84. <https://doi.org/10.1186/s12974-017-0858-x>.
- [152] Haghani A, Johnson R, Safi N, Zhang H, Thorwald M, Mousavi A, et al. Toxicity of urban air pollution particulate matter in developing and adult mouse brain: Comparison of total and filter-eluted nanoparticles. *Environment International* 2020;136:105510. <https://doi.org/10.1016/j.envint.2020.105510>.
- [153] Thomson EM, Kumarathasan P, Calderón-Garcidueñas L, Vincent R. Air pollution alters brain and pituitary endothelin-1 and inducible nitric oxide synthase gene expression. *Environmental Research* 2007;105:224–33. <https://doi.org/10.1016/j.envres.2007.06.005>.
- [154] Haghani A, Cacciottolo M, Doty KR, D’Agostino C, Thorwald M, Safi N, et al. Mouse brain transcriptome responses to inhaled nanoparticulate matter differed by sex and APOE in Nrf2-Nfkb interactions. *eLife* 2020;9:e54822. <https://doi.org/10.7554/eLife.54822>.
- [155] Bell ML, Dominici F, Ebisu K, Zeger SL, Samet JM. Spatial and Temporal Variation in PM_{2.5} Chemical Composition in the United States for Health Effects Studies. *Environ Health Perspect* 2007;115:989–95. <https://doi.org/10.1289/ehp.9621>.
- [156] Cory-Slechta DA, Merrill A, Sobolewski M. Air Pollution–Related Neurotoxicity Across the Life Span. *Annu Rev Pharmacol Toxicol* 2023;63:143–63. <https://doi.org/10.1146/annurev-pharmtox-051921-020812>.
- [157] Malashock DA, Delang MN, Becker JS, Serre ML, West JJ, Chang K-L, et al. Global trends in ozone concentration and attributable mortality for urban, peri-urban, and rural areas between 2000 and 2019: a modelling study. *The Lancet Planetary Health* 2022;6:e958–67. [https://doi.org/10.1016/S2542-5196\(22\)00260-1](https://doi.org/10.1016/S2542-5196(22)00260-1).
- [158] Zhang J (Jim), Wei Y, Fang Z. Ozone Pollution: A Major Health Hazard Worldwide. *Frontiers in Immunology* 2019;10. <https://doi.org/10.3389/fimmu.2019.02518>.

- [159] Brook RD, Brook JR, Urch B, Vincent R, Rajagopalan S, Silverman F. Inhalation of Fine Particulate Air Pollution and Ozone Causes Acute Arterial Vasoconstriction in Healthy Adults. *Circulation* 2002;105:1534–6. <https://doi.org/10.1161/01.CIR.0000013838.94747.64>.
- [160] Goldberg MS. Associations between Daily Cause-specific Mortality and Concentrations of Ground-level Ozone in Montreal, Quebec. *American Journal of Epidemiology* 2001;154:817–26. <https://doi.org/10.1093/aje/154.9.817>.
- [161] World Health Organization, editor. Air quality guidelines: global update 2005: particulate matter, ozone, nitrogen dioxide, and sulfur dioxide. Copenhagen, Denmark: World Health Organization; 2006.
- [162] Chitano P, Hosselet J, Mapp C, Fabbri L. Effect of oxidant air pollutants on the respiratory system: insights from experimental animal research. *Eur Respir J* 1995;8:1357–71. <https://doi.org/10.1183/09031936.95.08081357>.
- [163] Seltzer J, Bigby BG, Stulbarg M, Holtzman MJ, Nadel JA, Ueki IF, et al. O₃-induced change in bronchial reactivity to methacholine and airway inflammation in humans. *Journal of Applied Physiology* 1986;60:1321–6. <https://doi.org/10.1152/jappl.1986.60.4.1321>.
- [164] Pryor WA, Squadrito GL, Friedman M. A new mechanism for the toxicity of ozone. *Toxicology Letters* 1995;82–83:287–93. [https://doi.org/10.1016/0378-4274\(95\)03563-X](https://doi.org/10.1016/0378-4274(95)03563-X).
- [165] Frampton MW, Pryor WA, Cueto R, Cox C, Morrow PE, Utell MJ. Ozone Exposure Increases Aldehydes in Epithelial Lining Fluid in Human Lung. *American Journal of Respiratory and Critical Care Medicine* 1999;159:1134–7. <https://doi.org/10.1164/ajrccm.159.4.9807057>.
- [166] Sokolowska M, Quesniaux VFJ, Akdis CA, Chung KF, Ryffel B, Togbe D. Acute Respiratory Barrier Disruption by Ozone Exposure in Mice. *Front Immunol* 2019;10:2169. <https://doi.org/10.3389/fimmu.2019.02169>.
- [167] Enweasor C, Flayer CH, Haczku A. Ozone-Induced Oxidative Stress, Neutrophilic Airway Inflammation, and Glucocorticoid Resistance in Asthma. *Front Immunol* 2021;12:631092. <https://doi.org/10.3389/fimmu.2021.631092>.
- [168] Atkinson CE, Kesic MJ, Hernandez ML. Ozone in the Development of Pediatric Asthma and Atopic Disease. *Immunology and Allergy Clinics of North America* 2022;42:701–13. <https://doi.org/10.1016/j.iac.2022.06.001>.
- [169] Tétreault L-F, Doucet M, Gamache P, Fournier M, Brand A, Kosatsky T, et al. Childhood Exposure to Ambient Air Pollutants and the Onset of Asthma: An Administrative Cohort Study in Québec. *Environ Health Perspect* 2016;124:1276–82. <https://doi.org/10.1289/ehp.1509838>.

- [170] Fang X, Huang S, Zhu Y, Lei J, Xu Y, Niu Y, et al. Short-term exposure to ozone and asthma exacerbation in adults: A longitudinal study in China. *Front Public Health* 2023;10:1070231. <https://doi.org/10.3389/fpubh.2022.1070231>.
- [171] Ho K, Weimar D, Torres-Matias G, Lee H, Shamsi S, Shalosky E, et al. Ozone impairs endogenous compensatory responses in allergic asthma. *Toxicology and Applied Pharmacology* 2023;459:116341. <https://doi.org/10.1016/j.taap.2022.116341>.
- [172] Thurston GD. Air Pollution as an Underappreciated Cause of Asthma Symptoms. *JAMA* 2003;290:1915. <https://doi.org/10.1001/jama.290.14.1915>.
- [173] Gao H, Wang K, W. Au W, Zhao W, Xia Z. A Systematic Review and Meta-Analysis of Short-Term Ambient Ozone Exposure and COPD Hospitalizations. *IJERPH* 2020;17:2130. <https://doi.org/10.3390/ijerph17062130>.
- [174] Breitner S, Steckling-Muschack N, Markevych I, Zhao T, Mertes H, Nowak D, et al. The Burden of COPD Due to Ozone Exposure in Germany. *Deutsches Ärzteblatt International* 2021. <https://doi.org/10.3238/arztebl.m2021.0258>.
- [175] Paulin LM, Gassett AJ, Alexis NE, Kirwa K, Kanner RE, Peters S, et al. Association of Long-term Ambient Ozone Exposure With Respiratory Morbidity in Smokers. *JAMA Intern Med* 2020;180:106. <https://doi.org/10.1001/jamainternmed.2019.5498>.
- [176] Calderón-Garcidueñas L, Azzarelli B, Acuna H, Garcia R, Gambling TM, Osnaya N, et al. Air Pollution and Brain Damage. *Toxicol Pathol* 2002;30:373–89. <https://doi.org/10.1080/01926230252929954>.
- [177] Croze ML, Zimmer L. Ozone Atmospheric Pollution and Alzheimer’s Disease: From Epidemiological Facts to Molecular Mechanisms. *Journal of Alzheimer’s Disease* 2018;62:503–22. <https://doi.org/10.3233/JAD-170857>.
- [178] Calderón-Garcidueñas L, Reed W, Maronpot RR, Henriquez-Roldán C, Delgado-Chavez R, Calderón-Garcidueñas A, et al. Brain Inflammation and Alzheimer’s-Like Pathology in Individuals Exposed to Severe Air Pollution. *Toxicol Pathol* 2004;32:650–8. <https://doi.org/10.1080/01926230490520232>.
- [179] Calderón-Garcidueñas L, Reynoso-Robles R, Vargas- Martínez J, Gómez-Maqueo-Chew A, Pérez-Guillé B, Mukherjee PS, et al. Prefrontal white matter pathology in air pollution exposed Mexico City young urbanites and their potential impact on neurovascular unit dysfunction and the development of Alzheimer’s disease. *Environmental Research* 2016;146:404–17. <https://doi.org/10.1016/j.envres.2015.12.031>.
- [180] Calderón-Garcidueñas L, Mora-Tiscareño A, Ontiveros E, Gómez-Garza G, Barragán-Mejía G, Broadway J, et al. Air pollution, cognitive deficits and brain

abnormalities: A pilot study with children and dogs. *Brain and Cognition* 2008;68:117–27. <https://doi.org/10.1016/j.bandc.2008.04.008>.

- [181] Calderón-Garcidueñas L, Mora-Tiscareño A, Styner M, Gómez-garza G, Zhu H, Torres-Jardón R, et al. White Matter Hyperintensities, Systemic Inflammation, Brain Growth, and Cognitive Functions in Children Exposed to Air Pollution. *JAD* 2012;31:183–91. <https://doi.org/10.3233/JAD-2012-120610>.
- [182] Rodríguez-Martínez E, Martínez F, Espinosa-García MT, Maldonado P, Rivas-Arancibia S. Mitochondrial dysfunction in the hippocampus of rats caused by chronic oxidative stress. *Neuroscience* 2013;252:384–95. <https://doi.org/10.1016/j.neuroscience.2013.08.018>.
- [183] Hernández-Zimbrón LF, Rivas-Arancibia S. Oxidative stress caused by ozone exposure induces β -amyloid 1–42 overproduction and mitochondrial accumulation by activating the amyloidogenic pathway. *Neuroscience* 2015;304:340–8. <https://doi.org/10.1016/j.neuroscience.2015.07.011>.
- [184] Guerrero AL, Dorado-Martínez C, Rodríguez A, Pedroza-Ríos K, Borgonio-Pérez G, Rivas-Arancibia S. Effects of vitamin E on ozone-induced memory deficits and lipid peroxidation in rats: *NeuroReport* 1999;10:1689–92. <https://doi.org/10.1097/00001756-199906030-00012>.
- [185] Dorado-Martínez C, Paredes-carbajal C, Mascher D, Borgonio-Pérez G, Rivas-arancibia S. Effects of Different Ozone Doses on Memory, Motor Activity and Lipid Peroxidation Levels, in Rats. *International Journal of Neuroscience* 2001;108:149–61. <https://doi.org/10.3109/00207450108986511>.
- [186] Erickson MA, Banks WA, Baumann KK. Measurement of Blood-Brain Barrier Disruption in Mice Following Ozone Exposure Using Highly Sensitive Radiotracer Assays. *Current Protocols* 2022;2. <https://doi.org/10.1002/cpz1.460>.
- [187] Rivas-Arancibia S, Hernández-Zimbrón LF, Rodríguez-Martínez E, Borgonio-Pérez G, Velumani V, Durán-Bedolla J. Chronic exposure to low doses of ozone produces a state of oxidative stress and blood-brain barrier damage in the hippocampus of rat. *ABB* 2013;04:24–9. <https://doi.org/10.4236/abb.2013.411A2004>.
- [188] Heusinkveld HJ, Wahle T, Campbell A, Westerink RHS, Tran L, Johnston H, et al. Neurodegenerative and neurological disorders by small inhaled particles. *NeuroToxicology* 2016;56:94–106. <https://doi.org/10.1016/j.neuro.2016.07.007>.
- [189] Wang J, Liu Y, Jiao F, Lao F, Li W, Gu Y, et al. Time-dependent translocation and potential impairment on central nervous system by intranasally instilled TiO₂ nanoparticles. *Toxicology* 2008;254:82–90. <https://doi.org/10.1016/j.tox.2008.09.014>.

- [190] Oberdörster G, Sharp Z, Atudorei V, Elder A, Gelein R, Kreyling W, et al. Translocation of Inhaled Ultrafine Particles to the Brain. *Inhalation Toxicology* 2004;16:437–45. <https://doi.org/10.1080/08958370490439597>.
- [191] Patchin ES, Anderson DS, Silva RM, Uyeminami DL, Scott GM, Guo T, et al. Size-Dependent Deposition, Translocation, and Microglial Activation of Inhaled Silver Nanoparticles in the Rodent Nose and Brain. *Environ Health Perspect* 2016;124:1870–5. <https://doi.org/10.1289/EHP234>.
- [192] Adani G, Filippini T, Garuti C, Malavolti M, Vinceti G, Zamboni G, et al. Environmental Risk Factors for Early-Onset Alzheimer’s Dementia and Frontotemporal Dementia: A Case-Control Study in Northern Italy. *IJERPH* 2020;17:7941. <https://doi.org/10.3390/ijerph17217941>.
- [193] Knobel P, Litke R, Mobbs CV. Biological age and environmental risk factors for dementia and stroke: Molecular mechanisms. *Front Aging Neurosci* 2022;14:1042488. <https://doi.org/10.3389/fnagi.2022.1042488>.
- [194] Armstrong TD, Suwannasual U, Kennedy CL, Thasma A, Schneider LJ, Phillippi D, et al. Exposure to Traffic-Generated Pollutants Exacerbates the Expression of Factors Associated with the Pathophysiology of Alzheimer’s Disease in Aged C57BL/6 Wild-Type Mice. *JAD* 2020;78:1453–71. <https://doi.org/10.3233/JAD-200929>.
- [195] Richardson JR, Roy A, Shalat SL, Von Stein RT, Hossain MM, Buckley B, et al. Elevated Serum Pesticide Levels and Risk for Alzheimer Disease. *JAMA Neurol* 2014;71:284. <https://doi.org/10.1001/jamaneurol.2013.6030>.
- [196] Bolton JL, Marinero S, Hassanzadeh T, Natesan D, Le D, Belliveau C, et al. Gestational Exposure to Air Pollution Alters Cortical Volume, Microglial Morphology, and Microglia-Neuron Interactions in a Sex-Specific Manner. *Front Synaptic Neurosci* 2017;9:10. <https://doi.org/10.3389/fnsyn.2017.00010>.
- [197] Calderón-Garcidueñas L, Leray E, Heydarpour P, Torres-Jardón R, Reis J. Air pollution, a rising environmental risk factor for cognition, neuroinflammation and neurodegeneration: The clinical impact on children and beyond. *Revue Neurologique* 2016;172:69–80. <https://doi.org/10.1016/j.neurol.2015.10.008>.
- [198] Block ML, Calderón-Garcidueñas L. Air pollution: mechanisms of neuroinflammation and CNS disease. *Trends in Neurosciences* 2009;32:506–16. <https://doi.org/10.1016/j.tins.2009.05.009>.
- [199] Paul KC, Haan M, Mayeda ER, Ritz BR. Ambient Air Pollution, Noise, and Late-Life Cognitive Decline and Dementia Risk. *Annual Review of Public Health* 2019;40:203–20. <https://doi.org/10.1146/annurev-publhealth-040218-044058>.
- [200] Iaccarino L, La Joie R, Lesman-Segev OH, Lee E, Hanna L, Allen IE, et al. Association Between Ambient Air Pollution and Amyloid Positron Emission

Tomography Positivity in Older Adults With Cognitive Impairment. *JAMA Neurology* 2021;78:197. <https://doi.org/10.1001/jamaneurol.2020.3962>.

- [201] Semmens EO, Leary CS, Fitzpatrick AL, Ilango SD, Park C, Adam CE, et al. Air pollution and dementia in older adults in the Ginkgo Evaluation of Memory Study. *Alzheimer's & Dementia* 2023;19:549–59. <https://doi.org/10.1002/alz.12654>.
- [202] Zare Sakhvidi MJ, Yang J, Lequy E, Chen J, De Hoogh K, Letellier N, et al. Outdoor air pollution exposure and cognitive performance: findings from the enrolment phase of the CONSTANCES cohort. *The Lancet Planetary Health* 2022;6:e219–29. [https://doi.org/10.1016/S2542-5196\(22\)00001-8](https://doi.org/10.1016/S2542-5196(22)00001-8).
- [203] Shi L, Wu X, Danesh Yazdi M, Braun D, Abu Awad Y, Wei Y, et al. Long-term effects of PM_{2.5} on neurological disorders in the American Medicare population: a longitudinal cohort study. *The Lancet Planetary Health* 2020;4:e557–65. [https://doi.org/10.1016/S2542-5196\(20\)30227-8](https://doi.org/10.1016/S2542-5196(20)30227-8).
- [204] Bhatt DP, Puig KL, Gorr MW, Wold LE, Combs CK. A Pilot Study to Assess Effects of Long-Term Inhalation of Airborne Particulate Matter on Early Alzheimer-Like Changes in the Mouse Brain. *PLoS ONE* 2015;10:e0127102. <https://doi.org/10.1371/journal.pone.0127102>.
- [205] Air Quality - National Summary n.d. <https://www.epa.gov/air-trends/air-quality-national-summary>.
- [206] U.S. EPA. Integrated Science Assessment (ISA) for Ozone and Related Photochemical Oxidants (Final Report, Feb 2013). U.S. Environmental Protection Agency, Washington, DC, EPA/600/R-10/076F, 2013. n.d.
- [207] Zhao N, Pinault L, Toyib O, Vanos J, Tjepkema M, Cakmak S. Long-term ozone exposure and mortality from neurological diseases in Canada. *Environment International* 2021;157:106817. <https://doi.org/10.1016/j.envint.2021.106817>.
- [208] Chen J-C, Schwartz J. Neurobehavioral effects of ambient air pollution on cognitive performance in US adults. *NeuroToxicology* 2009;30:231–9. <https://doi.org/10.1016/j.neuro.2008.12.011>.
- [209] Kodavanti PRS, Valdez M, Richards JE, Agina-Obu DI, Phillips PM, Jarema KA, et al. Ozone-induced changes in oxidative stress parameters in brain regions of adult, middle-age, and senescent Brown Norway rats. *Toxicology and Applied Pharmacology* 2021;410:115351. <https://doi.org/10.1016/j.taap.2020.115351>.
- [210] Rivas-Arancibia S, Zimbrón LFH, Rodríguez-Martínez E, Maldonado PD, Borgonio Pérez G, Sepúlveda-Parada M. Oxidative stress-dependent changes in immune responses and cell death in the substantia nigra after ozone exposure in rat. *Front Aging Neurosci* 2015;7. <https://doi.org/10.3389/fnagi.2015.00065>.

- [211] Cheng H, Saffari A, Sioutas C, Forman HJ, Morgan TE, Finch CE. Nanoscale Particulate Matter from Urban Traffic Rapidly Induces Oxidative Stress and Inflammation in Olfactory Epithelium with Concomitant Effects on Brain. *Environ Health Perspect* 2016;124:1537–46. <https://doi.org/10.1289/EHP134>.
- [212] Johnson NF, Hotchkiss JA, Harkema JR, Henderson RF. Proliferative responses of rat nasal epithelia to ozone. *Toxicology and Applied Pharmacology* 1990;103:143–55. [https://doi.org/10.1016/0041-008X\(90\)90270-5](https://doi.org/10.1016/0041-008X(90)90270-5).
- [213] Hardy J, Allsop D. Amyloid deposition as the central event in the aetiology of Alzheimer's disease. *Trends in Pharmacological Sciences* 1991;12:383–8. [https://doi.org/10.1016/0165-6147\(91\)90609-V](https://doi.org/10.1016/0165-6147(91)90609-V).
- [214] Mattsson-Carlgrén N, Andersson E, Janelidze S, Ossenkoppele R, Insel P, Strandberg O, et al. A β deposition is associated with increases in soluble and phosphorylated tau that precede a positive Tau PET in Alzheimer's disease. *Sci Adv* 2020;6:eaz2387. <https://doi.org/10.1126/sciadv.aaz2387>.
- [215] Liu C-C, Hu J, Zhao N, Wang J, Wang N, Cirrito JR, et al. Astrocytic LRP1 Mediates Brain A β Clearance and Impacts Amyloid Deposition. *J Neurosci* 2017;37:4023–31. <https://doi.org/10.1523/JNEUROSCI.3442-16.2017>.
- [216] Nielsen HM, Mulder SD, Beliën JAM, Musters RJP, Eikelenboom P, Veerhuis R. Astrocytic A β 1-42 uptake is determined by A β -aggregation state and the presence of amyloid-associated proteins: Uptake of A β 1-42 Oligomers and Fibrils. *Glia* 2010;58:1235–46. <https://doi.org/10.1002/glia.21004>.
- [217] Holmes C, Cunningham C, Zotova E, Woolford J, Dean C, Kerr S, et al. Systemic inflammation and disease progression in Alzheimer disease. *Neurology* 2009;73:768–74. <https://doi.org/10.1212/WNL.0b013e3181b6bb95>.
- [218] Sadleir KR, Eimer WA, Cole SL, Vassar R. A β reduction in BACE1 heterozygous null 5XFAD mice is associated with transgenic APP level. *Mol Neurodegeneration* 2015;10:1. <https://doi.org/10.1186/1750-1326-10-1>.
- [219] Sadleir KR, Popovic J, Vassar R. ER stress is not elevated in the 5XFAD mouse model of Alzheimer's disease. *Journal of Biological Chemistry* 2018;293:18434–43. <https://doi.org/10.1074/jbc.RA118.005769>.
- [220] Yanai H, Matsuda A, An J, Koshiba R, Nishio J, Negishi H, et al. Conditional ablation of HMGB1 in mice reveals its protective function against endotoxemia and bacterial infection. *Proc Natl Acad Sci USA* 2013;110:20699–704. <https://doi.org/10.1073/pnas.1320808110>.
- [221] Hinnert RG, Burkart JK, Punte CL. Animal Inhalation Exposure Chambers. *Archives of Environmental Health: An International Journal* 1968;16:194–206. <https://doi.org/10.1080/00039896.1968.10665043>.

- [222] Hatch GE, Slade R, Harris LP, McDonnell WF, Devlin RB, Koren HS, et al. Ozone dose and effect in humans and rats. A comparison using oxygen-18 labeling and bronchoalveolar lavage. *Am J Respir Crit Care Med* 1994;150:676–83. <https://doi.org/10.1164/ajrccm.150.3.8087337>.
- [223] Plopper CG, Hyde DM. The non-human primate as a model for studying COPD and asthma. *Pulmonary Pharmacology & Therapeutics* 2008;21:755–66. <https://doi.org/10.1016/j.pupt.2008.01.008>.
- [224] Ballinger CA, Cueto R, Squadrito G, Coffin JF, Velsor LW, Pryor WA, et al. Antioxidant-mediated augmentation of ozone-induced membrane oxidation. *Free Radical Biology and Medicine* 2005;38:515–26. <https://doi.org/10.1016/j.freeradbiomed.2004.11.009>.
- [225] Segura P, Montaña LM, Bazán-Perkins B, Gustin P, Vargas MH. Ozone at high-pollution urban levels causes airway hyperresponsiveness to substance P but not to other agonists. *Environmental Toxicology and Pharmacology* 1997;3:91–5. [https://doi.org/10.1016/S1382-6689\(96\)00144-5](https://doi.org/10.1016/S1382-6689(96)00144-5).
- [226] Paxinos G, Franklin KBJ, Franklin KBJ. *The mouse brain in stereotaxic coordinates*. 2nd ed. San Diego: Academic Press; 2001.
- [227] Escartin C, Galea E, Lakatos A, O’Callaghan JP, Petzold GC, Serrano-Pozo A, et al. Reactive astrocyte nomenclature, definitions, and future directions. *Nat Neurosci* 2021;24:312–25. <https://doi.org/10.1038/s41593-020-00783-4>.
- [228] Michalovicz LT, Kelly KA, Vashishtha S, Ben-Hamo R, Efroni S, Miller JV, et al. Astrocyte-specific transcriptome analysis using the ALDH1L1 bacTRAP mouse reveals novel biomarkers of astrogliosis in response to neurotoxicity. *J Neurochem* 2019;150:420–40. <https://doi.org/10.1111/jnc.14800>.
- [229] Mucke L, Yu G-Q, McConlogue L, Rockenstein EM, Abraham CR, Masliah E. Astroglial Expression of Human α 1-Antichymotrypsin Enhances Alzheimer-like Pathology in Amyloid Protein Precursor Transgenic Mice. *The American Journal of Pathology* 2000;157:2003–10. [https://doi.org/10.1016/S0002-9440\(10\)64839-0](https://doi.org/10.1016/S0002-9440(10)64839-0).
- [230] Drobny A, Prieto Huarcaya S, Dober J, Kluge A, Bunk J, Schlothauer T, et al. The role of lysosomal cathepsins in neurodegeneration: Mechanistic insights, diagnostic potential and therapeutic approaches. *Biochimica et Biophysica Acta (BBA) - Molecular Cell Research* 2022;1869:119243. <https://doi.org/10.1016/j.bbamcr.2022.119243>.
- [231] Dejanovic B, Wu T, Tsai M-C, Graykowski D, Gandham VD, Rose CM, et al. Complement C1q-dependent excitatory and inhibitory synapse elimination by astrocytes and microglia in Alzheimer’s disease mouse models. *Nat Aging* 2022;2:837–50. <https://doi.org/10.1038/s43587-022-00281-1>.

- [232] Davidson KR, Ha DM, Schwarz MI, Chan ED. Bronchoalveolar lavage as a diagnostic procedure: a review of known cellular and molecular findings in various lung diseases. *J Thorac Dis* 2020;12:4991–5019. <https://doi.org/10.21037/jtd-20-651>.
- [233] Garza-Lombó C, Thang M, Greve HJ, Mumaw CL, Messenger EJ, Ahmed C, et al. Circulating HMGB1 is elevated in veterans with Gulf War Illness and triggers the persistent pro-inflammatory microglia phenotype in male C57Bl/6J mice. *Transl Psychiatry* 2021;11:390. <https://doi.org/10.1038/s41398-021-01517-1>.
- [234] Shin S, Bai L, Burnett RT, Kwong JC, Hystad P, Van Donkelaar A, et al. Air Pollution as a Risk Factor for Incident Chronic Obstructive Pulmonary Disease and Asthma. A 15-Year Population-based Cohort Study. *Am J Respir Crit Care Med* 2021;203:1138–48. <https://doi.org/10.1164/rccm.201909-1744OC>.
- [235] Nair AK, Van Hulle CA, Bendlin BB, Zetterberg H, Blennow K, Wild N, et al. Asthma amplifies dementia risk: Evidence from CSF biomarkers and cognitive decline. *A&D Transl Res & Clin Interv* 2022;8. <https://doi.org/10.1002/trc2.12315>.
- [236] Wang J, Li X, Lei S, Zhang D, Zhang S, Zhang H, et al. Risk of dementia or cognitive impairment in COPD patients: A meta-analysis of cohort studies. *Front Aging Neurosci* 2022;14:962562. <https://doi.org/10.3389/fnagi.2022.962562>.
- [237] Rostami J, Mothes T, Kolahdouzan M, Eriksson O, Moslem M, Bergström J, et al. Crosstalk between astrocytes and microglia results in increased degradation of α -synuclein and amyloid- β aggregates. *J Neuroinflammation* 2021;18:124. <https://doi.org/10.1186/s12974-021-02158-3>.
- [238] Smith CD, Andersen AH, Kryscio RJ, Schmitt FA, Kindy MS, Blonder LX, et al. Altered brain activation in cognitively intact individuals at high risk for Alzheimer's disease. *Neurology* 1999;53:1391–1391. <https://doi.org/10.1212/WNL.53.7.1391>.
- [239] Bookheimer SY, Strojwas MH, Cohen MS, Saunders AM, Pericak-Vance MA, Mazziotta JC, et al. Patterns of Brain Activation in People at Risk for Alzheimer's Disease. *N Engl J Med* 2000;343:450–6. <https://doi.org/10.1056/NEJM200008173430701>.
- [240] Ruitenberg A, Den Heijer T, Bakker SLM, Van Swieten JC, Koudstaal PJ, Hofman A, et al. Cerebral hypoperfusion and clinical onset of dementia: The Rotterdam study. *Annals of Neurology* 2005;57:789–94. <https://doi.org/10.1002/ana.20493>.
- [241] Paul J, Strickland S, Melchor JP. Fibrin deposition accelerates neurovascular damage and neuroinflammation in mouse models of Alzheimer's disease. *The Journal of Experimental Medicine* 2007;204:1999–2008. <https://doi.org/10.1084/jem.20070304>.

- [242] Zipser BD, Johanson CE, Gonzalez L, Berzin TM, Tavares R, Hulette CM, et al. Microvascular injury and blood–brain barrier leakage in Alzheimer’s disease. *Neurobiology of Aging* 2007;28:977–86. <https://doi.org/10.1016/j.neurobiolaging.2006.05.016>.
- [243] Yan SF, Ramasamy R, Schmidt AM. The RAGE Axis: A Fundamental Mechanism Signaling Danger to the Vulnerable Vasculature. *Circulation Research* 2010;106:842–53. <https://doi.org/10.1161/CIRCRESAHA.109.212217>.
- [244] Thomas T, Thomas G, McLendon C, Sutton T, Mullan M. β -Amyloid-mediated vasoactivity and vascular endothelial damage. *Nature* 1996;380:168–71. <https://doi.org/10.1038/380168a0>.
- [245] Liu X, Li Z, Zhang J, Guo M, Lu F, Xu X, et al. The association between ozone and ischemic stroke morbidity among patients with type 2 diabetes in Beijing, China. *Science of The Total Environment* 2022;818:151733. <https://doi.org/10.1016/j.scitotenv.2021.151733>.
- [246] Han M-H, Yi H-J, Kim Y-S, Ko Y, Kim Y-S. Association between Diurnal Variation of Ozone Concentration and Stroke Occurrence: 24-Hour Time Series Study. *PLoS ONE* 2016;11:e0152433. <https://doi.org/10.1371/journal.pone.0152433>.
- [247] Xu X, Sun Y, Ha S, Talbott EO, Lissaker CTK. Association between Ozone Exposure and Onset of Stroke in Allegheny County, Pennsylvania, USA, 1994–2000. *Neuroepidemiology* 2013;41:2–6. <https://doi.org/10.1159/000345138>.
- [248] Carlsen HK, Forsberg B, Meister K, Gíslason T, Oudin A. Ozone is associated with cardiopulmonary and stroke emergency hospital visits in Reykjavík, Iceland 2003–2009. *Environ Health* 2013;12:28. <https://doi.org/10.1186/1476-069X-12-28>.
- [249] Zhu L, Fratiglioni L, Guo Z, Agüero-Torres H, Winblad B, Viitanen M. Association of Stroke With Dementia, Cognitive Impairment, and Functional Disability in the Very Old: A Population-Based Study. *Stroke* 1998;29:2094–9. <https://doi.org/10.1161/01.STR.29.10.2094>.
- [250] Honig LS, Tang M-X, Albert S, Costa R, Luchsinger J, Manly J, et al. Stroke and the Risk of Alzheimer Disease. *Arch Neurol* 2003;60:1707. <https://doi.org/10.1001/archneur.60.12.1707>.
- [251] Sweeney MD, Ayyadurai S, Zlokovic BV. Pericytes of the neurovascular unit: key functions and signaling pathways. *Nat Neurosci* 2016;19:771–83. <https://doi.org/10.1038/nn.4288>.
- [252] Kisler K, Nelson AR, Rege SV, Ramanathan A, Wang Y, Ahuja A, et al. Pericyte degeneration leads to neurovascular uncoupling and limits oxygen supply to brain. *Nat Neurosci* 2017;20:406–16. <https://doi.org/10.1038/nn.4489>.

- [253] Hall CN, Reynell C, Gesslein B, Hamilton NB, Mishra A, Sutherland BA, et al. Capillary pericytes regulate cerebral blood flow in health and disease. *Nature* 2014;508:55–60. <https://doi.org/10.1038/nature13165>.
- [254] Mishra A, Reynolds JP, Chen Y, Gourine AV, Rusakov DA, Attwell D. Astrocytes mediate neurovascular signaling to capillary pericytes but not to arterioles. *Nat Neurosci* 2016;19:1619–27. <https://doi.org/10.1038/nn.4428>.
- [255] Dai W, Lopez OL, Carmichael OT, Becker JT, Kuller LH, Gach HM. Mild Cognitive Impairment and Alzheimer Disease: Patterns of Altered Cerebral Blood Flow at MR Imaging. *Radiology* 2009;250:856–66. <https://doi.org/10.1148/radiol.2503080751>.
- [256] Ma HR, Pan PL, Sheng LQ, Dai ZY, Wang GD, Luo R, et al. Aberrant pattern of regional cerebral blood flow in Alzheimer’s disease: a voxel-wise meta-analysis of arterial spin labeling MR imaging studies. *Oncotarget* 2017;8:93196–208. <https://doi.org/10.18632/oncotarget.21475>.
- [257] Michels L, Warnock G, Buck A, Macaudo G, Leh SE, Kaelin AM, et al. Arterial spin labeling imaging reveals widespread and A β -independent reductions in cerebral blood flow in elderly apolipoprotein epsilon-4 carriers. *J Cereb Blood Flow Metab* 2016;36:581–95. <https://doi.org/10.1177/0271678X15605847>.
- [258] Koike MA, Green KN, Blurton-Jones M, LaFerla FM. Oligemic Hypoperfusion Differentially Affects Tau and Amyloid- β . *The American Journal of Pathology* 2010;177:300–10. <https://doi.org/10.2353/ajpath.2010.090750>.
- [259] Wang X, Xing A, Xu C, Cai Q, Liu H, Li L. Cerebrovascular Hypoperfusion Induces Spatial Memory Impairment, Synaptic Changes, and Amyloid- β Oligomerization in Rats. *JAD* 2010;21:813–22. <https://doi.org/10.3233/JAD-2010-100216>.
- [260] Korte N, Nortley R, Attwell D. Cerebral blood flow decrease as an early pathological mechanism in Alzheimer’s disease. *Acta Neuropathol* 2020;140:793–810. <https://doi.org/10.1007/s00401-020-02215-w>.
- [261] Sun X, He G, Qing H, Zhou W, Dobie F, Cai F, et al. Hypoxia facilitates Alzheimer’s disease pathogenesis by up-regulating *BACE1* gene expression. *Proc Natl Acad Sci USA* 2006;103:18727–32. <https://doi.org/10.1073/pnas.0606298103>.
- [262] Zhang X, Zhou K, Wang R, Cui J, Lipton SA, Liao F-F, et al. Hypoxia-inducible Factor 1 α (HIF-1 α)-mediated Hypoxia Increases BACE1 Expression and β -Amyloid Generation. *Journal of Biological Chemistry* 2007;282:10873–80. <https://doi.org/10.1074/jbc.M608856200>.
- [263] Verghese PB, Castellano JM, Garai K, Wang Y, Jiang H, Shah A, et al. ApoE influences amyloid- β (A β) clearance despite minimal apoE/A β association in

physiological conditions. Proc Natl Acad Sci USA 2013;110.
<https://doi.org/10.1073/pnas.1220484110>.

- [264] Zhao Z, Sagare AP, Ma Q, Halliday MR, Kong P, Kisler K, et al. Central role for PICALM in amyloid- β blood-brain barrier transcytosis and clearance. Nat Neurosci 2015;18:978–87. <https://doi.org/10.1038/nn.4025>.
- [265] Nortley R, Korte N, Izquierdo P, Hirunpattarasilp C, Mishra A, Jaunmuktane Z, et al. Amyloid β oligomers constrict human capillaries in Alzheimer’s disease via signaling to pericytes. Science 2019;365:eaav9518.
<https://doi.org/10.1126/science.aav9518>.
- [266] Hartz AMS, Zhong Y, Wolf A, LeVine H, Miller DS, Bauer B. A β 40 Reduces P-Glycoprotein at the Blood–Brain Barrier through the Ubiquitin–Proteasome Pathway. J Neurosci 2016;36:1930–41. <https://doi.org/10.1523/JNEUROSCI.0350-15.2016>.
- [267] Hartz AMS, Bauer B, Soldner ELB, Wolf A, Boy S, Backhaus R, et al. Amyloid- β Contributes to Blood–Brain Barrier Leakage in Transgenic Human Amyloid Precursor Protein Mice and in Humans With Cerebral Amyloid Angiopathy. Stroke 2012;43:514–23. <https://doi.org/10.1161/STROKEAHA.111.627562>.
- [268] Wan W, Cao L, Liu L, Zhang C, Kalionis B, Tai X, et al. A β 1–42 oligomer-induced leakage in an *in vitro* blood–brain barrier model is associated with up-regulation of RAGE and metalloproteinases, and down-regulation of tight junction scaffold proteins. Journal of Neurochemistry 2015;134:382–93.
<https://doi.org/10.1111/jnc.13122>.
- [269] Zarow C, Barron E, Chui HC, Perlmutter LS. Vascular Basement Membrane Pathology and Alzheimer’s Disease. Annals of the New York Academy of Sciences 1997;826:147–59. <https://doi.org/10.1111/j.1749-6632.1997.tb48467.x>.
- [270] Schultz N, Brännström K, Byman E, Moussaud S, Nielsen HM, The Netherlands Brain Bank, et al. Amyloid-beta 1-40 is associated with alterations in NG2+ pericyte population ex vivo and in vitro. Aging Cell 2018;17:e12728.
<https://doi.org/10.1111/accel.12728>.
- [271] Carrano A, Hoozemans JJM, Van Der Vies SM, Rozemuller AJM, Van Horssen J, De Vries HE. Amyloid Beta Induces Oxidative Stress-Mediated Blood–Brain Barrier Changes in Capillary Amyloid Angiopathy. Antioxidants & Redox Signaling 2011;15:1167–78. <https://doi.org/10.1089/ars.2011.3895>.
- [272] Park L, Wang G, Zhou P, Zhou J, Pitstick R, Previti ML, et al. Scavenger receptor CD36 is essential for the cerebrovascular oxidative stress and neurovascular dysfunction induced by amyloid- β . Proc Natl Acad Sci USA 2011;108:5063–8.
<https://doi.org/10.1073/pnas.1015413108>.

- [273] Kimbrough IF, Robel S, Roberson ED, Sontheimer H. Vascular amyloidosis impairs the gliovascular unit in a mouse model of Alzheimer's disease. *Brain* 2015;138:3716–33. <https://doi.org/10.1093/brain/awv327>.
- [274] Wilcock DM, Vitek MP, Colton CA. Vascular amyloid alters astrocytic water and potassium channels in mouse models and humans with Alzheimer's disease. *Neuroscience* 2009;159:1055–69. <https://doi.org/10.1016/j.neuroscience.2009.01.023>.
- [275] Sun N, Akay LA, Murdock MH, Park Y, Galiana-Melendez F, Bubnys A, et al. Single-nucleus multiregion transcriptomic analysis of brain vasculature in Alzheimer's disease. *Nat Neurosci* 2023;26:970–82. <https://doi.org/10.1038/s41593-023-01334-3>.
- [276] Merlini M, Meyer EP, Ulmann-Schuler A, Nitsch RM. Vascular β -amyloid and early astrocyte alterations impair cerebrovascular function and cerebral metabolism in transgenic arcA β mice. *Acta Neuropathol* 2011;122:293–311. <https://doi.org/10.1007/s00401-011-0834-y>.
- [277] Oppenheim HA, Lucero J, Guyot A-C, Herbert LM, McDonald JD, Mabondzo A, et al. Exposure to vehicle emissions results in altered blood brain barrier permeability and expression of matrix metalloproteinases and tight junction proteins in mice. *Part Fibre Toxicol* 2013;10:62. <https://doi.org/10.1186/1743-8977-10-62>.
- [278] Disdier C, Chalansonnet M, Gagnaire F, Gaté L, Cosnier F, Devoy J, et al. Brain Inflammation, Blood Brain Barrier dysfunction and Neuronal Synaptophysin Decrease after Inhalation Exposure to Titanium Dioxide Nano-aerosol in Aging Rats. *Sci Rep* 2017;7:12196. <https://doi.org/10.1038/s41598-017-12404-5>.
- [279] Suwannasual U, Lucero J, McDonald JD, Lund AK. Exposure to traffic-generated air pollutants mediates alterations in brain microvascular integrity in wildtype mice on a high-fat diet. *Environmental Research* 2018;160:449–61. <https://doi.org/10.1016/j.envres.2017.10.029>.
- [280] Guan L, Geng X, Shen J, Yip J, Li F, Du H, et al. PM2.5 inhalation induces intracranial atherosclerosis which may be ameliorated by omega 3 fatty acids. *Oncotarget* 2018;9:3765–78. <https://doi.org/10.18632/oncotarget.23347>.
- [281] Hartz AMS, Bauer B, Block ML, Hong J-S, Miller DS. Diesel exhaust particles induce oxidative stress, proinflammatory signaling, and P-glycoprotein up-regulation at the blood-brain barrier. *FASEB j* 2008;22:2723–33. <https://doi.org/10.1096/fj.08-106997>.
- [282] Ruiz De Almodovar C, Lambrechts D, Mazzone M, Carmeliet P. Role and Therapeutic Potential of VEGF in the Nervous System. *Physiological Reviews* 2009;89:607–48. <https://doi.org/10.1152/physrev.00031.2008>.

- [283] Shibuya M. Vascular Endothelial Growth Factor (VEGF) and Its Receptor (VEGFR) Signaling in Angiogenesis: A Crucial Target for Anti- and Pro-Angiogenic Therapies. *Genes & Cancer* 2011;2:1097–105. <https://doi.org/10.1177/1947601911423031>.
- [284] Jais A, Solas M, Backes H, Chaurasia B, Kleinridders A, Theurich S, et al. Myeloid-Cell-Derived VEGF Maintains Brain Glucose Uptake and Limits Cognitive Impairment in Obesity. *Cell* 2016;165:882–95. <https://doi.org/10.1016/j.cell.2016.03.033>.
- [285] Tang H, Mao X, Xie L, Greenberg DA, Jin K. Expression level of vascular endothelial growth factor in hippocampus is associated with cognitive impairment in patients with Alzheimer’s disease. *Neurobiology of Aging* 2013;34:1412–5. <https://doi.org/10.1016/j.neurobiolaging.2012.10.029>.
- [286] Apátiga-Pérez R, Soto-Rojas LO, Campa-Córdoba BB, Luna-Viramontes NI, Cuevas E, Villanueva-Fierro I, et al. Neurovascular dysfunction and vascular amyloid accumulation as early events in Alzheimer’s disease. *Metab Brain Dis* 2022;37:39–50. <https://doi.org/10.1007/s11011-021-00814-4>.
- [287] Ojo JO, Reed JM, Crynen G, Vallabhaneni P, Evans J, Shackleton B, et al. Molecular Pathobiology of the Cerebrovasculature in Aging and in Alzheimers Disease Cases With Cerebral Amyloid Angiopathy. *Front Aging Neurosci* 2021;13:658605. <https://doi.org/10.3389/fnagi.2021.658605>.
- [288] Paris D, Patel N, DelleDonne A, Quadros A, Smeed R, Mullan M. Impaired angiogenesis in a transgenic mouse model of cerebral amyloidosis. *Neuroscience Letters* 2004;366:80–5. <https://doi.org/10.1016/j.neulet.2004.05.017>.
- [289] Fischer VW, Siddiqi A, Yusufaly Y. Altered angioarchitecture in selected areas of brains with Alzheimer’s disease. *Acta Neuropathol* 1990;79:672–9. <https://doi.org/10.1007/BF00294246>.
- [290] Brown WR, Moody DM, Thore CR, Challa VR, Anstrom JA. Vascular dementia in leukoaraiosis may be a consequence of capillary loss not only in the lesions, but in normal-appearing white matter and cortex as well. *Journal of the Neurological Sciences* 2007;257:62–6. <https://doi.org/10.1016/j.jns.2007.01.015>.
- [291] Lepelletier F -X., Mann DMA, Robinson AC, Pinteaux E, Boutin H. Early changes in extracellular matrix in Alzheimer’s disease. *Neuropathology Appl Neurobio* 2017;43:167–82. <https://doi.org/10.1111/nan.12295>.
- [292] Buée L, Hof PR, Bouras C, Delacourte A, Perl DP, Morrison JH, et al. Pathological alterations of the cerebral microvasculature in Alzheimer’s disease and related dementing disorders. *Acta Neuropathol* 1994;87:469–80. <https://doi.org/10.1007/BF00294173>.

- [293] Wang D-S, Dickson DW, Malter JS. β -Amyloid Degradation and Alzheimer's Disease. *Journal of Biomedicine and Biotechnology* 2006;2006:1–12. <https://doi.org/10.1155/JBB/2006/58406>.
- [294] Manzano RN, Chaze T, Rubinstein E, Matondo M, Zurzolo C, Brou C. Proteomic landscape of tunneling nanotubes reveals CD9 and CD81 tetraspanins as key regulators. *Cell Biology*; 2022. <https://doi.org/10.1101/2022.12.21.521537>.
- [295] Reyes R, Cardeñes B, Machado-Pineda Y, Cabañas C. Tetraspanin CD9: A Key Regulator of Cell Adhesion in the Immune System. *Front Immunol* 2018;9:863. <https://doi.org/10.3389/fimmu.2018.00863>.
- [296] Schenk GJ, Dijkstra S, Van Het Hof AJ, Van Der Pol SMA, Drexhage JAR, Van Der Valk P, et al. Roles for HB-EGF and CD9 in multiple sclerosis. *Glia* 2013;61:1890–905. <https://doi.org/10.1002/glia.22565>.
- [297] Rössler K, Neuchrist C, Kitz K, Scheiner O, Kraft D, Lassmann H. Expression of leucocyte adhesion molecules at the human blood-brain barrier (BBB). *J of Neuroscience Research* 1992;31:365–74. <https://doi.org/10.1002/jnr.490310219>.
- [298] Musunuri S, Khoonsari PE, Mikus M, Wetterhall M, Häggmark-Mänberg A, Lannfelt L, et al. Increased Levels of Extracellular Microvesicle Markers and Decreased Levels of Endocytic/Exocytic Proteins in the Alzheimer's Disease Brain. *JAD* 2016;54:1671–86. <https://doi.org/10.3233/JAD-160271>.
- [299] Mathieu M, Névo N, Jouve M, Valenzuela JI, Maurin M, Verweij FJ, et al. Specificities of exosome versus small ectosome secretion revealed by live intracellular tracking of CD63 and CD9. *Nat Commun* 2021;12:4389. <https://doi.org/10.1038/s41467-021-24384-2>.
- [300] Kumar A, Hughes TM, Craft S, Deep G. A novel approach to isolate brain-cell-derived exosomes from plasma to better understand pathogenesis of Alzheimer's disease: Biomarkers (non-neuroimaging) / plasma/serum/urine biomarkers. *Alzheimer's & Dementia* 2020;16:e044894. <https://doi.org/10.1002/alz.044894>.
- [301] Andrés IE, Toborek M. Extracellular vesicles of the blood-brain barrier. *Tissue Barriers* 2016;4:e1131804. <https://doi.org/10.1080/21688370.2015.1131804>.
- [302] Andrés IE, Leda A, Contreras MG, Bertrand L, Park M, Skowronska M, et al. Extracellular vesicles of the blood-brain barrier: Role in the HIV-1 associated amyloid beta pathology. *Molecular and Cellular Neuroscience* 2017;79:12–22. <https://doi.org/10.1016/j.mcn.2016.12.006>.
- [303] Forner S, MODEL-AD. Deep phenotyping of the 5xfAD mouse model by MODEL-AD: Development of new models and analysis methods/validation of pre-clinical methods. *Alzheimer's & Dementia* 2020;16:e036468. <https://doi.org/10.1002/alz.036468>.

- [304] Liddelow SA, Guttenplan KA, Clarke LE, Bennett FC, Bohlen CJ, Schirmer L, et al. Neurotoxic reactive astrocytes are induced by activated microglia. *Nature* 2017;541:481–7. <https://doi.org/10.1038/nature21029>.
- [305] Haruwaka K, Ikegami A, Tachibana Y, Ohno N, Konishi H, Hashimoto A, et al. Dual microglia effects on blood brain barrier permeability induced by systemic inflammation. *Nature Communications* 2019;10. <https://doi.org/10.1038/s41467-019-13812-z>.
- [306] Scaffidi P, Misteli T, Bianchi ME. Release of chromatin protein HMGB1 by necrotic cells triggers inflammation. *Nature* 2002;418:191–5. <https://doi.org/10.1038/nature00858>.
- [307] Papadopoulos Z, Herz J, Kipnis J. Meningeal Lymphatics: From Anatomy to Central Nervous System Immune Surveillance. *The Journal of Immunology* 2020;204:286–93. <https://doi.org/10.4049/jimmunol.1900838>.

CURRICULUM VITAE

Chandrama Ahmed

EDUCATION

PhD in Medical Neuroscience Aug 2018 – Jun 2024
Indiana University, USA

M.S. in Biomedical Engineering Aug 2015 - Dec 2017
Indiana University – Purdue University Indianapolis, USA

B.S. in Applied Physics, Electronics and Communication Engineering Feb 2010 - Dec 2014
University of Dhaka, Bangladesh

RESEARCH EXPERIENCE

Graduate Research Assistant Aug 2018-Present
Medical Neuroscience | Indiana University School of Medicine
Advisor: Michelle Block, PhD
Projects:

- Characterizing astrocytic and neurovascular dysregulation from air pollution and their roles in air pollution induced aggravated amyloid pathology in Alzheimer's disease.
- Investigate role of HMGB1 in lung–brain axis and astrocytic dysregulation in Alzheimer disease.
- Exploring neuroinflammation in parkinsonian model from paraquat toxicity.

Visiting Research Associate Jun 2018-Aug 2018
Anatomy and Cell Biology | Indiana University School of Medicine
Advisor: Michelle Block, PhD
Project:

- Paraquat induced Parkinsonian neurodegeneration model development in mice.

Visiting Research Associate Jan 2018-Apr 2018
Biomedical Engineering | Indiana University – Purdue University Indianapolis
Advisor: Ken Yoshida, PhD
Projects:

- Development of computational models to design electrodes for nerve conduction block with electrical stimulation.
- Development of in-vivo and ex-vivo proof of concept for reversible nerve conduction block with earthworm and canine vagus nerve respectively.

Graduate Research Assistant Aug 2015 - Dec 2017
Biomedical Engineering | Indiana University – Purdue University Indianapolis
Advisor: Ken Yoshida, PhD
Projects:

- System characterization of Universal Invertible Amplifier using bio-electric

contamination with Kalman filter algorithm.

- Design and development of a second order Universal Invertible Amplifier to capture entire spectrum of bioelectric signals with single device.
- Peripheral nerve conduction block using low-frequency alternating current.

Undergraduate Student Researcher

Jul 2013 - Dec 2014

Applied Physics, Electronics and Communication Engineering | University of Dhaka

Advisor: MAR Ahad, PhD

Project:

- Pedestrian action recognition using Support Vector Machine and Motion History Image.

TEACHING EXPERIENCE

Teaching Assistant: Probability Statistics & Application in

Biomedical Engineering

Jan 2017–May 2017

Purdue School of Engineering and Technology

- Was responsible for grading the homework and project.
- Held weekly office hours to help students with their problems.

Tutor: Science tutor for high school students

Jan 2012 - Dec 2014

PUBLICATION

Ahmed C, Greve HJ, Garza-Lombó C, Malley J, Johnson JA Jr, Oblak AL and Block ML. Peripheral HMGB1 is linked to O₃ pathology of disease-associated astrocytes and amyloid. *Alzheimer's & Dementia*. (In press).

Greve HJ, Dunbar AL, Garza-Lombó C, **Ahmed C**, Thang M, Messenger EJ, Mumaw CL, Johnson JA Jr, Kodavanti UP, Oblak AL, and Block ML. The bidirectional lung brain-axis of amyloid- β pathology: ozone dysregulates the peri-plaque microenvironment, *Brain*, 2022;, awac113, <https://doi.org/10.1093/brain/awac113>.

Garza-Lombó C, Thang M, Greve HJ, Mumaw CL, Messenger EJ, **Ahmed C**, Quinn E, Sullivan K, Block ML. Circulating HMGB1 is elevated in veterans with Gulf War Illness and triggers the persistent pro-inflammatory microglia phenotype in male C57Bl/6J mice. *Transl Psychiatry*. 2021 Jul 12;11(1):390. doi: 10.1038/s41398-021-01517-1. PubMed PMID: 34253711; PubMed Central PMCID: PMC8275600.

Ladd TB, Johnson JA Jr, Mumaw CL, Greve HJ, Xuei X, Simpson E, Barnes MA, Green BJ, Croston TL, **Ahmed C**, Lemons A, Beezhold DH, Block ML. Aspergillus versicolor Inhalation Triggers Neuroimmune, Glial, and Neuropeptide Transcriptional Changes. *ASN Neuro*. 2021 Jan-Dec; 13:17590914211019886. doi: 10.1177/17590914211019886. PubMed PMID: 34098774; PubMed Central PMCID: PMC8191080.

Mueid, R., **Ahmed, C.**, & Ahad, MAR. Pedestrian activity classification using patterns of motion and histogram of oriented gradient. *Journal on Multimodal User Interfaces*. 2016; 10(4), 299-305.

Horn, MR., **Ahmed, C.**, and Yoshida, K. Low Frequency Alternating Current Block - A New Method to Stop or Slow Conduction of Action Potentials. *2019 9th International IEEE/EMBS Conference on Neural Engineering (NER)*. 2019; 787-790, doi: 10.1109/NER.2019.8717160.

ACADEMIC ACTIVITIES

- Poster presentation at Big Ten Neuroscience Annual Meeting 2023 Jun 2023
- Poster presentation at Society of Toxicology (SOT) Annual Meeting Mar 2023
- Poster presentation at Neuroscience 2022 Nov 2022
- Oral presentation at BIG Ten Neuroscience Seminar Aug 2022
- Poster presentation at Americas School of Neuroimmunology (ASNI) Jul 2022
- Platform presentation at Ohio Valley Society of Toxicology (OVSOT) Trainee Meeting Jul 2022
- Oral presentation at Stark Summer Symposium 2022 Jul 2022
- Poster presentation at Greater Indiana Society for Neuroscience Meeting 2022. Apr 2022
- Poster presentation at Society of Toxicology (SOT) Annual Meeting. Mar 2022

AWARDS AND ACCOLADES

- SOT Graduate student travel award Mar 2023
- Trainee Professional Development Award, Society for Neuroscience Nov 2022
- Best presenter award at Ohio Valley Society of Toxicology (OVSOT) Trainee Meeting July 2022
- Stark Neuroscience Research Institute Travel Award May 2022
- IUPUI Graduate Office Travel Fellowship Award Nov 2022

EXTRACURRICULAR ACTIVITIES

- **SOT reporter:** Society of Toxicology Annual Meeting 2022. Mar 2022
- **General Secretary:** Bangladesh Student Association (BDSA) Aug 2018 – Aug 2019
- **Secretary:** Biomedical Engineering Graduate Student Association (BMEGSA), IUPUI. Aug 2016 - May 2017
- **Executive Member:** Electrical and Electronics Club at University of Dhaka. Jan 2013 - Dec 2014

- **Editor:** Utsob. Yearly magazine of the Department of Applied Physics.
- **Organizing Volunteer:** 2012 Int'l Conference on Informatics, Electronics and Vision.

Sep 2013 - Dec 2013

May 2012